UNIVERSITY OF CALIFORNIA SAN DIEGO

Development of magnetic assays for quantification of serum proteins and enzymatic activity

A Dissertation submitted in partial satisfaction of the requirements
for the degree Doctor of Philosophy

in

Bioengineering

by

Michael Sveiven

Committee in charge:

Professor Drew Hall, Co-Chair
Professor Anthony O'Donoghue, Co-Chair
Professor Stephanie Fraley, Co-Chair
Professor Louise Laurent
Professor Geert Schmid-Schoenbein
Professor Douglas Conrad

2024

The Dissertation of Michael Sveiven is approved, and it is acceptable in quality and form for publication on microfilm and electronically.

University of California San Diego

2024

DEDICATION

To my grandfather, Butch. You always challenged my thinking. Your love for people and learning left an indelible mark on me. Rest in peace.

TABLE OF CONTENTS

LIST OF FIGURES

LIST OF TABLES

ACKNOWLEDGEMENTS

I want to acknowledge Professor Anthony O'Donoghue and Professor Drew Hall for their support and guidance throughout my graduate education. Professor Hall, you allowed me to enter your lab as a master's student before I transitioned to the PhD program. I grew in skill and confidence in your lab because of the environment you fostered. Your lab is full of bright, curious minds exploring the cutting-edge of research with joy because you give them the resources and freedom to be curious. One thing I admire most about you is your ability to manage a lab full of students while you parent two young children. Your success as a father and a professional is so aspirational. I still want a rematch at go-kart racing, so you'll have to let me know the next time you go to K1 Speed. Thank you for allowing me to become educated in one of the best programs in the country and giving me all the tools I needed to succeed. Professor O'Donoghue, the time I spent with you in your office problem-solving was critical in my growth as a scientist. Seeing how you thought greatly shaped my critical thinking and experimental design. In addition, the memories I made with you and your lab during happy hours and lab retreats will stay with me for a long time. Whether ripping through the desert in a dune buggy or down the Mammoth slopes on a snowboard, your sense of fun and adventure is unmatched. Thank you for making my PhD journey so memorable and fulfilling.

I would also like to acknowledge all the lab members who made my PhD studies enjoyable and educational. You were all so helpful, collaborative, and friendly. I am so thankful for you all. I want to specifically acknowledge Sandeep Adem, Saeromi Chung, Matthew Holden, Naveen Singh, Xiahan Zhou, Tyler Hack, Aditi Jain, Corentin Pinochet, Chih-Cheng Huang, Omid Ghadami, Joshua Rosenberg, Matthew Chan, Sonal Jain, Elany Barbosa Da Silva, Pavla Fajtova,

Brianna Hurysz, Lawrence Liu, Von Phan, Stephanie Luedtke, Ana K Serrano, Kavya Balaji, and all my other labmates who have made the experience so special.

In addition, I would like to thank all my collaborators. You provided me with resources and insights that were invaluable to my success. I'd like to specifically thank Professor Louise Laurent, Professor Doug Conrad, Andrew Gassman, PhD, Jay Boniface, PhD, Tracey Fleischer, PhD, and Aaron Smargon, PhD.

I would like to thank my family and friends. Enjoying time with you always gave me a comforting perspective. Earning a PhD is full of challenges and failures, which makes it so valuable, but that does take a toll on your spirits. My loved ones never failed to support me and lift my spirits. I am glad I chose to pursue a graduate degree in a city close to home because my weekends home for family events always fortified my efforts. I want to specifically thank all my friends. Holly, Matt, Nate, Jon, Hank, Deval, Ashu, Ariel, Dave, Jeffry, Sara, Nicole, Michael, Lindsey, Sebastian, Dana, Miranda, Marcus, Nik, Albert, Fernando, and Rachel made my early twenties some of the best years of my life!

My parents have been great role models all my life. Your insistence on hard work and sacrifice for us children has been the foundation my life was built on. The family you have built is a delightful achievement that will fill my heart always. I hope that I live up to your example. I treasure you greatly and will never stop appreciating your impact on my life.

Finally, I have to give a specific acknowledgement to my partner, Holly. I gained so much during my time at UCSD, but nothing I treasure more than my relationship with you. Although I was pining after you the whole time, our platonic friendship during the first few years of our graduate program brightened my life. But creating a partnership with you has genuinely surpassed

my expectations of what a relationship can give. I love you so much and I am so glad that our graduate education brought us together.

Chapter 2, in part, is a reprint of the journal article "A GMR Enzymatic Assay for Quantifying Nuclease and Peptidase Activity" as it appears in *Frontiers in Bioengineering and Biotechnology* by Michael Sveiven, Ana Serrano, Joshua Rosenberg, Doug Conrad, Drew A. Hall, and Anthony J. O'Donoghue, Mar 2024. In addition, Chapter 2, in part, is a reprint of the journal article "A Dual-Binding, Magnetic Immunoassay to Predict Spontaneous Preterm Birth" as it appears in *Frontiers in Bioengineering and Biotechnology* by Michael Sveiven, Andrew Gassman, Joshua Rosenberg, Jay Boniface, Matthew Chan, Anthony J. O'Donoghue, Louise Laurent, and Drew A. Hall, Sep 2023. The dissertation author was the first author of these papers.

Chapter 3, in part, is a reprint of the journal article "A Dual-Binding, Magnetic Immunoassay to Predict Spontaneous Preterm Birth" as it appears in *Frontiers in Bioengineering and Biotechnology* by Michael Sveiven, Andrew Gassman, Joshua Rosenberg, Jay Boniface, Matthew Chan, Anthony J. O'Donoghue, Louise Laurent, and Drew A. Hall, Sep 2023. In addition, Chapter 3, in part, is a reprint of the journal article "A CMOS Magnetoresistive Sensor Front-End with Mismatch-Tolerance and Sub-ppm Sensitivity for Magnetic Immunoassays" as it appears in *IEEE Transactions on Biomedical Circuits* (TBioCAS) by Xiahan Zhou, Michael Sveiven, and Drew Hall, Dec 2019. The dissertation author was the first author of the first paper and the second author of the other paper.

Chapter 4, in part, is a reprint of the journal article "A GMR Enzymatic Assay for Quantifying Nuclease and Peptidase Activity" as it appears in *Frontiers in Bioengineering and Biotechnology* by Michael Sveiven, Ana Serrano, Joshua Rosenberg, Doug Conrad, Drew A. Hall, and Anthony J. O'Donoghue, Mar 2024. In addition, Chapter 4, in part, is a reprint of the journal

article “Giant Magnetoresistive Biosensors for Real-Time Quantitative Detection of Protease Activity” as it appears in *Nature Scientific Reports* by Sandeep Adem, Sonal Jain, Michael Sveiven, Xiahan Zhou, Anthony J. O’Donoghue, and Drew A. Hall, May 2020. The dissertation author was the first author of the first paper and the third author of the second paper.

Chapter 5, in part, is a reprint of the journal article “A GMR Enzymatic Assay for Quantifying Nuclease and Peptidase Activity” as it appears in *Frontiers in Bioengineering and Biotechnology* by Michael Sveiven, Ana Serrano, Joshua Rosenberg, Doug Conrad, Drew A. Hall, and Anthony J. O’Donoghue, Mar 2024. In addition, Chapter 5, in part, is a reprint of the journal article “A Dual-Binding, Magnetic Immunoassay to Predict Spontaneous Preterm Birth” as it appears in *Frontiers in Bioengineering and Biotechnology* by Michael Sveiven, Andrew Gassman, Joshua Rosenberg, Jay Boniface, Matthew Chan, Anthony J. O’Donoghue, Louise Laurent, and Drew A. Hall, Sep 2023. The dissertation author was the first author of these papers.

VITA

2017 Bachelor of Science in Biomedical Engineering, University of Arizona

2024 Doctor of Philosophy in Bioengineering, University of California San Diego

PUBLICATIONS

Michael Sveiven, Ana Serrano, Joshua Rosenberg, Doug Conrad, Drew A. Hall, and Anthony J. O'Donoghue, "A GMR Enzymatic Assay for Quantifying Nuclease and Peptidase Activity," *Frontiers in Bioengineering and Biotechnology*, vol. 11, Mar 2024.

Michael Sveiven, Andrew Gassman, Joshua Rosenberg, Matthew Chan, Jay Boniface, Anthony J. O'Donoghue, Louise C. Laurent, and Drew A. Hall, "A Dual-Binding Magnetic Immunoassay to Predict Spontaneous Preterm Birth," *Frontiers in Bioengineering and Biotechnology*, vol. 11, Sep 2023.

Xiahan Zhou, **Michael Sveiven**, and Drew Hall, "A CMOS Magnetoresistive Sensor Front-End with Mismatch-Tolerance and Sub-ppm Sensitivity for Magnetic Immunoassays," *IEEE Transactions on Biomedical Circuits* (TBioCAS), Dec 2019.

Xiahan Zhou, **Michael Sveiven**, and Drew Hall, "A Fast-Readout, Mismatch-Insensitive Magnetoresistive Biosensor Front-End Achieving Sub-ppm Sensitivity," *IEEE International Solid-State Circuits Conference* (ISSCC), Feb 2019.

Xiahan Zhou, Enhan Mai, **Michael Sveiven**, Corentin Pochet, Haowei Jiang, Chih-Cheng Huang, et al., "A 9.7-nTrms, 704-ms Magnetic Biosensor Front-End for Detecting Magneto-Relaxation," *IEEE Journal of Solid-State Circuits* (JSSC), Jul 2021.

Sandeep Adem, Sonal Jain, **Michael Sveiven**, Xiahan Zhou, Anthony J. O'Donoghue, and Drew A. Hall, "Giant Magnetoresistive Biosensors for Real-Time Quantitative Detection of Protease Activity," *Nature Scientific Reports*, May 2020.

Naveen Singh, Saeromi Chung, **Michael Sveiven**, and Drew Hall, "Cortisol Detection in Undiluted Human Serum Using a Sensitive Electrochemical Structure Switching Aptamer over an Antifouling Nanocomposite Layer," *ACS Omega*, Oct 2021.

ABSTRACT OF THE DISSERTATION

Development of magnetic assays for quantification of serum proteins and enzymatic activity

by

Michael Sveiven

Doctor of Philosophy in Bioengineering

University of California San Diego, 2024

Professor Drew Hall, Co-Chair

Professor Anthony O'Donoghue, Co-Chair

Professor Stephanie Fraley, Co-Chair

This research focused on using giant magnetoresistive (GMR) biosensors for point-of-care testing to improve disease diagnosis and monitoring, thereby aiding healthcare decision-making. With their ability to detect subtle changes in local magnetic fields, GMR sensors offer a multiplexed and highly sensitive solution for various biomedical applications. By optimizing the

surface chemistry for stable and reproducible conjugation of various biomolecules, the versatile platform enabled specific protein binding, including antibodies for Insulin-like Growth Factor Binding Protein-4 (IBP4) and Sex Hormone Binding Globulin (SHBG), as well as double-stranded DNA substrates for nuclease activity quantitation and protease substrates for quantitation of proteases such as papain and human neutrophil elastase. This work resulted in proof-of-concept of a sensitive, multiplexed, and point-of-care assay for predicting spontaneous preterm birth in pregnant mothers, critical as the complications posed by preterm birth (delivery before 37 weeks of pregnancy) are a leading cause of newborn morbidity and mortality. The assays were validated against mass spectrometry, showing high agreement. These assays have the potential to revolutionize prenatal care by providing timely and precise information to healthcare providers, ultimately improving outcomes for both mothers and infants. We expanded the capabilities of GMR sensors to multiplexed hydrolase quantification, including proteases and nucleases in biological samples. This development is vital for diseases marked by recurrent bacterial lung infections, such as chronic obstructive pulmonary disease and cystic fibrosis. This work highlights the transformative potential of GMR sensors in offering rapid and comprehensive insights into patients' health to enhance healthcare decision-making and improve patient outcomes.

CHAPTER 1: INTRODUCTION

1.1 Biosensors

Utilizing a variety of bioreceptors, such as enzymes, antibodies, cells, aptamers, and nanoparticles, biosensors transduce the presence or activity of biological analytes into detectable signals. These sophisticated instruments are pivotal for accessing biological information, both internal and external to the human body. In healthcare, biosensors are indispensable tools for revolutionizing disease diagnosis, health monitoring, and substance abuse observation. They play a crucial role in ensuring food quality control by rapidly identifying contaminants, spoilage, and adulteration in food products. Biosensors also contribute significantly to environmental monitoring, agriculture, and bioprocess monitoring, detecting pollutants, and ensuring product quality and process efficiency. Additionally, biosensors are integral to drug discovery processes, facilitating rapid screening of potential drug candidates and enhancing drug development pipelines. However, perhaps their most vital application lies in healthcare, where biosensors empower timely and accurate diagnostics, disease management, and treatment monitoring.

Since their commercially successful inception in 1975 with the introduction of the blood glucose test by Yellow Springs Instruments, biosensors have witnessed exponential growth (Yoo and Lee, 2010). According to a report by MarketsandMarkets, the biosensors market is expected to reach $36.7 billion USD by 2026 with a compound annual growth rate of 7.5%. This expansion further underscores biosensors' indispensable role in accessing and interpreting biological information across diverse fields, with healthcare as their most prominent domain.

Historically, the complexity and cost of data analysis systems, such as the readout station from Yellow Springs Instrument Company, have confined their use to centralized laboratories for interpreting biosensor responses. However, a key trend shaping the field of biosensors is the

decentralization of sensing modalities. Empowering users with the ability to deploy sensors directly enables more frequent data collection, shorter turnaround times, and enhanced accessibility, expanding the utility of biosensors across a multitude of applications.

Researchers face several critical challenges to realize the potential of biosensors with point-of-care or point-of-use capabilities, including managing assay complexity, ensuring reagent stability, and selecting appropriate equipment. Overcoming these challenges is essential for developing user-friendly, robust biosensors that can seamlessly integrate into diverse healthcare settings. By embracing these trends and addressing associated challenges, biosensors hold immense promise for revolutionizing healthcare delivery, empowering individuals with timely and accurate health information, and ultimately enhancing the quality of life for people worldwide.

1.2 Giant magnetoresistive sensors

The discovery of giant magnetoresistance earned Albert Fert and Peter Grünberg the Nobel Prize in Physics in 2007. They found that structures containing multiple, alternating thin-film layers of conductive ferromagnetic and nonmagnetic materials change electrical resistance in response to magnetic fields. This phenomenon arises from a quantum mechanical effect known as spin-dependent scattering. When the magnetization of the layers of ferromagnetic material (separated by films of nonmagnetic material) are aligned by an external magnetic field, electrons will move through the structure with less resistance than if the ferromagnetic layers were magnetized antiparallel to each other. This occurs because the scattering of the electrons as they flow through the conductive material depends on whether the spin of the electrons is parallel or antiparallel to the magnetization of the ferromagnetic layer. GMR spin-valve (GMR SV) sensors are the most commonly used GMR sensors (Barnaś et al., 1990; Osterfeld et al., 2008; Prinz, 1998; Wolf et al., 2001; Wu et al., 2022). They are composed of a “free-layer” made of a thin-film of

ferromagnetic material adjacent to a nonmagnetic layer. The “free-layer” will orient its magnetization in the direction of any applied external magnetic field. Beneath the nonmagnetic layer is another ferromagnetic layer, which is “pinned” by an adjacent antiferromagnetic layer. The “pinned” ferromagnetic layer is kept in a specific magnetic orientation. Due to magnetic shape anisotropy, the “pinned-layer” and the “free-layer” have 90º alignment when the GMR SV sensors are kept in zero external magnetic field. When the external magnetic field orients the “free-layer” antiparallel to the “pinned-layer,” the resistance increases. A critical metric in evaluating GMR sensors is the magnetoresistance (MR) ratio, which quantifies the sensor's sensitivity to changes in magnetic field. This ratio is calculated as the percentage difference between the resistance of the sensor when the ferromagnetic layers are in an antiparallel configuration (R_{AP}) and the resistance when they are in a parallel configuration (R_P), divided by the resistance in the parallel state ($[R_{AP} - R_P] / R_P$). Although the MR ratio is lower for GMR SV sensors when compared to sensors containing more layers of ferromagnetic material, GMR SV sensors are the best candidate for many applications due to their linear response to changes in magnetic fields.

1.3 Biomedical applications of giant magnetoresistive sensors

Initially, GMR sensors found applications in computer systems, particularly in components such as hard-disk drives. Subsequently, their value became evident in bioassays. In the realm of biomedical applications, the integration of GMR SV sensors has proven to be advantageous for several reasons. As highlighted by various researchers, magnetic sensors offer a unique set of benefits, including their ability to be arrayed for multiplex detection, amenability to miniaturization, and exceptional sensitivity (Klein et al., 2019; Krishna et al., 2016; Osterfeld et al., 2008; S. Gaster et al., 2011). What sets GMR sensors apart in biomedical contexts is their agnosticism towards the sample matrix (Gaster et al., 2009). Unlike traditional methods, GMR

sensors operate seamlessly regardless of the sample type, be it urine, saliva, serum, or others, thereby streamlining sample preparation procedures, often requiring nothing more than dilution. Because of their unique blend of advantageous properties, GMR SV sensors are particularly attractive for point-of-care or point-of-use settings.

Utilizing GMR sensors in bioassays requires using a magnetic label, often achieved with magnetic nanoparticles (MNPs). MNPs induce a change in the local magnetic field surrounding the GMR sensors. When subjected to an external magnetic field, these MNPs generate stray magnetic fields in the antiparallel direction of the external field. If these MNPs are tethered near the sensor surface, their stray magnetic fields will provoke a change in the magnetization of the sensor's "free-layer," which can be quantified as a change in magnetoresistance. This approach offers distinct advantages over traditional fluorescent detection molecules, which are plagued by issues such as auto-fluorescence and photobleaching.

Currently, there is evidence supporting the substitution of GMR SV sensors for conventional ELISAs, marking a promising development. However, there is potential for even further expansion. This work aims to advance the application of GMR sensors in creating bioassays that capitalize on their unique advantages, thus contributing significantly to the biomedical field. Integrating GMR sensors can democratize essential biomedical insights, enhancing accessibility to health information for patients, healthcare professionals, and researchers alike.

CHAPTER 2: SURFACE FUNCTIONALIZATION TECHNIQUES

2.1 Overview

In the realm of bioengineering, the interplay between biological systems and engineered materials is central to the advancement of biosensing technologies, particularly in disease monitoring and diagnosis. Among these technologies, GMR sensors have emerged as promising platforms due to their sensitivity, multiplexing ability, agnosticism towards sample matrices, miniaturization capabilities, and potential use in point-of-care devices. However, the successful application of GMR sensors in this context hinges on the strategic use of surface chemistry to functionalize these sensors effectively.

Surface chemistry plays a pivotal role in tailoring the functionality of GMR sensors, facilitating the specific binding of biomolecules known as bioreceptors, such as antibodies and enzyme substrates, to the sensor surface. These bioreceptors are integral in transducing biological interactions into electrical signals, thus forming the basis of immunoassays and enzymatic activity assays crucial for disease diagnosis and monitoring. The ability to bind amine-containing reagents reproducibly and efficiently to the sensor surface is paramount, as is ensuring the stability of these surface-bound moieties in assay buffers and biological samples.

This thesis endeavors to address the critical role of surface chemistry in the development of GMR-based biosensing platforms for disease monitoring and diagnosis. Through systematic investigation and optimization of surface modification techniques, the objective is to achieve robust and stable immobilization of bioreceptors on the sensor surface. By enhancing the specificity, sensitivity, and reproducibility of GMR-based assays, this research aims to contribute

significantly to the field of bioanalytical technologies, with implications spanning medical diagnostics and disease monitoring.

2.2 Materials and methods

2.2.1 Materials

Poly (allylamine) solution (PAAM; #479144) and poly (ethylene alt maleic anhydride) (PEMA; #188050 were purchased from Sigma-Aldrich. Streptavidin-coated magnetic nanoparticles (#130-048-101) were acquired from Miltenyi Biotec. Fine crystalline 2-(4-Morpholino)ethane Sulfonic Acid (MES) (#BP300-100) was purchased from Fisher Scientific.

2.2.2 Methods

Surface functionalization: Sensors were cleaned with sequential addition and removal of 600 µL of acetone, methanol, and isopropanol. The sensor arrays were then placed in an ultraviolet (UV)-Ozone Cleaner (Uvotech Systems, Helios 500) for 10 min. Immediately afterward, a 100 µL solution of 1% Poly(allylamine) in pH 6.0 MES buffer is placed in the sensor wells for 10 min and then washed with 600 µL of deionized (DI) water. The sensors were baked for 90 min at 110°C in a Precision Compact Oven (Thermo Scientific #PR305225G). Poly(ethylene alt-maleic anhydride) (PEMA) is made aqueous by placing it in a 170°C water bath for 90 min directly before adding it to the sensor surface. Then the 100 µL solution of 1.5% aqueous PEMA in pH 6.0 MES buffer is passed through a 0.22 µm filter before addition to the sensors for 5 min. We also tested combinations of 2% PEMA at 200° C and 0.45 µm filters to discover these optimized conditions. The sensors are rinsed with 1 mL DI water, air-dried with an aspirator, and baked for 1 h at 160°C. The protocol was adapted from previous methods (Kim et al., 2013).

Stability assay: To assess the stability of the functionalized sensors, EZ-Link™ Amine-PEG_{11}-Biotin (Thermo Fisher #26136) is coupled to the sensor, as described above. 1%

ethanolamine is added and incubated for 30 min at room temperature. The sensor is placed in the GMR readout station, and 50 µL of streptavidin-coated magnetic nanoparticles (Miltenyi Biotec #130–048–101) is added and incubated for 15 min. The sensor is washed with 1 mL of PBS and then incubated for 21 days at 4° C under humid conditions by placing wet Kim wipes in a Petri dish with parafilm to create a seal. The stability evaluation is initiated by returning the assay to the GMR readout station for measurement. Next, the sensors are washed with 1 mL PBS, and streptavidin is blocked by incubating with 100 µL of 1 mM biotin in PBS. Stability is assessed by incubating the sensor array for 5 min each with 0.2, 1, and 5 M NaCl in water. The sensor is then washed briefly with water and sequentially incubated with PBS at 22, 4, and 50°C for 5 min each. For pH stability, the sensor is incubated in PBS adjusted to pH 3 with HCl. It is then incubated in PBS pH 7.2 and PBS adjusted to pH 9 and pH 13.5 with NaOH.

2.3 Exploration of surface functionalization techniques

Immobilizing bioreceptors, such as antibodies and hydrolase enzyme substrates, to the sensor surface is critical in biosensing. Several immobilization chemistries were explored (e.g., Polyethylenimine, (3-Aminopropyl)triethoxysilane, N-Hydroxysuccinimide with 1-Ethyl-3-(3-dimethylaminopropyl)carbodiimide (NHS-EDC), Diaza-Silane, and PEMA-PAAM), and evaluated based on their stability, reactivity, and coverage (Figure 2.1). A biotinylated-BSA reagent was used as a positive control. The biotin will bind to the streptavidin-coated magnetic nanoparticles (MNPs). The negative control is BSA without biotin, which will have no mechanism for tethering the MNPs close to the sensor surface. If the surface chemistry functions as expected, the sensors functionalized with biotinylated-BSA will exhibit high signal while the sensors functionalized with the unmodified BSA will exhibit a lack signal. PEMA-PAAM consistently

performed the best, in terms of the positive control sensors' signal amplitude compared to the negative control sensors' signal amplitude, and was used for all subsequent experiments.

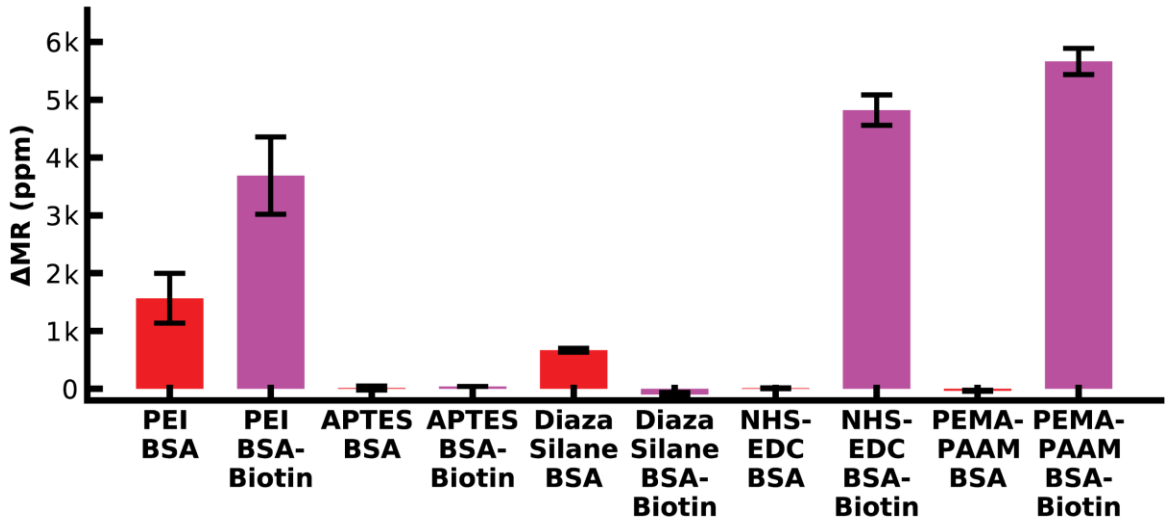

Figure 2.1: Surface chemistry alternatives. Positive (magenta) and negative (red) control values for surface chemistries explored.

2.4 Poly(ethylene alt-maleic anhydride) with poly(allylamine)

2.4.1 Mechanism

The reactions necessary to use poly(ethylene alt-maleic anhydride) with poly(allylamine) to bind amine-containing reagents to the surface of GMR sensors are outlined as follows. The GMR sensors are coated with a SiO_2 passivation layer. Silanol groups can form on this layer due to moisture in the air. This passivation layer gains a negative charge due to the polar bonds between oxygen and silicon or hydrogen. When an aqueous solution of poly(allylamine) (PAAM) is applied to the sensor in a pH 6 buffer, the amine groups of PAAM become protonated, forming positively charged ammonium ions. The opposite charge between the passivation layer and the protonated PAAM promotes the adhesion of PAAM to the sensor's surface. This adhesion is further strengthened by baking. While PAAM is being baked onto the sensor, poly(ethylene-alt-maleic

anhydride) (PEMA) is hydrolyzed in a water bath, leading to the formation of carboxylic acids (Figure 2.2A). When these carboxylic acid groups are added to the sensor surface, they become deprotonated by the amines of PAAM, forming ionic salts. Heating promotes the reaction of some of these carboxylic acids with the amines of PAAM to form amide bonds (Figure 2.2B). Additionally, the sensors are baked to cure the PEMA, converting any unreacted carboxylic acid species back to their maleic anhydride form (Figure 2.2A). An excess of PEMA is used compared to PAAM to ensure enough reactive groups are available for subsequent reactions. When substrates containing primary amines are introduced to the sensor surface, the maleic anhydride groups of

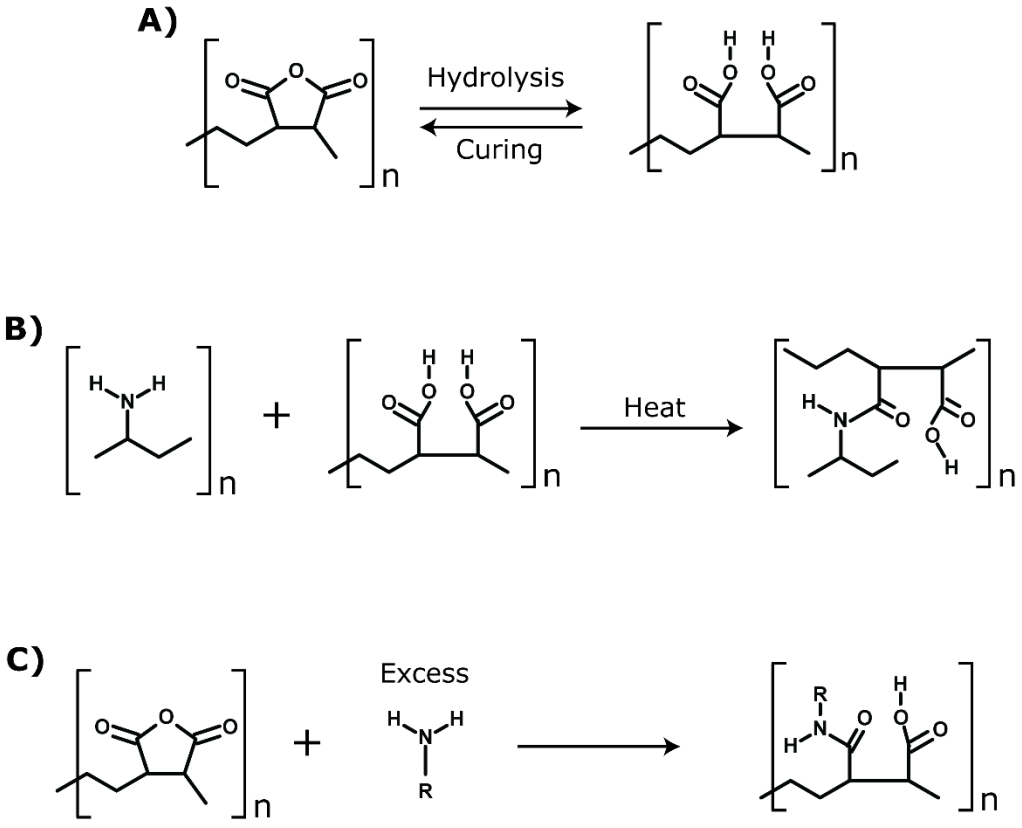

Figure 2.2: Surface chemistry reactions. (A) Hydrolysis and curing of poly(ethylene alt-maleic anhydride). (B) Amide formation with poly(allylamine) and poly(ethylene alt-maleic anhydride). (C) Functionalization of amine-containing substrates to poly(ethylene alt-maleic anhydride).

PEMA form amide bonds with the primary amines of the substrates (Figure 2.2C). This reaction follows a nucleophilic addition-elimination mechanism.

2.4.2 Immunoassay functionalization

PEMA-PAAM was used for all immunoassay experiments to covalently couple the free amines of the interleukin-6 (IL-6), sex hormone-binding globulin (SHBG), and insulin-like growth factor-binding protein 4 (IBP4) antibodies to the silicon dioxide surface via the anhydride groups. Unbound anhydride groups were blocked by adding an excess of BSA. The sample (in buffer or serum) containing the protein of interest was added with a non-ionic surfactant (Tween-20) to facilitate binding to the surface-immobilized antibodies and minimize nonspecific interactions. The analyte was detected by adding a biotinylated antigen-specific antibody, followed by streptavidin-coated MNPs. The MNPs bind to the detection antibodies via a biotin-streptavidin interaction, leading to a change in the local magnetic field proportional to the analyte concentration. With 80 sensors available on each array, multiplex detection of IL-6, SHBG, and IBP4, in addition to positive and negative controls, is possible.

UV-ozone and oxygen plasma treatments have been used to create conditions conducive to coupling antibodies to the surface of the sensor arrays. However, prior experiments have shown that UV-ozone is preferable because oxygen plasma can damage the sensor (Figure 2.3). We optimized other conditions promoting antibody coupling, such as the PEMA concentration, temperature, and filtration pore size (Figure 2.4). We designed a simple assay consisting of a linker molecule (PEG with an amine group on one end and biotin on the other) to quantify the change in magnetoresistance (ΔMR) upon binding of streptavidin-coated MNPs. The best response (signal amplitude relative to standard deviation) was for 1.5% PEMA, 170°C, and a 0.22 μm filter. These conditions were used for all subsequent assays.

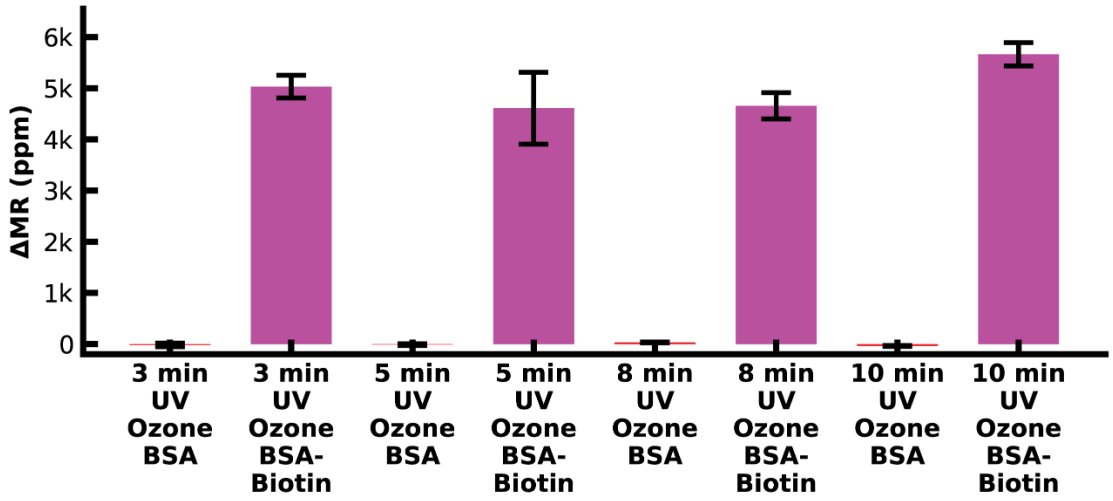

Figure 2.3: UV ozone times for PEMA-PAAM surface chemistry. Positive (magenta) and negative (red) control values for UV Ozone times explored.

2.4.3 Hydrolase activity assays

The feasibility of using the GMR sensor platform to measure hydrolase activity hinges upon optimizing surface chemistry to ensure robustness and adaptability. This is crucial as instability of the immobilized substrate can affect the measurement of enzymatic activity and the sensor's ability to be assembled and stored for use in a point-of-care setting. Using the PEMA-PAAM surface chemistry approach, we coupled an amine-PEG_{11}-biotin linker molecule to a GMR surface via an amine reaction with maleic anhydride (Figure 2.5A). Upon addition of streptavidin-coated MNPs, an average increase in resistance of 5,380 ppm was quantified on the 2 sensors containing amine-PEG_{11}-biotin, while sensors that lacked this molecule had an average increase in resistance of 304 ppm, revealing that the biotin groups on the PEG linker are responsible for binding to the MNPs (Figure 2.5B). Following extensive washing with PBS, we obtained no noticeable reduction in signal, indicating that the MNPs are tightly bound to the sensor surface.

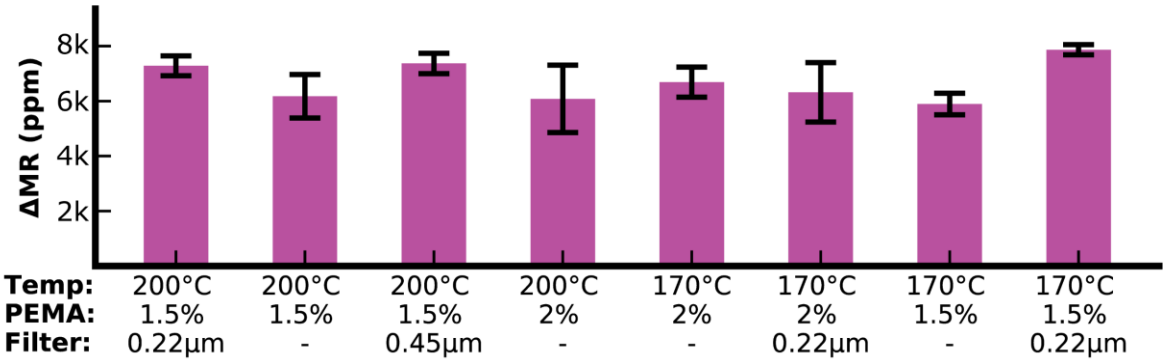

Figure 2.4: Magnetic assay optimization. Optimization of surface chemistry parameters with positive control (amine-PEG_{11}-biotin).

The functionalized sensor chip was stored at 4°C for 21 days to evaluate the long-term stability and then placed back in the GMR readout station. We then performed extensive washing steps using a range of buffer conditions to determine if the signal decreased. Little change (<5%) in resistance was quantified in excess biotin, revealing that PEG_{11}-biotin was tightly bound to streptavidin-MNP and could not be competed off. Sequentially adding an increasing concentration of NaCl or changing the temperature from 22°C (room temperature) to 4°C did not alter the signal more than 5% of the saturated signal after MNP addition. When the temperature was changed from 4°C to 50°C, the signal increased by 9.6% of the saturated signal after MNP addition. The sensor was then washed with reagents buffered at various pH values. Changing the pH from neutral to pH 3 increased the signal by 4.9%, then decreased by 15.2% when the buffer was changed back to pH 7. Increasing the pH further to pH 9.0 has little effect on the signal (<5%). However, adding pH 13.5 buffer reduced the signal by 4,970 ppm, corresponding to a 92.5% reduction of the saturated signal after MNP addition (Figure 2.5C). By monitoring the real-time chemical release of MNPs under extreme alkaline conditions, we showed that the signal decreased rapidly within 3 min and then stabilized (Figure 2.5D). These data revealed that the sensor chip stored at 4°C for 21 days retained the PEG_{11} linker sequence and the streptavidin-coated MNPs and that this

complex was only broken by treatment with a strong alkaline solution. From these studies, it was unclear if the decrease in signal was due to the breakage of the amine-maleic anhydride bond or the streptavidin–biotin bond. To determine if the signal reduction was due to the release of the streptavidin–biotin, a reaction was set up whereby the linker-MNP complex was treated with a pH 13.5 solution, washed with PBS at neutral pH, and then incubated with fresh streptavidin-MNPs. The resistance signal decreased by nearly 75% upon treatment with pH 13.5 but then increased to 97% of its original signal upon adding fresh MNPs (Figure 2.6). These studies reveal that the amine–maleic anhydride bond is stable in extreme alkaline conditions, but the biotin–streptavidin bond is broken, most likely due to the denaturation of streptavidin. The stability of the substrate-MNP complex on the sensor surface is compatible with the buffer conditions needed for hydrolase

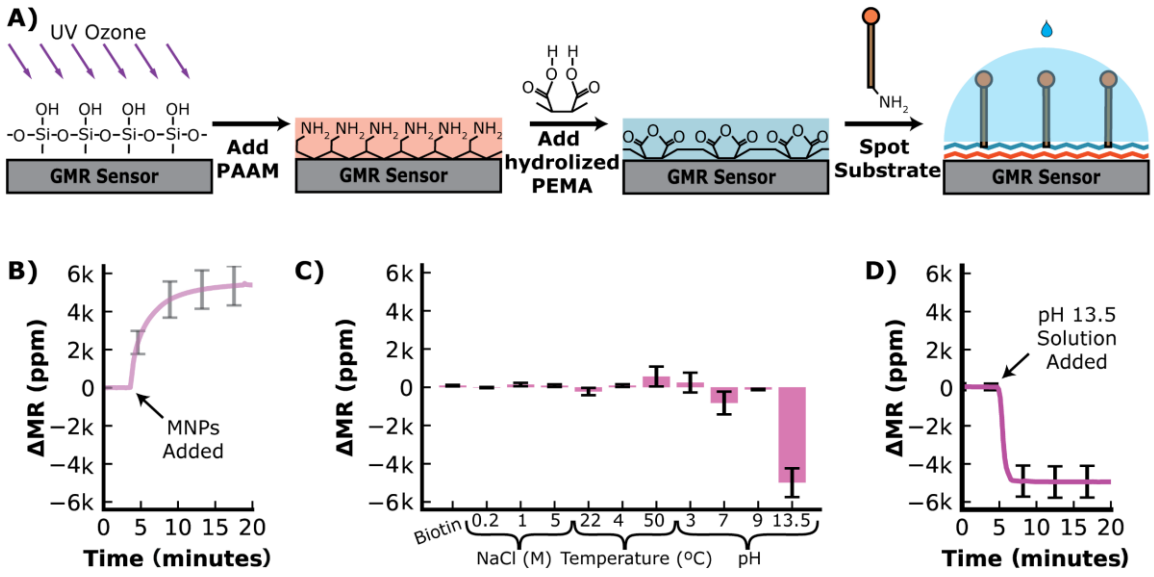

Figure 2.5: Sensor functionalization and stability of the substrate. (A) The sensor surface is cleaned and activated by ultraviolet-ozone treatment before poly (allylamine) (PAAM) is added. The hydrolyzed poly (ethylene-alt-maleic anhydride) (PEMA) is added to create a layer of maleic groups. When the amine-containing substrate is spotted on the sensor surface, the maleic groups form a covalent bond with the amines on the substrate. (B) Time-dependent loading of streptavidin-MNP onto a sensor surface containing PEG_{11}-biotin. (C) Change in magnetoresistance for a fully assembled PEG_{11}-MNP complex that was stored for 21 days at 4°C and then sequentially incubated at various conditions. The change is recorded from one condition to the next. (D) Time-dependent decrease in signal in the presence of an extremely basic reagent (pH 13.5).

activity assays, as there are no documented human enzymes that require extreme alkaline conditions to be functional.

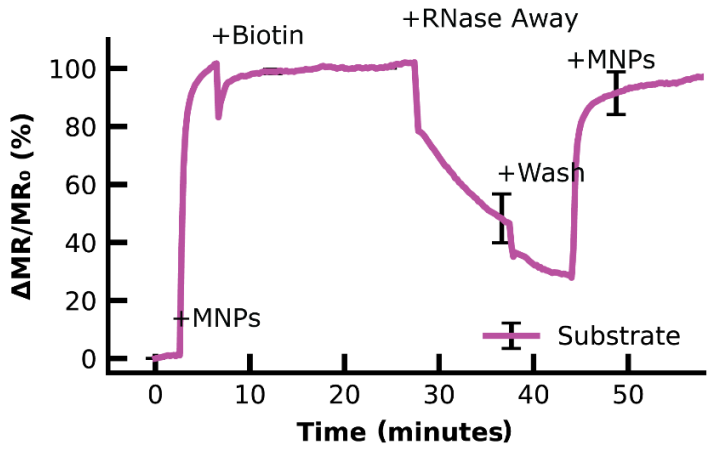

Figure 2.6: Signal reduction and restoration. Demonstration of the loss of substrate signal due the addition of pH 13.5 solution, but the restoration of that signal after washing and the addition of MNPs.

Acknowledgements

Chapter 2, in part, is a reprint of the journal article "A GMR Enzymatic Assay for Quantifying Nuclease and Peptidase Activity" as it appears in *Frontiers in Bioengineering and Biotechnology* by Michael Sveiven, Ana Serrano, Joshua Rosenberg, Doug Conrad, Drew A. Hall, and Anthony J. O'Donoghue, Mar 2024. In addition, Chapter 2, in part, is a reprint of the journal article "A Dual-Binding, Magnetic Immunoassay to Predict Spontaneous Preterm Birth" as it appears in *Frontiers in Bioengineering and Biotechnology* by Michael Sveiven, Andrew Gassman, Joshua Rosenberg, Jay Boniface, Matthew Chan, Anthony J. O'Donoghue, Louise Laurent, and Drew A. Hall, Sep 2023. The dissertation author was the first author of these papers.

CHAPTER 3: MAGNETIC IMMUNOASSAYS

3.1 Overview

The average length of human gestation is approximately 40 weeks, and birth is considered preterm before 37 weeks. Globally, preterm births affect 15 million infants annually and are strongly associated with adverse postnatal outcomes, such as developmental and intellectual disabilities, including cerebral palsy, attention deficit hyperactivity disorder, depression, and anxiety (Liu et al., 2012; Luu et al., 2017). Preterm birth is also associated with long-term pulmonary complications, such as asthma and bronchopulmonary dysplasia. In addition, preterm birth increases the risk of diabetes, dental problems, hearing loss, and infections (Boyle et al., 2017; Li et al., 2014; Parkinson et al., 2013; Saigal and Doyle, 2008). The UN Inter-agency Group for Child Mortality Estimation reported in 2019 that preterm births caused 35% of global neonatal deaths. About 1 in 10 babies in the United States are born preterm, at an estimated $25 billion cost to the healthcare system annually (Waitzman et al., 2021). The earlier the birth, the more serious the health and financial consequences are, indicating that prolonging pregnancies would yield important gains (Petrou et al., 2019; Waitzman et al., 2021).

Currently, the treatment of preterm labor is largely reactive, with tocolytics, antenatal corticosteroids, and magnesium sulfate being offered to pregnant individuals with signs or symptoms of preterm labor (Conde-Agudelo et al., 2018; Haghighi et al., 2017). Antenatal corticosteroids, such as betamethasone and dexamethasone, are administered to pregnant women at high risk of delivery within the subsequent 2 weeks to accelerate infant lung development and prevent perinatal complications, such as respiratory distress syndrome, intraventricular hemorrhage, and necrotizing enterocolitis (Autran et al., 2018; Conde-Agudelo et al., 2018). Magnesium sulfate administered shortly before early preterm birth (prior to 34 weeks gestational

age) decreases the risk of cerebral palsy (Costantine and Weiner, 2009; Doyle et al., 2009). Tocolytics such as beta-adrenergic receptor agonists, calcium channel blockers, and nonsteroidal anti-inflammatory drugs can delay labor—but only for a few days; fortunately, this delay is often sufficient for the administration of antenatal corticosteroids and magnesium sulfate (Flenady et al., 2014; Haas et al., 2012; Wilson et al., 2022).

For pregnant individuals with an elevated risk of preterm birth due to a history of preterm birth or an ultrasound finding of a short cervix, weekly intramuscular treatments with 17-hydroxyprogesterone or daily treatments with vaginal progesterone are initiated between 16–24 weeks gestational age (GA). These treatments have been shown to prevent preterm birth, although their efficacy across different categories of at-risk individuals has been debated (Akinwunmi and Ming, 2022; Boelig et al., 2022; Conde-Agudelo and Romero, 2022; Fonseca et al., 2007; Lin and Nie, 2022; Meis et al., 2003; Nelson et al., 2022). Alternatively, care management, which encompasses coordinated care aimed at providing a more comprehensive and supportive environment, may improve the environmental, behavioral, social, and psychological factors contributing to the risk of preterm birth (Garite and Manuck, 2022). Unfortunately, nearly 70% of spontaneous preterm births (sPTBs) occur in first pregnancies or in pregnancies where the mothers have no history of preterm birth, and for these individuals, progesterone or monitoring of cervical length is not offered (Goldenberg et al., 2008). Thus, accurate and feasible risk assessment for sPTB has the potential to enable personalized clinical management with improved outcomes.

Diagnostic tools for monitoring pregnancy today are broadly classified into imaging and biomolecular tests. Serial transvaginal ultrasound measurement of cervical length is commonly used in pregnancies at high risk for sPTB, and a mid-trimester ultrasound screening of cervical length either transabdominally or transvaginally is routinely performed (Booker et al., 2021;

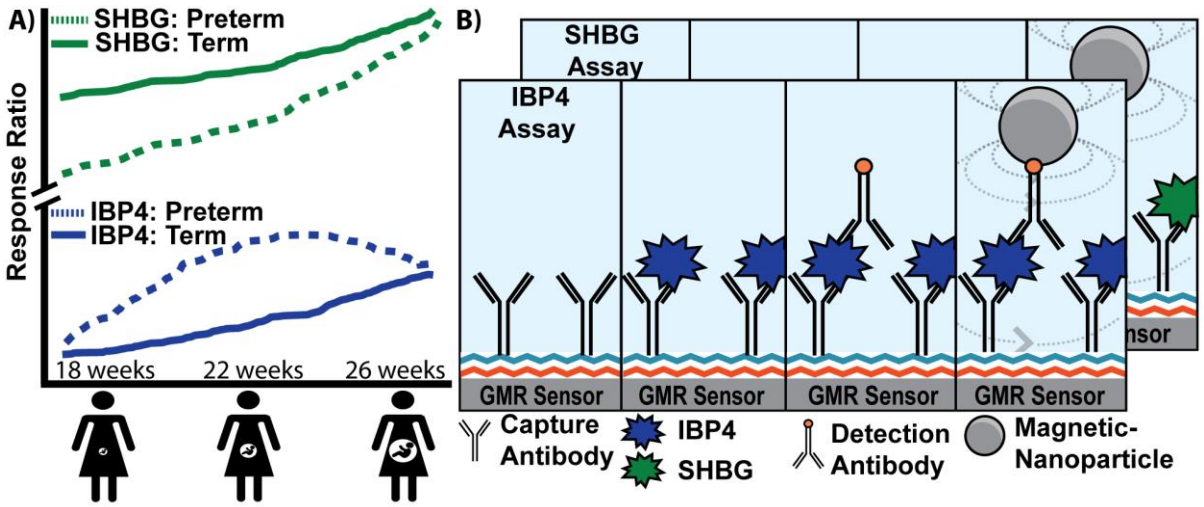

Figure 3.1: Magnetic immunoassay to identify pregnant women at high risk of preterm birth. (A) Illustration showing the increase of two proteins, SHBG and IBP4, in serum as pregnancy progresses. Women at high risk of preterm birth have abnormal levels of SHBG and IBP4 at different stages in the pregnancy where a proteomic score can be derived from the ratio of these proteins. (B) Magnetic immunoassay to quantify SHBG and IBP4 using a capture antibody bound to the sensor surface and a detection antibody that recruits magnetic nanoparticles (MNPs) close to the surface. The recruited MNPs perturb the local magnetic field, which is read out using the underlying giant magnetoresistive sensors. The IBP4 and SHBG immunoassays differ only by the antibody and analyte used, and therefore, the individual steps of the SHBG assay have been hidden to avoid redundancy in the image.

Orzechowski et al., 2016). Serum biomarkers are used to evaluate ectopic and other nonviable pregnancies in the first trimester and to perform screening for open neural tube defects and fetal aneuploidy (PAPP-A, bHCG, AFP, Inhibin-A, and estriol) (Betz and Fane, 2022; Biggio et al., 2004; Brock et al., 1975; Xu et al., 2020). Fetal fibronectin found in cervicovaginal fluid is associated with preterm birth (Lockwood et al., 1991) with tests performed on vaginal swab specimens from gravidas at high risk of preterm delivery between 24–36 weeks GA to assess the risk of delivery within the following 1–2 weeks (Peaceman et al., 1997; Swamy et al., 2005). However, the utility of fetal fibronectin is limited by its poor positive predictive value of 17%–30% and the lack of evidence of its utility in improving clinical outcomes (Son and Miller, 2017; Swamy et al., 2005). Recently, proteomics has been used to predict complex diseases and

outcomes. Sex hormone-binding globulin (SHBG) and insulin-like growth factor-binding protein 4 (IBP4) were identified as biomarkers for mothers at risk of sPTB (Bradford et al., 2017; Saade et al., 2016). Both proteins increase throughout pregnancy, but the trajectories diverge in pregnancies destined for preterm vs. term delivery (Figure 3.1A) (Kearney et al., 2018). Throughout pregnancy, SHBG increases 5- to 10-fold in human serum (Anderson, 1974; O'Leary et al., 1991), and its function is to bind hormones (e.g., testosterone and oestradiol) to quench their activities. Insulin-like growth factor (IGF) is a hormone that stimulates body growth and development by acting on metabolic organs, including the liver, bone, and skeletal muscle. IBP4 regulates IGF activity through binding. In addition, IBP4 was previously identified as a biomarker for fetal growth restriction (Qiu et al., 2012).

From mass spectrometry assays, the algorithmic determination of sPTB risk using the combination of IBP4/SHBG biomarker abundance and clinical factors was found to have a high predictive value (Burchard et al., 2021; Saade et al., 2016). In pregnancies that subsequently deliver preterm, serum abundance of IBP4 is higher than normal, and SHBG levels are lower than normal between 18 and 22 weeks. A proteomic score combining the IBP4 and SHBG response ratios (the mass spectrometry response to an unknown sample divided by the response of a calibrant) can predict sPTB (Burchard et al., 2021). Mass spectrometry-based quantitation of SHBG and IBP4 is ideal for biomarker discovery and has successfully been extended to the clinic (Kearney et al., 2018), but it is not currently suitable in a point-of-care setting. Immunoassays are better suited for the rapid turnaround time of clinical samples. Two common immunoassay formats are the enzyme-linked immunosorbent assay (ELISA) and electrochemiluminescence immunoassay (ECLIA) (Crowther, 2008; Richter, 2004). ELISA uses an enzyme to convert substrate into a colorimetric or fluorogenic product. ECLIA uses electrodes to induce a

luminophore into an excited state where it will emit light. Both assay formats require plate readers to capture the signal change. Thus, these tests require maternal blood samples to be sent off for processing and analysis. Processing requires expensive, highly specialized equipment and technical expertise exclusive to advanced laboratories. The optimal GA window to use SHBG and IBP4 for sPTB risk assessment is in gestation weeks 18–20. Decreasing the turnaround time may allow patients and clinicians to act sooner with interventional strategies. For example, the recommended GA window for initiating progesterone to prevent preterm birth is 16–24 weeks, and other interventional strategies, such as case management (Garite and Manuck, 2022), may benefit from early initiation. Moreover, failure to appropriately follow up results occurs in 7%–62% of laboratory tests (Callen et al., 2012; Casalino et al., 2009; Norwitz and Caughey, 2011). Test effectiveness may be improved to the extent that test result generation in a point-of-care setting can be coupled with better follow-up.

Recently, there has been a dramatic shift toward decentralizing diagnostic tests, making health information rapidly available to a patient's healthcare provider (Arshavsky-Graham and Segal, 2022; J. H.-K. Chen et al., 2020; Gong et al., 2019; Kumar et al., 2020; Mahmoudi et al., 2020). This adoption was further accelerated by the COVID-19 pandemic, where at-home testing became common. Point-of-care testing (POCT) brings the power of centralized labs directly to the patient, permitting testing in a healthcare office, at work, or at home. POCT for pregnant women may enable obstetricians to intervene quickly if a mother is at high risk for preterm birth. However, many POCT assay formats today (i.e., lateral flow immunoassays) only test a single analyte and are not quantitative, preventing their use for this type of bivariate assay. Other POCT formats include electrochemical and optical (Cao et al., 2020; Y.-T. Chen et al., 2020; Zhang et al., 2020). Magnetic sensors are particularly attractive for this application as they can be arrayed for multiplex

detection, are already miniaturized, and are highly sensitive (Klein et al., 2019; Krishna et al., 2016; Osterfeld et al., 2008; S. Gaster et al., 2011). Giant magnetoresistive (GMR) sensors are thin-film proximity-based magnetic sensors where the local magnetic field is transduced into resistance change through a quantum mechanical effect (Barnaś et al., 1990; Osterfeld et al., 2008; Prinz, 1998; Wolf et al., 2001). As biological samples (e.g., urine, saliva, serum, etc.) lack a magnetic background, this readout format is agnostic to the sample matrix, which greatly simplifies the sample preparation, which is often just dilution (Gaster et al., 2009). This constellation of properties may make magnetic sensors ideal for monitoring pregnant women in a point-of-use setting as they progress throughout their pregnancies.

In this study, we developed an immunoassay to quantify SHBG and IBP4 in serum samples that is amenable to point-of-care testing, thereby allowing the quantification of selected biomarkers clinically relevant to sPTB. Figure 3.1B illustrates the two assays where capture antibodies are immobilized on the sensor surface. When the maternal serum sample is added, the target analytes (IBP4 and SHBG) bind to their respective capture antibodies. Biotinylated detection antibodies are added and bind to the antigen forming a sandwich assay. The addition of streptavidin-coated magnetic nanoparticles (MNPs) results in binding to the detection antibodies quantitatively readout using the underlying GMR sensors. The change in magnetic signal during the assay is proportional to the target biomarker's concentration in the serum sample. The GMR immunoassays quantify SHBG and IBP4 with sufficient sensitivity and accuracy in blood serum with a high degree of correlation to the proteins measured from a centralized laboratory assay based on mass spectrometry. Capable of being run in a point-of-care setting with minimal training required, the assay could provide obstetricians with a powerful tool to predict spontaneous preterm births and intervene when necessary.

3.2 Materials and methods

3.2.1 Materials

Tween-20 (#P9416) and human serum (#H6914) were purchased from Sigma-Aldrich. Bovine serum albumin (BSA; #37525) was procured from Thermo-Scientific. Streptavidin-coated magnetic nanoparticles (#130-048-101) were acquired from Miltenyi Biotec. Tris-buffered saline (TBS, 10×) pH 7.4 (#J60764.K2) was purchased from Fisher Scientific (#BP300-100). Lauryl Maltose Neopentyl Glycol (#NG310) was bought from Anatrace. Phosphate-Buffered Saline (10×) pH 7.4, RNase-free (#AM9625), Pierce Bovine Serum Albumin, Biotinylated (#29130), and EZ-Link AminePEG_{11}-Biotin (#26136) were procured through Thermo Fisher. Magnetic polyvinyl alcohol beads (#CMG-216) were procured through Perkin Elmer. Mouse Anti-Mouse IgD (#BDB553509) was obtained from Thermo Fisher. Betaine, 5M solution, molecular biology grade, Ultrapure (#AAJ77507AB) was acquired from Fisher Scientific. 2,3-Butanediol (#MFCD00004523) was obtained from Sigma Aldrich. Ethylene Glycol (#E178-500) was ordered from Fisher Chemical. Protein, Recombinant Human IL-6 (#206IL010), Polyclonal Primary Biotin (#BAF206), and Human/Primate IL-6 Antibody (MAB206) was acquired from R&D Systems. Sera Prognostics provided SHBG and IBP4 antigens, monoclonal capture and detection antibodies against IBP4 and SHBG (Table 3.1), and serum samples pooled from multiple unidentified female donors.

Table 3.1: Antibody properties.

	Host	K_a [$M^{-1}s^{-1}$]	K_d [s^{-1}]	K_D [nM]
IBP4 Capture #2	Mouse	9.03E+04	9.21E-04	10.2
IBP4 Detection #1	Mouse	3.80E+04	6.00E-04	15
SHBG Capture #1	Mouse	6.35E+04	1.50E-04	2.36
SHBG Detection #2	Mouse	4.54E+05	1.50E-04	0.33

3.2.2 Methods

GMR sensor arrays: GMR SV sensor arrays were purchased from MagArray, Inc. (#BZ0078). Each GMR SV sensor array has 80 sensors arranged in an 8 × 10 matrix where each sensor is 120 × 120 μm2 on a 280 μm pitch with a nominal resistance (R0) of 1464 Ω and a mean magnetoresistance (MR) ratio of 7.99% (Figure 3.2). Each one of the 80 sensors can be independently addressed. A custom holder was fabricated from Teflon to create a 100 μL reaction well with an o-ring on top of the sensor array. GMR reader The measurement setup consists of a computer, a power amplifier, a Helmholtz coil, and custom readout electronics, as shown in Figure 3.3A (Hall et al., 2010a). A double modulation readout scheme was used to reject 1/f noise from the sensors and electronics, and a temperature compensation technique was used to reduce the temperature drift (Hall et al., 2010b). The computer digitally adjusted the frequencies and amplitudes of sensor bias voltage and magnetic field through a National Instruments data acquisition card (PCIe-6351) and a LabVIEW graphical user interface. Specifically, the power amplifier controlled by the computer provides current to the Helmholtz coil, which creates a homogenous magnetic field (23—34 Oerms based on the sensor MR) for the sensor array. The readout electronics contain 8× transimpedance amplifiers to convert the currents to voltages that

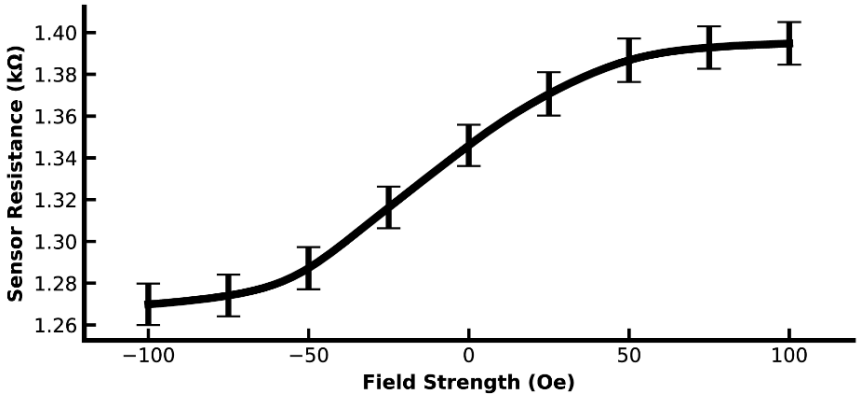

Figure 3.2: GMR SV transfer curve. Measured resistance versus magnetic field applied for GMR SV sensor.

were quantized by the acquisition card. Time-multiplexing was applied to read the 8 × 10 sensor array with a 10 s update rate. The measured signal is the change in MR from the initial MR in parts-per-million (ppm).

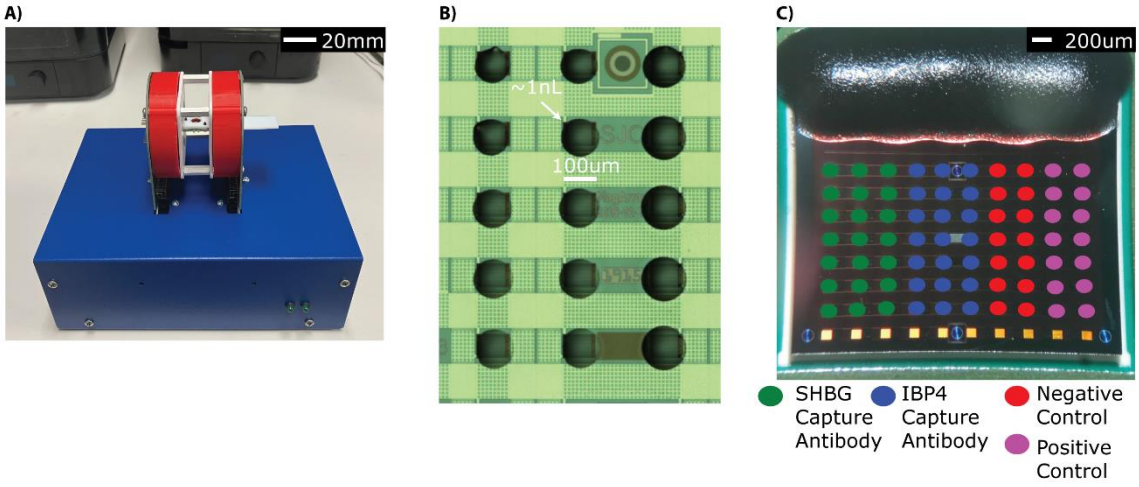

Figure 3.3: GMR reader. (A) Photograph of GMR SV reader station with a sensor inside the Helmholtz coil. (B) Photograph of the GMR SV sensor array with sensors spotted with reagents. (C) Photograph of the GMR SV sensor array with 80 sensors arranged in an 8×10 matrix where each sensor is 120×120 µm2 on a 280 µm pitch with an example spotting map.

Antibody biotinylation: Sulfo-NHS-LC Biotin with a 22.4-Å spacer (Thermo Scientific, #A39257) was diluted in ultrapure water and added at a 20:1 ratio of label to purified detection antibodies diluted in PBS pH 7.4. The conjugation was incubated for 2 h on ice. Unincorporated biotin was removed using a desalting spin column with a 7 kDa molecular weight cut-off (Thermo Scientific, #89882).

Antibody spotting: Individual sensors were spotted with capture antibodies using an iTWO-300P automated spotter (axiVEND, Florida). Twenty droplets of ~100 pL were spotted on each sensor to cover the sensor surface (Figure 3.3B). A printing buffer (1 M Betaine and 12.5% 2,3- Butanediol in PBS) is needed for the IBP4 capture antibodies. IBP4 capture antibody was spotted on each sensor by transferring 100 pL twice from a stock of 0.34 mg/mL. The SHBG

capture antibody is spotted in 10% glycol in PBS at 0.125 mg/mL. In general, 16 sensors are spotted with the capture antibodies, while the remaining sensors are spotted with either 1% BSA (a negative control to monitor for nonspecific MNP binding), 0.1 mg/mL IL-6 capture antibody (a negative control for nonspecific antibody interactions), and 1 mg/mL BSA-Biotin (a positive control for biotin-streptavidin interactions), or an amine-PEG-Biotin substrate (another positive control for biotin-streptavidin interactions), as shown in Figure 3.3C. After spotting, the automated spotter chamber is brought to 70% humidity for 1 h then the sensors are left to incubate overnight in the chamber.

Magnetic immunoassay: The sensor array is placed in a Teflon holder with silicon o-rings. Then the sensors are washed with 600 µL of Buffer 1 (0.1% BSA, 0.1% Tween-20 in 1 × PBS) and blocked for 30 min using 5% BSA in PBS. Following an additional wash with 600 µL of Buffer 1, the sample containing antigen is diluted in Buffer 1 and then added to the sensors for 1 h. The sensors are washed 5 × with 600 µL of Buffer 1. Biotinylated detection antibodies are diluted in PBS to 10 µg/mL, and 100 µL is added to the sensors for 1 h. Then, the sensors are washed 3 × with 600 µL of Buffer 1 and submerged in 100 µL PBS. The sensor array is placed into the magnetic reading station, and 50 µL of magnetic nanoparticles are added to the reaction well.

Dual-binding magnetic immunoassay: The assay is similar to the magnetic immunoassay described above, but additional steps are added at the end. After the MNPs have reached binding equilibrium with the detection antibodies (~30 min), the unbound MNPs are washed away, and 10 mM free biotin is added for 15 min before being washed away with 600 µL of Buffer 1. Then 50 µL of 10 nM SHBG is added and incubated for 40 min with 20 µL of 75 µg/mL detection antibody for the last 20 min. The well is then washed with 600 µL of Buffer 1

before 25 µL of MNPs are added for 20 min for an additional binding curve. The normalization ratio is calculated by dividing the first curve's saturation value by the second curve's saturation value on a sensor-by-sensor basis.

Anti-mouse assay: After antibody spotting and overnight incubation, the surface is blocked with 30 min of 100 µL at 5% BSA. Subsequently, 100 µL at 10 µg/mL of anti-mouse detection antibodies are incubated for 1 h. Then, the detection antibodies are washed away before PBS is added. The assay is then run with 50 µL of MNPs, and the change in magnetic resistance is quantified after signal saturation.

Mass spectrometry (MS) assay: Pools of serum samples were generated to span low to high levels of IBP4 and SHBG, respectively (10 pools total). After pooling the individual samples, aliquots were analyzed according to the standard operating procedure. Briefly, pooled serum (50 µL) was immunodepleted of the top fourteen most abundant plasma proteins (Agilent Technologies, #MARS14). Depleted serum was digested with trypsin, spiked with purified stable isotype standard (SIS) peptides, and desalted. Peptides were separated by reverse-phase liquid chromatography and analyzed by multiple reactions monitoring mass spectrometry, with IBP4 and SHBG measured in each of the ten pools. Two relative peptide amounts were quantified as the response ratio (RR) of the endogenous peak area divided by the SIS peak area. Proteomic scores were calculated as the ln (RRIBP4/ RRSHBG).

Depleted serum: Pooled serum (1 mL) from female donors was diluted 1:4 in TBS with 0.05% Lauryl Maltose Neopentyl Glycol and mixed with magnetic polyvinyl alcohol beads coupled with anti-IBP4 antibody (6 mg) and anti-SHBG antibody (10 mg). The diluted serum was rotated with beads for 75 min at room temperature, and the depleted serum was removed. This

serum was then subjected to a second depletion by the same procedure, resulting in a protein concentration of 16.5 mg/mL and the removal of ~95% of the detectable IBP4 and SHBG proteins.

Statistical analysis: All data shown are the mean values with one median absolute deviation as error bars. The limit of blank (LOB) is calculated as 1.645 × the standard deviation of the blank plus the mean of the blank, whereas the limit of detection (LOD) is defined as the LOB plus 1.645 × the standard deviation of the lowest concentration sample (Armbruster and Pry, 2008). The concentration corresponding to the LOD is calculated using the four-parameter logistic (4-PL) coefficients (Table 3.2). 4-PL curve fitting was performed using NumPy (v1.18.5) in Python (v3.8) with least squares optimization on the spiked samples in the calibration curve, and the fit parameters were used to back-calculate the concentration of unknown samples. Statistical analysis (Pearson's coefficient and Deming analysis) was done with NumPy (v1.18.5) and SciPy (v1.6.0) in Python (v3.8). Receiver operator characteristic (ROC) curves were calculated using scikit-learn (v1.0.2) in Python (v3.8).

Table 3.2: Four-parameter logistic curve fitting parameters.

$$f(x) = \frac{a - d}{1 + \left(\frac{x}{c}\right)^b} + d$$

	a	*b*	*c*	*d*
IBP4 in Buffer	0.88	1.09	5.45	230
IBP4 in Serum	2.93	1.23	6.34	209
SHBG in Buffer	181	-1.11	0.57	3.99
SHBG in Serum	0.87	-0.80	1.02	0.069

3.3 Interleukin-6 assay

To optimize the magnetic immunoassay without using the limited SHBG and IBP4 antibody reserves, an assay for human Interleukin-6 (IL-6) was developed using commercially available IL-6 antibodies. Once the IL-6 assay performed well, the magnetic immunoassay could be adapted for SHBG and IBP4 quantitation. Biological experiments were conducted to validate

the system performance. Sensors were functionalized with biotinylated-bovine serum albumin (Biotin-BSA) for use as a positive control, a captured antibody for human IL-6, a cancer biomarker, and BSA for use as a negative control to monitor non-specific binding. The reference sensor was covered by epoxy, preventing it from sensing signal from the MNPs. To functionalize the sensor surface with the BSA or IL-6 antibodies, chips were washed with acetone, methanol, and IPA. After 5 minutes of cleaning with oxygen plasma, 1% Poly(allylamine) in distilled water (DIW) was added for another 5 minutes. After baking for 1 hour at 110 °C, 2% aqueous Poly(ethylene-alt-maleic anhydride) in DIW was added to the chips for 5 minutes. Finally, the chips were baked for 1 hour at 160 °C. Capture reagents were spotted on the sensors and incubated at 4 °C overnight.

Figure 3.4a shows overlaid transient measurement results for the negative control, positive control, and various concentrations of IL-6. In each assay, the sensors were washed with phosphate-buffered saline (PBS) 1 minute after starting, and MNPs (Streptavidin microbeads, catalog number #130-048-101, Miltenyi Biotec) were added afterward. The system continuously measured the real-time binding curves in the high gain mode. After the binding curves saturated, a washing step was performed to remove any non-specific binding. Multiple experiments showed that the signal after washing did not drop, indicating that the binding was highly specific. The averages of each measurement (n = 6 sensors) are compiled to obtain the calibration curve shown in Figure 3.4b. The resulting data is fit with a 4-parameter logistical (4-PL) regression with an R^2 value of 0.986. The LOD, calculated based on (Armbruster and Pry, 2008), is 0.96 pM.

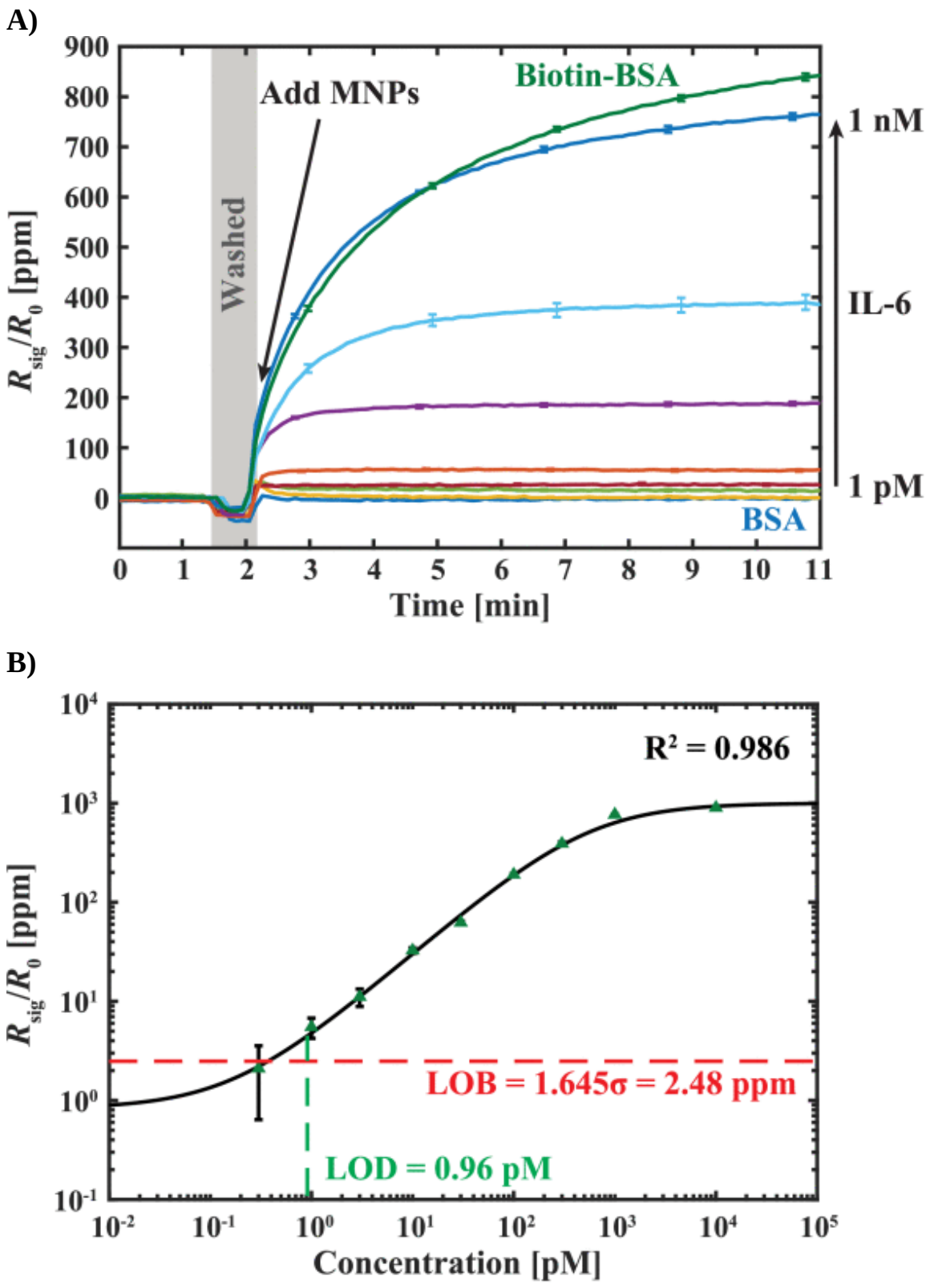

Figure 3.4: IL-6 Assay. (a) Measured binding curves for negative control (BSA), positive control (Biotin-BSA), and IL-6 at different concentrations; (b) IL-6 calibration curve.

3.4 Antibody immobilization and assay optimization

To quantify the loading of the mouse capture antibodies to the sensor surface, we utilized biotinylated anti-mouse antibodies that directly bind to the capture antibodies and compared the binding to a positive control sensor that was functionalized with biotinylated BSA (Figure 3.5A). Based on proximity-based detection, GMR sensors are primarily influenced by magnetic nanoparticles close to the sensor surface (Osterfeld et al., 2008). Antibodies (~8.4—13.7 nm, depending on the orientation) are larger than biotinylated BSA (~7 nm); thus, we expected that the MNPs bound by the antibodies would be further away from the sensor surface than in the BSA assay, resulting in a lower signal (Tan et al., 2008; Yohannes et al., 2010). We found that the signal for each antibody was between 4.7 k and 5 k ppm, while the biotinylated BSA was 6.2 k ppm. These measurements demonstrated that the capture antibodies were anchored to the surface with sufficient density.

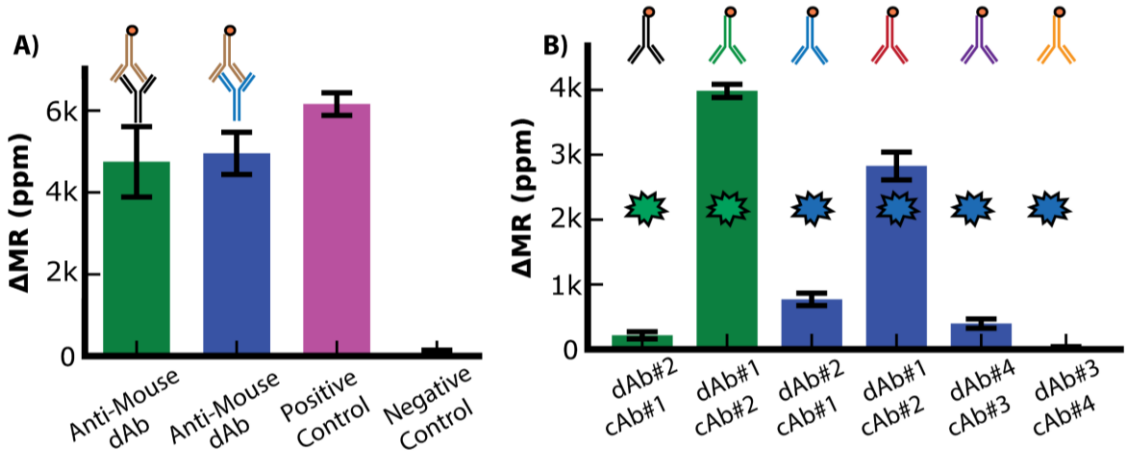

Figure 3.5: Assay optimization. (A) Anti-Mouse assay (10 µg/ mL biotinylated anti-mouse antibody) to analyze the surface density of capture antibodies with positive control (1 mg/mL biotinylated BSA), negative control (1% BSA), SHBG capture antibody (green bar), and IBP4 capture antibody (blue bar). (B) Antibody configuration optimization. The two green bars show the signal when the two SHBG antibodies (0.125 mg/mL) are used in both permutations for capture and detection antibodies (dAb). The blue bars show the signal when the two pairs of IBP4 antibodies (0.34 mg/mL) are run in each permutation.

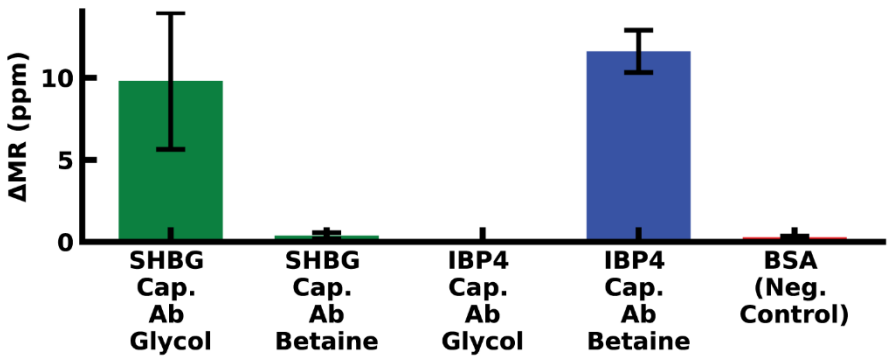

Figure 3.6: SHBG and IBP4 capture antibodies in printing buffers. 2 nM SHBG assay and 2.5 nM IBP4 assay with glycol printing buffer and betaine printing buffer.

Next, we optimized the antibody orientation (i.e., capture vs. detection and pairing) from the limited antibodies available. Immunoassays were run using all shown paired permutations of capture and detection antibodies with a fixed target analyte concentration of 10 nM in PBS with 0.1% BSA as a carrier protein. With anti-SHBG#1 as the capture antibody (cAb#1) and anti-SHBG#2 as the detection antibody (dAb#2), we measured a signal of 210 ± 50 ppm (Figure 3.5B). However, when these antibodies were set up in the reverse orientation (cAb#2 with dAb#1), the signal increased by 18.5-fold to 3.9 k ± 100 ppm, demonstrating the importance of this optimization experiment. The same experiment was performed for IBP4, where we found that anti-IBP4#4 as the capture antibody (cAb#4) and anti-IBP4#3 as the detection antibody (dAb#3) had the lowest signal (30 ± 10 ppm) while anti-IBP4#2 as the capture antibody (cAb#2) and anti-IBP4#1 as the detection antibody (dAb#1) had the highest signal of 2.8 k ± 200 ppm. We used these antibody combinations for all subsequent assays. While increasing the concentration of the detection antibodies above 20 μg/mL led to a small signal increase, the increase was not worth the cost of using twice the amount of detection antibodies per assay, so the detection antibody concentration was set at 10 μg/mL. In addition, the number of times the SHBG antibodies are run through the biotinylation protocol led to changes in signal when the reagents were bound directly

to the sensor surface, indicating that excess biotinylation prevents functionalization of the antibodies to the sensor surface, while insufficient biotinylation led to a decrease in MNP binding.

The sensors were spotted with an automated robotic spotter to reduce the sensor-to-sensor variation due to liquid handling. Each of the 120 × 120 μm2 sensors is covered by individual droplets (Figure 3.3B,C), eliminating edge effects (e.g., coffee ring) when manually spotting (which is limited to droplets covering 4-6 sensors). The antibody concentration was kept lower than 1 mg/mL, and a printing buffer was necessary to ensure accuracy and consistency in droplet volume. These buffers prevent the protein from binding to the spotter tip and preserve the reagent in solution on the sensor surface longer, prolonging the amine coupling time. Since the surface chemistry forms a covalent bond between anhydride groups and free amines (found in amino acids like lysine distributed throughout the antibodies), the orientation of the antibody on the surface is unpredictable. Some printing buffers can facilitate the orientation of antibodies, allowing for increased interactions between the epitopes of the antibodies and antigen in solution. The ability to spot individual sensors allows the capture antibody concentration and printing buffer to be optimized using a single sensor array. After a study exploring several printing buffers, it was found that 1 M Betaine and 12.5% 2,3-Butanediol in PBS for IBP4 capture antibodies and 10% ethylene-glycol in PBS for SHBG capture antibodies performed the best (Figure 3.6). The sensor array was spotted with a lower protein concentration multiple times to maintain the surface area of the spotted reagent while increasing the concentration.

3.4 Insulin-like growth factor-binding protein 4 assay

We then generated calibration curves by diluting IBP4 into PBS or spiking it into pooled human serum from pregnant donors depleted of endogenous IBP4, as shown in Figures 3.8A,B. The assay performed well in both sample matrices covering the physiological range (10—60 nM)

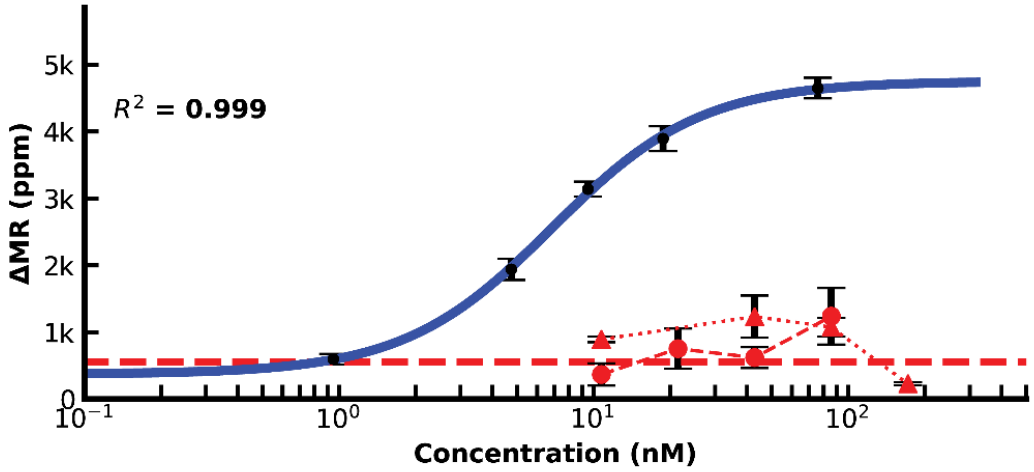

Figure 3.7: IBP4 at different serum dilutions. The blue line is 1/10 dilution, neat serum is the dashed red line, and 1/4 serum dilution is the dotted red line.

with a limit of detection (LOD) of 119 and 148 pM in PBS and serum, respectively. Prior experiments showed that a 1:10 dilution is needed to lower the serum's matrix effect on the anti-IBP4 antibodies (Figure 3.7). Without this dilution, the IBP4 assays were inconsistent. An assay with 2.5 nM IBP4 spiked in Buffer 1 was run multiple times (10 replicates with 3 sensor arrays) to assess the assay-to-assay variability. This concentration was selected considering the linear range of the assay. The average signal was 1.2 k ppm, and the coefficient of variation was 7% (Figure 3.8C). For comparison, the average of the negative control sensors (noncomplementary antibody or BSA) was 60 ± 5 ppm. We further quantified the accuracy of the assay through spike and recovery studies. Blinded serum pools were measured, with some having 2 nM IBP4 spiked into the sample. The concentrations were back-calculated using the serum calibration curve. The assays accurately quantified the spiked-in analyte within 15% (Figure 3.8D). Collectively, these data demonstrate the performance of the IBP4 assay showing repeatable, accurate detection in serum.

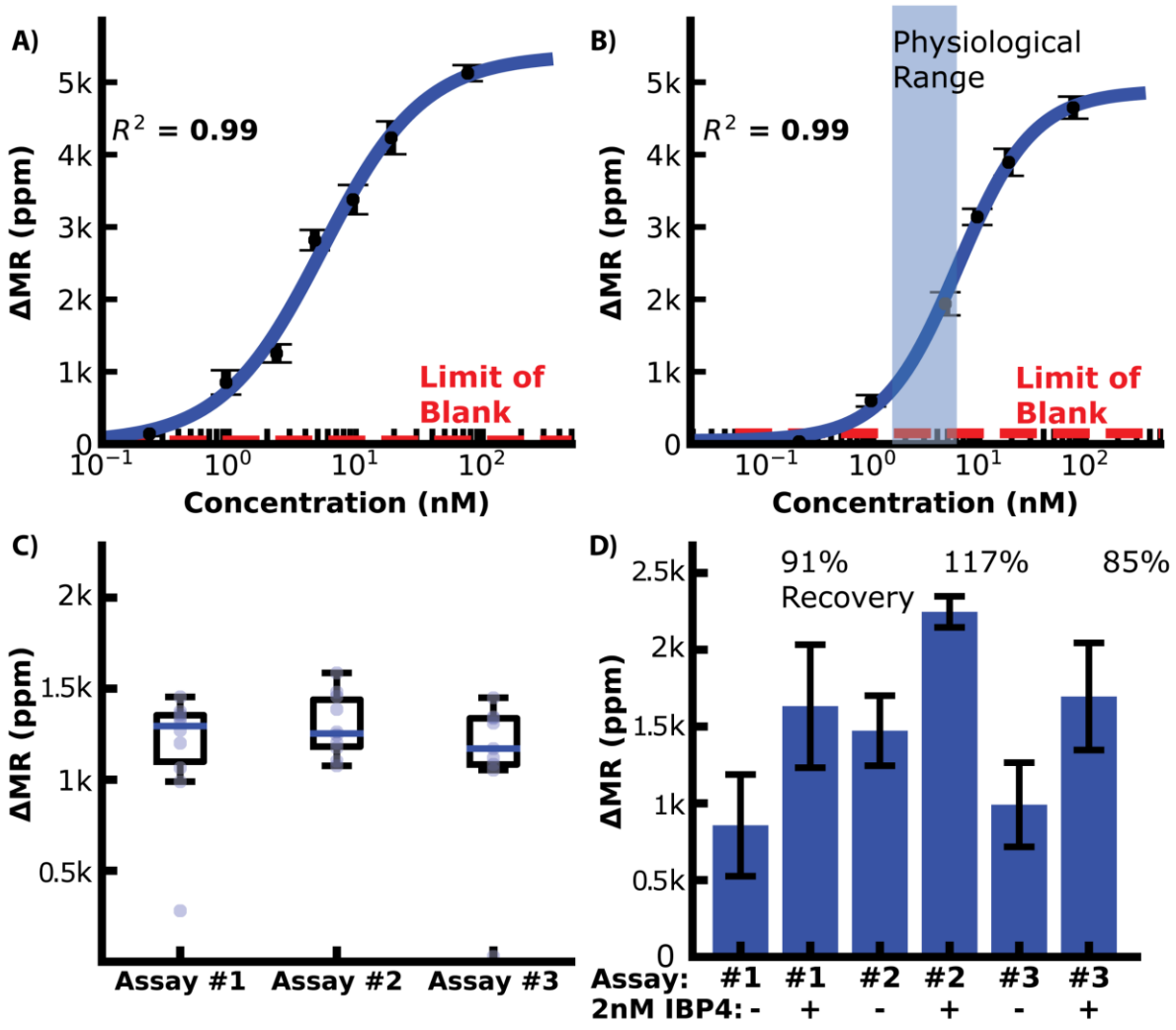

Figure 3.8: IBP4 assay data. (A) IBP4 spiked in PBS (LOD ~120 pM). (B) IBP4 spiked in 1:10 depleted serum (LOD ~150 pM). (C) Reproducibility of the 2.5 nM IBP4 assay in PBS. (D) Spike and recovery of 2 nM IBP4 in pooled serum.

3.6 Sex hormone-binding globulin dual-binding assay

We then generated a concentration curve with SHBG diluted into PBS with a LOD of 21 pM. A similar study as IBP4 was performed for the SHBG assay; however, the reproducibility was highly variable, with a coefficient of variation >17%. Many attempts to improve this using different antibody pairings and surface chemistries yielded mixed results but did not solve the

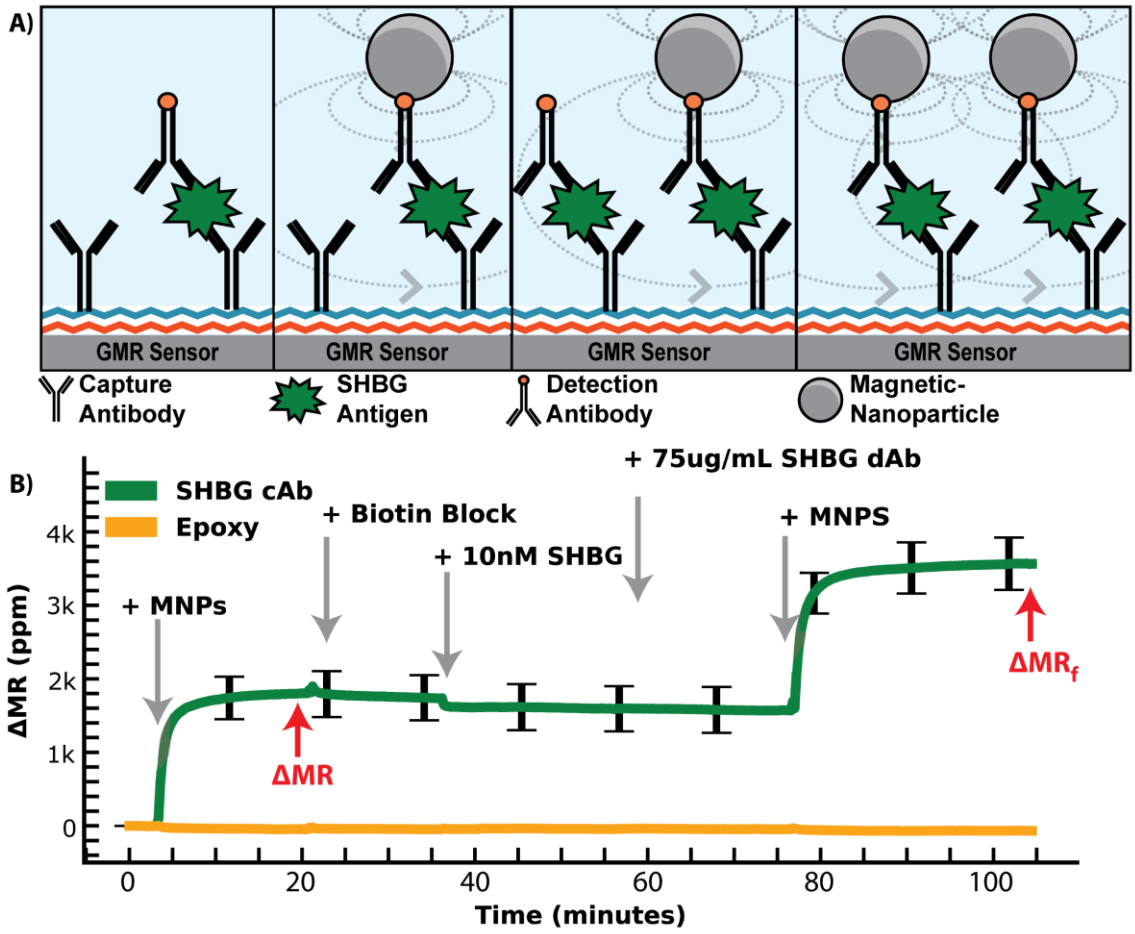

Figure 3.9: Dual-binding magnetic immunoassay. (A) Illustration of the dual-binding assay where a signal is first generated from the antigen in the sample. After binding has saturated, a known value of the calibrant is assayed on top of the existing assay. (B) Measured signal time course showing the binding curves from the dual-binding SHBG assay. The first binding curve is from 1 nM SHBG, then 10 nM SHBG is added. The ratio of the first to the second saturated value is used to normalize away assay variation.

underlying issue. There are several possible reasons for this variability, such as inconsistent surface antibody orientation and/ or analyte dimerization/aggregation that may complicate immunoassay results in some formats despite robust SHBG measurement by mass spectrometry and by clinical analyzers (Bradford et al., 2017; Grishkovskaya et al., 2000). Since the number of affinity reagents selected by our collaborator for this analyte was limited, we could not simply swap out affinity reagents; instead, we devised a way to deal with the variation at the assay level. Specifically, we modified the classical immunoassay by introducing another binding step with a known

concentration. As depicted in Figure 3.9, the first phase of the assay proceeds identically to the standard magnetic immunoassay with the functionalization of capture antibodies. After the first binding phase, we remove the unbound MNPs and add free biotin to block all unbound streptavidin on the tethered MNPs. This step is necessary to preserve the one-to-one relationship between the analyte and the MNPs (and thus the signal generated) and not deplete the biotinylated detection antibodies subsequently added. Next, we add a known concentration of SHBG protein on top of the already-bound protein. This complex is incubated for 20 min, followed by adding more biotinylated detection antibodies and MNPs. This "dual-binding" assay allows the signal from the first binding event to be normalized to the second binding event with a known concentration, resulting in a ratiometric signal. The important thing to note is that if there is inhomogeneity in the density of accessible capture antibody (due to surface chemistry, antibody orientation, etc.), it is also there for the second binding event and normalized out when taking the ratio. If it was a global effect that affected all antibodies similarly, one could normalize the signal to a housekeeping protein or an orthogonal spiked protein; however, this was not our situation. The issue was particular to the SHBG capture antibody, necessitating a different approach. The choice of 10 nM (vs. another concentration) spiked protein was based on the desire to operate in the linear region of the calibration curve—thus, any amount spiked on top of the sample required us to have sufficient dynamic range. The increase in signal after 10 nM SHBG incubation is correlated with the number of available antigen-binding sites after the sample incubation period, which means that the sample quantitation is less dependent on having the same number of initial antigen-binding sites on every sensor and across different assays. We also explored spiking in SHBG at a concentration that saturated the sensor, but this required significantly more reagents. While the

process is more complex than the magnetic immunoassay, we intend to automate it using a microfluidic cartridge so that the operator simply adds the sample.

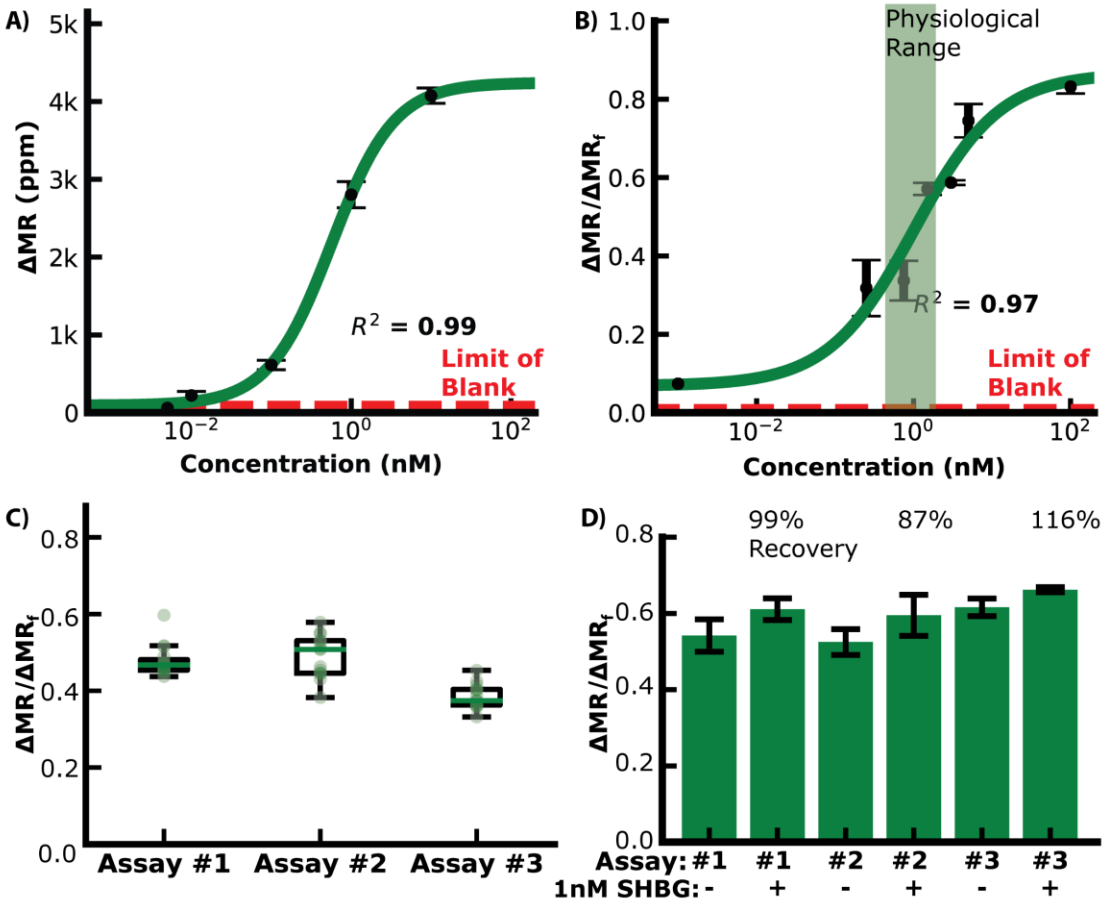

Figure 3.10: SHBG assay data. (A) Calibration curve in PBS (LOD ~20 pM). (B) Calibration curve in depleted serum (LOD ~15 pM). (C) Reproducibility assays with 1 nM SHBG in buffer. (D) Spike and recovery assays with 1 nM SHBG in pooled serum.

We measured SHBG in PBS and diluted serum using the dual-binding assay to generate a calibration curve (Figures 3.10A,B). The endogenous level of SHBG is high (100 nM), requiring a higher dilution of 1:1000 to bring it within the assay's dynamic range. The SHBG assay covered the physiological range of 100 nM for nonpregnant women, 600 nM in the first trimester, 1,000 nM in the second trimester, and 1,200 nM at delivery (Ekelund and Laurell, 1994) with a 13 pM LOD. The assay reproducibility is shown in Figure 3.10C, where the coefficient of variation for

multiple 1 nM SHBG dual-binding assays is 10%—a significant improvement over the classical magnetic immunoassay with a coefficient of variation of over 17%. Spike and recovery assays using the dual-binding assay with 1 nM SHBG in pooled serum had a quantitation accuracy within 15% (Figure 3.10D). These data demonstrate that the SHGB dual-binding assay can reproducibly and quantitatively detect the target analyte over the physiological range throughout gestation.

3.7 Validation

Nonspecific binding was measured by running an assay with serum depleted of SHBG and IBP4. Sensors with capture antibodies for SHBG and IBP4 developed little signal despite the addition of detection antibodies, which signifies that the antibodies are specific for SHBG and IBP4 (Figure 3.11). The SHBG capture antibodies developed 56 ± 14 ppm signal, while the IBP4 capture antibodies developed 51 ± 14 ppm of signal, similar to the 28 ± 5 ppm of signal from the negative control.

Despite running the previous assays in serum, we wanted to ensure that the assay was specific and had no cross-reactivity since quantitation is important for the proteomic score. The assay cross-reactivity was evaluated by adding 10 nM of SHBG to an IBP4 assay and 10 nM of

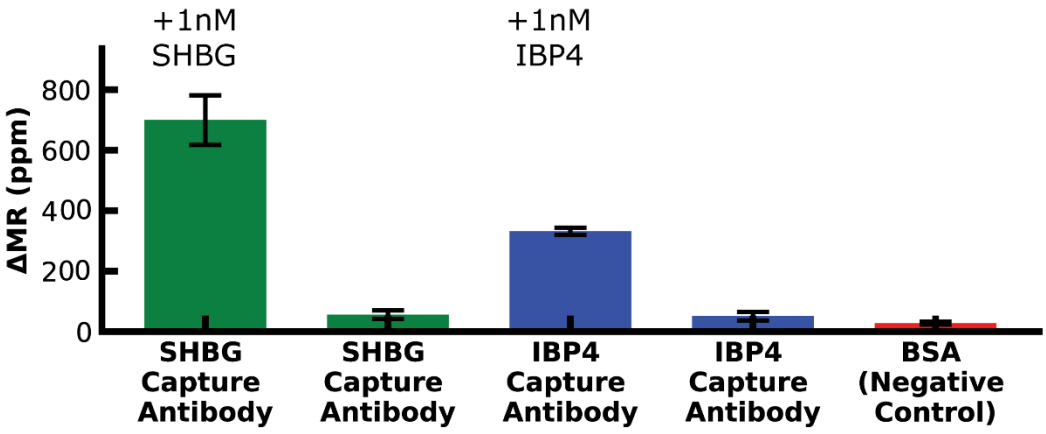

Figure 3.11: Nonspecific signal. Nonspecific binding SHBG and IBP4 assays in nonspiked depleted serum and 1nM analyte comparison.

IBP4 to an SHBG assay. The sensors spotted with off-target capture antibodies exhibited a negligible signal, no more than 120 ppm, similar to the negative control (BSA) sensors (Figure 3.12). Assays with serum immunodepleted of IBP4 and SHBG exhibited similarly low signals (Figure 3.11). These data demonstrate that the assay is highly specific to the target proteins with no detectable cross-reactivity.

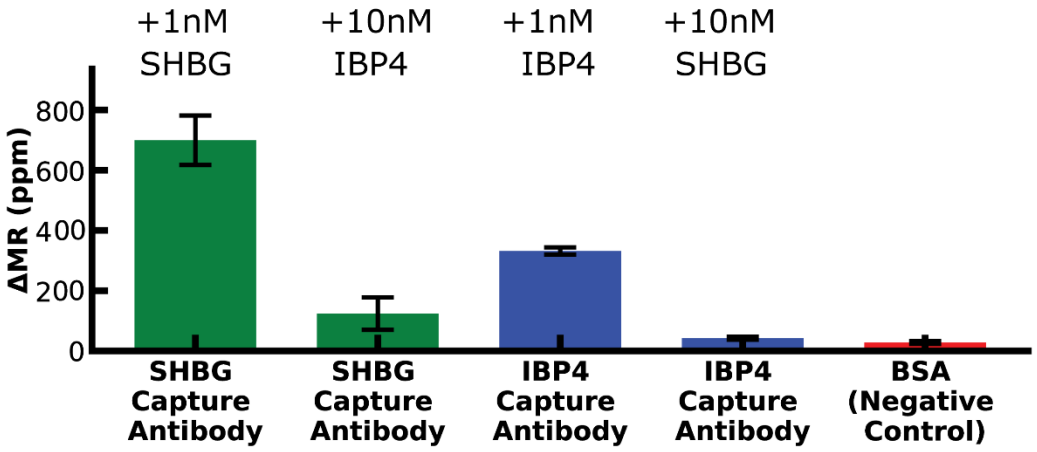

Figure 3.12: Cross-reactivity. Binding of SHBG and IBP4 assays with 10 nM of the opposite analyte; 1nM target analyte assays for comparison.

Serum patient pools were created and provided to the researchers blinded by collaborators at Sera Prognostics. The pools covered most of the physiological range of IBP4 (16—40 nM) and SHBG (567—1247 nM) throughout gestation. Each sample was run independently using the reported magnetic immunoassays and the clinically, analytically validated mass spectrometry assays. There was a strong correlation between the two different assays for IBP4 (n = 6) and SHBG (n = 4), as shown in Figures 3.13A,B. A proteomic score paired with clinical factors was shown to accurately predict spontaneous preterm birth, where the proteomic score is defined as the natural log of the IBP4 divided by SHBG response ratios (Saade et al., 2016). Because IBP4 and SHBG were not measured from the same pooled sample, to demonstrate the concordance of the proteomic

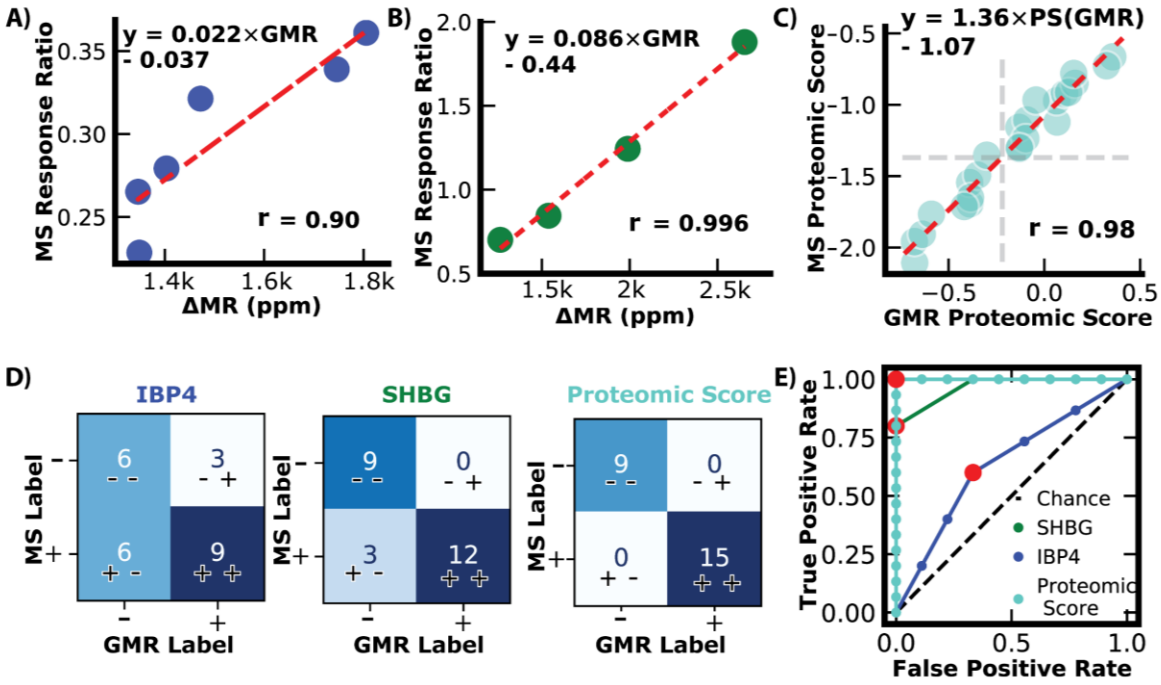

Figure 3.13: Assay verification. (A) IBP4 GMR values from pooled serum plotted against IBP4 response ratio values from mass spectrometry. (B) SHBG GMR values from pooled serum plotted against SHBG response ratio values from mass spectrometry. (C) Proteomic scores calculated from measurements of pooled serum combinations (n = 24) using the reported GMR assay and mass spectrometry. Proteomic scores are calculated by taking the natural log of the SHBG and IBP4 ratio. (D) Confusion matrices showing classification results from single biomarkers and proteomic scores. (E) Receiver operator curves for IBP4, SHBG, and proteomic score.

score between the assays, IBP4 values from the pools selected for their span of IBP4 concentrations (data in Figure 3.13A) were ratioed against pools selected for their SHBG concentrations (data in Figure 3.13B) with all possible permutations calculated (i.e., for each IBP4 value, a ratio was made using 4 different SHBG values, for a total of 24 combinations). The scores were calculated for both assays and plotted against each other. Figure 3.13C shows that the assays exhibit high similarity with a Pearson correlation coefficient of 0.98. The proteomic score threshold value for the mass spec assay is −1.37, which translates to a magnetic immunoassay score of −0.22. We then assessed the concordance of the two assays for each biomarker independently, and the scores derived from the ratio of the two using the mass spectrometry data as the "true" outcome. As shown in Figure 3.13D, using SHBG or IBP4 alone has lower concordance between the two assays. When

using the proteomic score, the reported assay has 100% positive and negative agreement. Finally, we calculated the ROC curve for the three cases to optimize the threshold value (Figure 3.13E). A −0.3 cut-off value for the proteomic score resulted in the best performance with an area under the curve (AUC) of 1, similar to the value predicted from the correlation analysis in Figure 3.13C. The sample size here was limited but perfectly agreed with the clinically validated mass spectrometry-based assay.

Acknowledgements

Chapter 3, in part, is a reprint of the journal article "A Dual-Binding, Magnetic Immunoassay to Predict Spontaneous Preterm Birth" as it appears in *Frontiers in Bioengineering and Biotechnology* by Michael Sveiven, Andrew Gassman, Joshua Rosenberg, Jay Boniface, Matthew Chan, Anthony J. O'Donoghue, Louise Laurent, and Drew A. Hall, Sep 2023. In addition, Chapter 3, in part, is a reprint of the journal article "A CMOS Magnetoresistive Sensor Front-End with Mismatch-Tolerance and Sub-ppm Sensitivity for Magnetic Immunoassays" as it appears in *IEEE Transactions on Biomedical Circuits* (TBioCAS) by Xiahan Zhou, Michael Sveiven, and Drew Hall, Dec 2019. The dissertation author was the first author of the first paper and the second author of the other paper.

CHAPTER 4: MAGNETIC HYDROLASE ACTIVITY ASSAYS

4.1 Overview

Enzymes play a pivotal role in various cellular processes, and their activities are tightly regulated to maintain cellular homeostasis. Monitoring enzymes is essential to understand cellular processes and disease mechanisms, and many enzyme-based disease biomarkers have been identified. For example, serum amylase and serum lipase assays are used to diagnose acute pancreatitis (Walkowska et al., 2022), alkaline phosphatase activity in blood is a marker for liver or bone conditions (Cannalire et al., 2023), creatine kinase tests diagnose Duchenne's Muscle Dystrophy in neonates (de Freitas Nakata et al., 2021), and elevated lactate dehydrogenase in blood is associated with poor prognosis in COVID-19 patients, potentially for use as a triage mechanism (Martha et al., 2022). Among enzymes, hydrolases are crucial in regulating intracellular pathways and, as a result, influence diverse physiological and pathological conditions. Hydrolases break down macromolecules such as lipids, carbohydrates, proteins, and nucleic acids. In humans, these enzymes are essential for food digestion, wound healing, cell signaling, and immune defense (W. Chen et al., 2020; Rack et al., 2020; Riise et al., 2019; Salhi et al., 2021). When these enzymes become dysfunctional, they become drivers of cancer, neurodegeneration, autoimmune disease, and heart disease (Liu et al., 2016; Moll et al., 2020; Mondanelli et al., 2019; Sama et al., 2020). Therefore, developing techniques to detect aberrant hydrolase activity as a disease biomarker provides an important tool for clinicians and researchers.

Nucleases are hydrolases that cleave the phosphodiester bonds between nucleotides in DNA and RNA (Garcia Gonzalez and Hernandez, 2022) and can be broadly divided into DNases and RNases based on their ability to cleave DNA or RNA, respectively (Santa et al., 2021). Nucleases hold great potential as biomarkers for many cancers (Balian and Hernandez, 2021). For

example, high DNase I activity is observed in patients with oral and breast cancers, while FEN I is a nuclease that is over-expressed in lung, prostate, brain, gastric, pancreatic, and breast cancer. In addition, RNase I is linked to pancreatic cancer (Balian and Hernandez, 2021; Lauková et al., 2020). Peptidases (or proteases) are hydrolases that cleave the peptide bonds between amino acids in a protein chain. Peptidases are involved in all biological processes, including food digestion, blood clotting, and immune defense (Armstrong, 2001; Kårlund et al., 2021; Shpacovitch et al., 2008; Walsh and Ahmad, 2002). Many diseases are characterized by dysfunctional peptidase activity, including cancer, arthritis, and Alzheimer's disease (Eatemadi et al., 2017; Lichtenthaler et al., 2022; Lucena and McDougall, 2021). Considering the vast influence of peptidases and nucleases on human health, measuring their activities in biofluids is of great interest.

Common nuclease measurement techniques include hybridization assays, immunohistochemistry, reverse-transcription polymerase chain reaction (PCR), enzyme-linked immunosorbent assay (ELISA), mass spectrometry, and western blots (Balian and Hernandez, 2021). Hybridization assays are qualitative and unsuitable for point-of-care testing (Singh et al., 2008), while immunohistochemistry assays are qualitative and require intensive processing (Wang et al., 2014). Reverse transcription-PCR is semi-quantitative and is usually a measurement of nuclease expression, not activity (Wang et al., 2014). ELISA uses fluorophores or chromogenic substrates that measure only enzyme concentration and can have photobleaching issues or incompatibility problems with sample matrices (Zhang et al., 2016). Many of these assays require a microplate reader to measure absorption or fluorescence (Balian and Hernandez, 2021; Lauková et al., 2020). While effective, they are limited by the size and complexity of the spectrophotometers, confining the assays to centralized labs.

Peptidases are typically quantified by fluorescent or colorimetric assays, where cleavage of a peptide sequence leads to a time-dependent increase in signal (Hao Ong and Yang, 2017; Wei et al., 2019; Zhang, 2004). These enzyme assays are amenable to microplate format and have been used extensively for high-throughput screening but have limitations regarding sensitivity, specificity, and adaptability (Hammond and Ferro, 2023; Nozeret et al., 2019; Oishi et al., 2008). Moreover, a persistent challenge inherent to these assays is their susceptibility to background

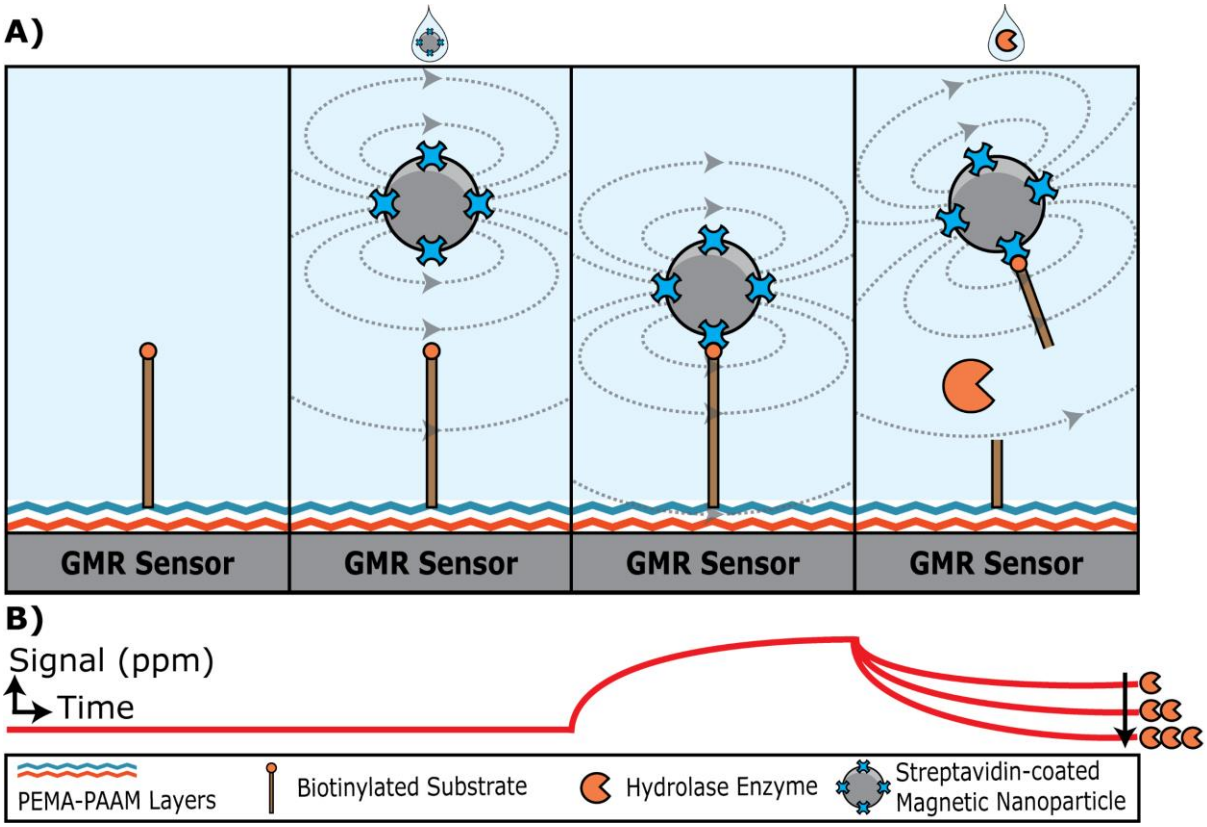

Figure 4.1: Graphical illustration of a hydrolase assay that uses magnetoresistance to quantify substrate cleavage. (A) A biotinylated substrate is covalently attached to the sensor surface through amine coupling. The addition of streptavidin-coated magnetic nanoparticles increases the magnetoresistance signal as the nanoparticles are tethered to the biotin substrate close to the sensor surface. The substrate is cleaved by a hydrolase enzyme and releases the magnetic nanoparticle. (B) Illustration of how the magnetoresistance signal changes with time. In the absence of magnetic nanoparticles, a low signal is detected. Upon the addition of streptavidin-coated magnetic nanoparticles, the signal increases with time as the particles bind to the substrate and are orientated close to the GMR sensor surface. The signal then decreases in proportion to the concentration of active hydrolase enzyme added.

signals, originating from non-specific interactions, autofluorescence, and photobleaching. This susceptibility can curtail the sensitivity and specificity of the measurements, often necessitating rigorous background correction procedures. Several surface-based (i.e., heterogeneous) peptidase assays have been developed that utilize electrochemical, surface plasmon resonance (SPR), or surface-enhanced Raman spectroscopy (SERS) detection. Electrochemical assays are sensitive and amenable to point-of-care use but susceptible to sample matrix effects (Chen et al., 2015; Menon et al., 2020). SPR sensors are label-free and real-time, but concerns exist over the complexity of the optical equipment required (Chang, 2021; Wang et al., 2019). SERS sensors have issues generating a reproducible colorimetric response, which means that the secondary enzyme will need specific conditions for activity (Ding and Yang, 2014). Overall, the assays described exhibit many desirable characteristics, but there is a need for new assays that overcome their shortcomings, especially regarding ease-of-use concerns and equipment complexity.

This study reports on a new technique that measures real-time hydrolase activity using giant magnetoresistive (GMR) sensors, as illustrated in Figure 4.1. GMR sensors are elaborately engineered thin-film stacks where the operation is deeply rooted in quantum mechanics; specifically, they exhibit a phenomenon known as spin-dependent scattering. This property makes them very sensitive to changes in the local magnetic field, enabling them to be used as ultrasensitive biosensors (Baselt et al., 1998; Wu et al., 2022). Past research has shown the utility of GMR sensors for measuring antigen levels using an antibody-antigen-antibody sandwich assay. The capture antibody is coupled to the GMR sensor and binds to the antigen. The bound antigen is then quantified using a biotinylated detection antibody as it recruits streptavidin-coated MNPs close to the sensor surface (Antarnusa et al., 2022; Gaster et al., 2013; Kim et al., 2013; Klein et al., 2019; Lin et al., 2019; Mostufa et al., 2023; Osterfeld et al., 2008; Sveiven et al., 2023; Zhou

et al., 2019). The increase in magnetoresistance directly correlates with the concentration of antigen. Miniaturization of the GMR system has been demonstrated, which allows for greater portability (Olazarra et al., 2022; S. Gaster et al., 2011; Yao et al., 2022). In the hydrolase assay described here, MNPs are tethered to the sensor substrate via a substrate sequence cleavable by the target enzyme. Therefore, the decrease in magnetic resistance over time directly correlates with the enzyme concentration.

A previous attempt to develop a GMR-based peptidase assay utilized a thioether linkage between a cysteine residue on the substrate and a maleimide-coated surface (Adem et al., 2020). However, the thioether bond was insufficiently stable in aqueous solutions and, therefore, not useful for point-of-care assays that require storage of the assembled substrate on the GMR sensor. We have recently functionalized GMR sensors for covalent binding to antibodies via primary amines and, therefore, used this approach to attach hydrolase substrates to the sensor surface. Prior to the addition of the hydrolase enzyme, the signal for the bound substrate can be quantified using streptavidin-coated MNPs. The signal decreases when the MNPs are released following substrate cleavage, enabling real-time, activity-dependent enzyme monitoring. The substrates consist of an amino acid sequence or a nucleic acid sequence to quantify the activity of a peptidase or nuclease. These substrates are flanked by a biotin molecule to capture streptavidin-coated MNPs and an amine chemical group to bind to the sensor surface. GMR sensors allow for a fast, kinetic, wash-free, portable assay with point-of-care capability. As this assay does not involve optical readout, the common issues of autofluorescence and photobleaching are avoided, enabling higher sensitivity. The GMR sensors are arrayed into 80 individually addressable sensors, creating multiplex ability. This study shows the viability of GMR sensors for quantifying hydrolase activity

using specific substrates and highlights the potential of this technology to provide physicians and patients with greater opportunities to detect and monitor diseases.

4.2 Materials and methods

GMR sensor arrays: GMR sensor arrays were purchased from MagArray, Inc (#BZ0078). Each GMR sensor array has 80 sensors arranged in an 8 × 10 matrix, where each sensor is 120 × 120 μm2 on a 280 μm pitch with a nominal resistance (R0) of 1.464 kΩ and a mean magnetoresistance (MR) ratio of 7.99% (Figure 3.2). Each of the 80 sensors can be independently addressed. A custom holder was fabricated from Teflon to create a 100 μL reaction well with an o-ring atop the sensor array.

GMR readout station: The measurement setup consists of a computer, a power amplifier (Texas Instruments, OPA549), a Helmholtz coil (180 turns of 22 gauge wire per coil, resulting in a 40.5 Oe/A coil constant), and custom readout electronics (Hall et al., 2010a), as shown in Figure 4.2. A double modulation readout scheme rejects 1/f noise from the sensors and electronics, and a temperature compensation technique is used to reduce the temperature drift (Hall et al., 2010b). The computer digitally adjusts the frequency and amplitude of the sensor bias voltage and magnetic field through a National Instruments data acquisition card (PCIe-6351) and a LabVIEW graphical user interface. Specifically, the power amplifier controlled by the computer provides a current to the Helmholtz coil, which creates a homogenous magnetic field (23–34 Oerms based on the sensor MR) for the sensor array. The readout electronics contain 8× transimpedance amplifiers to convert the currents to voltages that the data acquisition card quantizes. Time-multiplexing is applied to read the 8 × 10 sensor array with a 10 s update rate. The measured signal is the change in MR from the initial MR in parts-per-million (ppm).

Reagent spotting: Peptide, DNA, and PEG substrates are diluted in a printing buffer consisting of PBS, 1 M betaine, and 12.5% 2,3-butanediol. Individual sensors are spotted with the substrate using an iTWO300P automated spotter (axiVEND, Florida). Twenty droplets of ~100 pL are spotted on each sensor, sufficient to cover the sensor (Figure 4.3). The automated spotter chamber is then brought to 70% humidity for 1 h, and the sensors are incubated overnight.

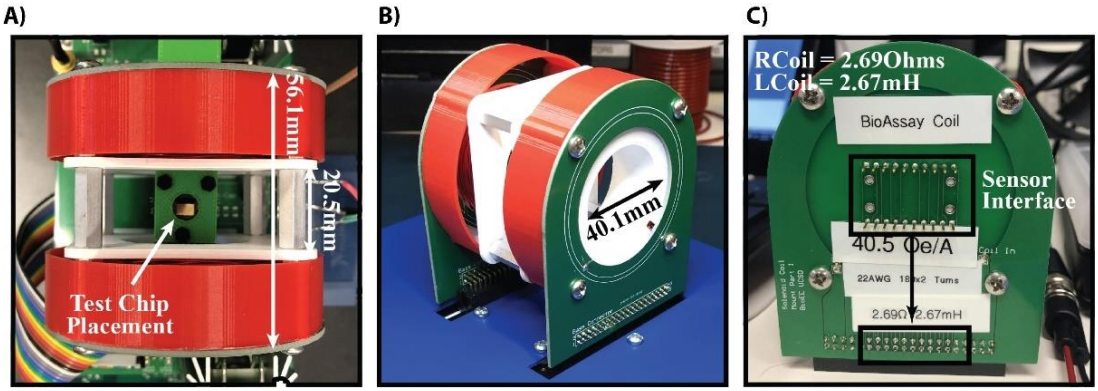

Figure 4.2: GMR reader. (A-C) Photographs of GMR SV reader station.

Magnetic enzyme activity assay: The sensors are functionalized with a substrate (specific to the target enzyme) containing a biotin on one end and an amine group on the other. After overnight incubation with the substrate, the sensors are blocked for 30 min using 1% ethanolamine, followed by a 1 mL wash with PBS. The sensors are placed into the GMR readout station, and 50 µL of MNPs (Miltenyi Biotec #130–048–101) is added. The sensor resistance is measured continuously for 15 min. Then, a 1 mM solution of biotin in PBS is added for 15 min followed by a wash with 1 mL PBS. The enzyme solution is added to the sensors to initiate the magnetic enzyme activity assay, and the MR signal is measured.

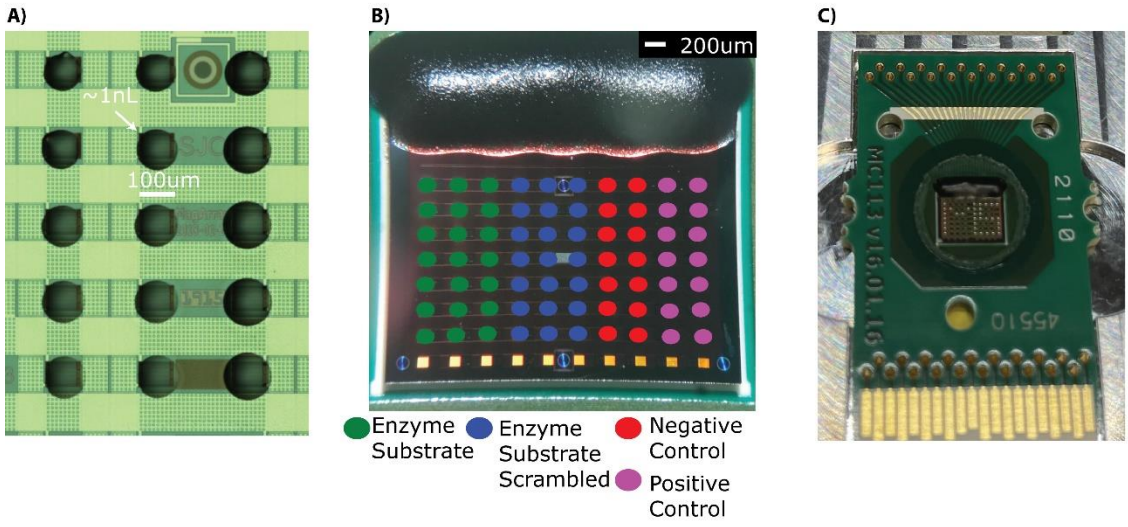

Figure 4.3: Reagent spotting. (A) Zoomed image of the GMR SV sensor array with sensors spotted with reagents. (B) The GMR SV sensor array with 80 sensors arranged in an 8×10 matrix where each sensor is 120×120 µm2 on a 280 µm pitch. Photograph shows an example mapping of the location of substrates and controls. (C) Demonstration of precise liquid dispensing using an iTWO-300P automated spotter. The 34 droplets were individually spotted on sensors in a defined pattern. The example shows a spotting pattern with the first author's initials (MS).

Nuclease assays: The sensors are functionalized with 9.56 ng of double-stranded DNA (5′– CCCCACTAGTAAAAAAAAAAAAAAAAAA–biotin–3′, Complementary: 5′–ACTAGTGGGGAAAAAAAAAAAAAA AAAAA–NH2–3′), where the 3′end of one strand is derivatized with biotin and the 3′end of the other strand is derivatized with an amine group. The Bcu I recognition site (ACTAGT) is underlined. A double-stranded DNA sequence containing a scrambled Bcu I site (TACATG) was also synthesized as a control. The assay setup is described in the magnetic enzyme activity assay section above. To initiate the nuclease assay, 15 µL of the restriction enzyme Bcu I (Thermo Scientific #FD1254) is mixed with 45 µL of fast digest buffer (Thermo Scientific #FD1254) and added onto the sensors. Activity is monitored for 25 min at room temperature. The DNase I is set up under similar conditions, except for 3 units (3 µL) of DNase I solution in 97 µL of DNase I buffer (Thermo Scientific #EN0521). For the sequential Bcu I/DNase I assay, the sensors were functionalized using the Bcu I DNA substrate and the scrambled

Bcu I sequence. 6.5 µL of Bcu I solution is combined with 43.5 µL of fast digest buffer for 15 min on the sensor. This is followed by a washing step with 1 mL of PBS before adding 5 units (5 µL) of DNase I in 45 µL of DNase I buffer for 10 min.

Peptidase assays: The peptidase assay setup follows the protocol described in the nuclease assay, except the sensors are functionalized with a linker sequence consisting of biotin-PEG_{36}-RQPVnWG-PEG_{36}-NH2 or a scrambled version of the same peptide, biotin-PEG_{36}-VWnRQGPPEG_{36}-NH2. The assay is initiated by adding 100 µL of 677 nM (20 µg/mL) human neutrophil elastase (Athens Research & Technology #16-14–051200) in PBS containing 0.01% Tween-20. To determine repeatability, three independent assays were performed using 100 µL of 500 nM human neutrophil elastase in PBS, 0.01% Tween-20, and the change in MR was recorded after 20 min of incubation. For the enzyme concentration curve assays, the enzyme was serially 2-fold diluted from 125 to 3.9 nM. For inhibition assays, the sensors are functionalized with the human neutrophil elastase substrate or its scrambled counterpart. The inhibitor, sivelestat sodium (VWR # 89161–706), is introduced at 0, 4, or 20 µg/mL in a 30 µL PBS, 0.01% Tween-20 onto the sensors for 10 min. Subsequently, 677 nM of HNE is introduced into the inhibitor solution, and the change in MR is recorded after 10 min.

Cystic fibrosis sputum fluorescent assay: Sputum samples were collected from adult cystic fibrosis patients (>18 years) according to a UC San Diego institutional review board-approved protocol for human subject research (#160078) from the UC San Diego Adult Cystic Fibrosis Clinic during routine visits (Quinn et al., 2019). Samples were diluted 1: 20 in PBS and stored at −20° C. Before use, samples are thawed, diluted 5-fold in PBS, and then mixed with an equal volume of 10 µM Ala-Ala-Pro-Val-7-amino-4-methylcoumarin (Alfa Aesar) in a black 384-well plate at a final volume of 30 µL such that the final dilution of sputum is 1 in 200. The reaction

is incubated at 37°C for 2 h assays in a Synergy HTX microplate reader (BioTek, VT, USA), and readings are obtained in 47 s intervals at excitation and emission wavelengths of 360 and 460 nm, respectively. Enzyme velocity in relative fluorescent units per sec (RFU/s) is calculated using the highest slope recorded for 10 consecutive fluorescent readings, and the mean and standard deviation are determined from three technical replicates.

Cystic fibrosis sputum magnetic assay: The cystic fibrosis sputum assay setup follows the protocol described above in the magnetic enzymatic activity assay section. The sensors are functionalized with the human neutrophil elastase substrate. Cystic fibrosis samples are prepared by diluting the frozen stocks 1:10 in PBS containing 0.01% Tween-20, then applying 50 µL of the diluted sample onto the sensors. The final dilution of sputum is 1 in 200.

Statistical analysis and exclusion criteria: All data shown are the mean values with one standard deviation as error bars. Sensors that show a signal of more than 117 ppm or less than −117 ppm before MNP addition were excluded. In the hydrolase assays, the sensor was excluded if it did not have sufficient loading after MNP addition (3,300 ppm for human neutrophil elastase substrates and 470 ppm for restriction enzyme substrates). Statistical analysis (Pearson's coefficient and Deming analysis) is done with custom-written code using NumPy (v1.18.5) and SciPy (v1.6.0) in Python (v3.8). The max negative velocity (-[ΔMR/MR0]/s) for the magnetic neutrophil elastase assays is calculated using LinearRegression from sklearn (v1.0).

4.3 Papain activity assay

Papain was the first hydrolase measured by a GMR activity assay. A sensor array containing immobilized SA-MNPs was incubated with 20 nM of papain for 160 minutes, and the MNPs were released from the surface in a time-dependent manner. After 160 minutes, 45% of the signal was reduced without any washing-steps being performed at pH 7.4 (Figure 4.4A). Under

the same conditions, sensors containing the non-cleavable linker sequence showed only 6% reduction in MNP signal. These studies confirmed that protease activity can be measured in real-time using a wash-free GMR SV sensor assay.

For a GMR sensor protease assay to have utility in a POC or POU setting, it should be able to rapidly quantify the protease concentration in a biofluid sample under a variety of assay conditions. Biofluids such as plasma, sputum, and wound fluid have a pH value close to neutral, and therefore, the prototype assay described above is suitable for detecting protease activity under these conditions. However, other biofluids, such as urine, have a pH of 6.052, and it was unclear if the assay was compatible with these mildly acidic conditions. Papain is enzymatically active at pH 6.0, so we evaluated the GMR sensor assay in these conditions. We show that 57% of the MNPs are released from the sensor surface after 160 minutes incubation with 20 nM of papain at pH 6.0 while only 4% of the linker is released (Figure 4.4A). Papain is more stable at acidic pH than at neutral pH, and therefore ,the greater release of MNPs at pH 6.0 relative to pH 7.4 is likely due to increased stability of the enzyme in the acidic environment.

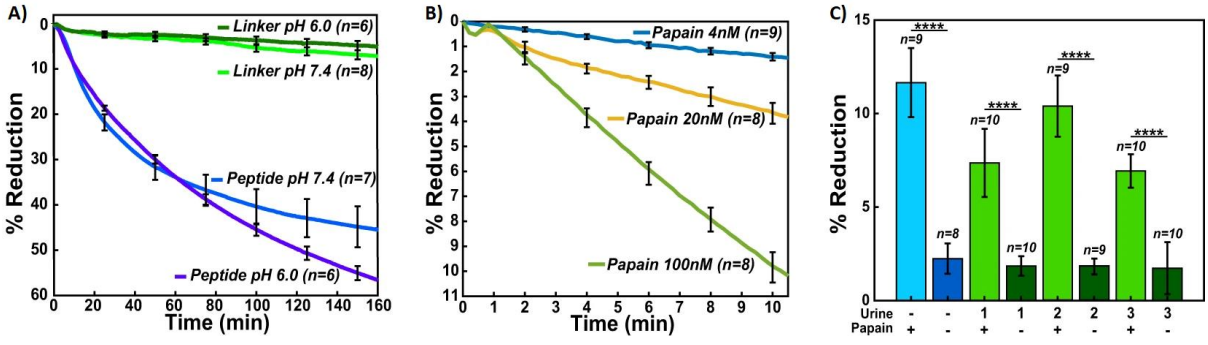

Figure 4.4: Measured real-time magnetometry papain digestion. (A) Normalized % reduction of peptide and linker sensors treated with 20 nM papain in pH 6.0 and pH 7.4 conditions. (B) Normalized % reduction data comparing the 4 nM (blue), 20 nM (yellow), and 100 nM (green) at pH 7.4 peptide treated sensors. Curves depicted are the mean signal of sensors that were functionalized. (C) Normalized % reduction of papain spiked urine samples and PBS. Error bars are ±1σ.

Next, we determined if the rate of MNP release correlates with enzyme concentration and if sufficient enzyme activity data can be generated within a shorter assay time. To do this, we assayed peptide and MNP-coated biochips with 4, 20, and 100 nM of papain for 10 minutes. The MNP release from the surface strongly correlates with the concentration of enzyme in the assay (Figure 4.4B). Therefore, the rate of change in MR can be used to quantify the amount of papain in the assay. The minimum assay time where protease cleavage can be quantified corresponds to the time when the SNR is greater than 2. Under these conditions, 4 nM of papain was detected after 3.49 minutes incubation, while 100 nM of papain can be quantified after 2.87 minutes incubation. These data validate using GMR SV sensors to rapidly quantify protease activity using a peptide release assay.

Urine is a commonly used biofluid for the diagnosis of urinary tract infections caused by either bacteria or yeast (Najeeb et al., 2015). Proteomic studies have shown that at least 41 proteases are present in urine from healthy individuals and fluorescent reporter peptides have been used to detect activity from these enzymes (Taylor et al., 2014). The most abundant urine proteases prefer cleaving one or two amino acids from the free N-terminus of proteins and peptides and therefore we predicted that these enzymes would not cleave the Biotin-PEG_{36}-TFSYnRWP-PEG_{12}-Cys peptide because the N-terminal threonine (T) residue is coupled to PEG_{36} and therefore blocked. Urine also contains a broad-acting cysteine protease inhibitor, cystatin C that potently inhibits papain. Using urine from three healthy individuals, cystatin C was inactivated with human cathepsin B. When these urine samples were added to the GMR SV sensor containing the peptide and incubated for 10 minutes, no significant reduction of MNPs was detected. This study shows that cathepsin B and the endogenous urine proteases are unable to cleave the papain peptide substrate. Adding 20 nM papain to these urine samples for 10 minutes resulted in a reduction in

MR comparable to papain assayed in PBS (Figure 4.4C). The average time for the SNR to be greater than 2 in these samples was 3.76 ± 0.25 minutes.

4.4 Human neutrophil elastase activity assay

After validating the MNP assay with papain, we evaluated the assay format for another peptidase, a hydrolase that cleaves peptide bonds. For these studies, we chose human neutrophil elastase (HNE) as the target enzyme as it has been established as a sputum biomarker for exacerbations associated with chronic obstructive pulmonary disease (COPD) and cystic fibrosis

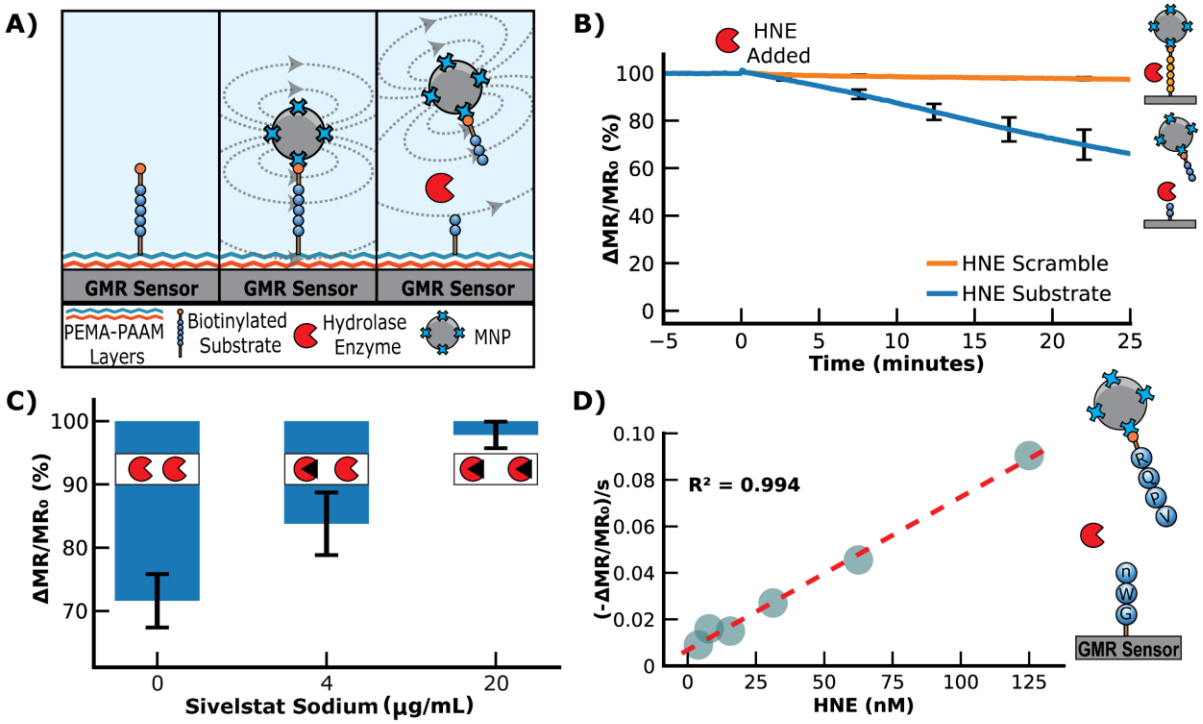

Figure 4.5: Human neutrophil elastase assay. (A) Illustration of the neutrophil elastase assay. The peptide substrate is covalently attached to the sensor surface and then bound to streptavidin-MNPs via a biotin group on the peptide. This results in an increase in magnetoresistance. The addition of human neutrophil elastase cleaves the substrate, decreasing the signal. (B) An example of how the signal is loaded and then reduced by adding human neutrophil elastase. The signal is displayed as a percentage of the loading signal after the magnetic nanoparticle binding has saturated. (C) Human neutrophil elastase assays with inhibition by sivelestat sodium. All three assays have 20 µg/mL of neutrophil elastase, but the inhibitor concentration increases from 0 to 20 µg/mL. (D) Human neutrophil elastase titration serial diluting from 125 nM to 3.9 nM by a factor of 2 in PBS containing 0.01% Tween-20. The magnetic assay results are shown as the maximum velocity.

(CF). During neutrophil degranulation, elastase from granules is released and efficiently kills bacteria; however, the excess enzyme also damages lung tissue by degrading extracellular matrix proteins that are important for lung structure and elasticity (Kafienah et al., 1998; Kawabata et al., 2002; Mecham et al., 1997; Saetta et al., 2001). The amount of neutrophil elastase in sputum is directly proportional to the amount of activated neutrophils. We have detected neutrophil elastase activity in the sputum of patients with CF using fluorogenic substrates and revealed that patients with severe disease and more pathogenic bacteria have higher levels of elastase activity (Quinn et al., 2019). While numerous assays have been developed to quantify this enzyme, we were interested in designing a point-of-care peptidase assay using the MNP sensor system.

We first needed to find a peptide efficiently cleaved by HNE. In previous studies by our group, we incubated HNE with 124 different 14-mer peptides, each highly diversified in sequence. The enzyme cleaved 78 of these peptides, and a substrate specificity profile was generated using the most frequently found amino acids in each position surrounding the cleavage site (O'Donoghue et al., 2013). A consensus peptide sequence consisting of Arg-Gln-Pro-Val*NleTrp-Gly (RQPVnWG) was developed as a sequence cleaved by HNE, where * is the cleavage site and Nle (n) is norleucine, a non-natural amino acid. In parallel, we identified a scrambled peptide sequence, VWnRQGP, that contains the same seven amino acids but is not cleaved by HNE. These peptides were synthesized with a PEG_{36} linker on each end. On the N-terminal PEG_{36}, an amine group was included to covalently attach to the sensor surface, while the C-terminal PEG_{36} contains a biotin group to bind MNPs (Figure 4.5A). Upon exposure of the sensor to a sample containing HNE, it

was predicted that the RQPVnWG peptide would be cleaved between V and n, while the scrambled peptide would not be cleaved.

Both peptides were coupled to the sensor surface using the protocol outlined previously for PEG_{11} and DNA, and upon the addition of MNPs, a signal increased by ~4,000 ppm, which confirmed the interaction between the biotin on the peptide with the streptavidin-coated MNPs. Following a wash step, the signal was monitored for 5 min to ensure stability, and then HNE was

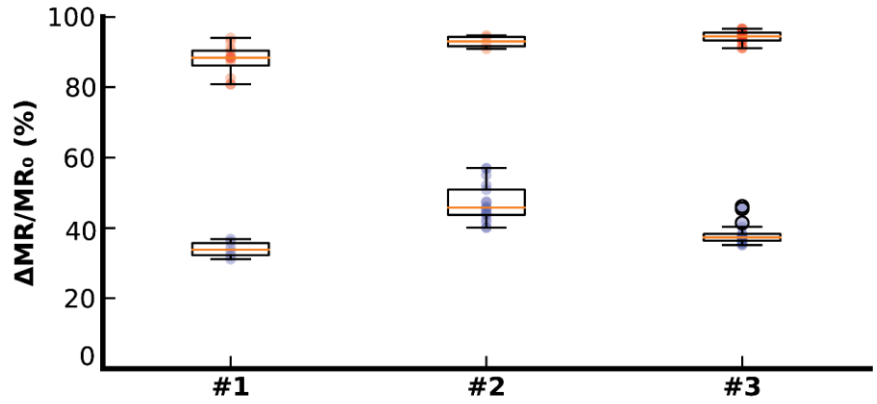

Figure 4.6: Evaluation of repeatability. Three independent assays were performed on replicate sensors to demonstrate repeatability. Sensors were functionalized with either the human neutrophil elastase substrate (blue) or the scrambled peptide (red). 500 nM of human neutrophil elastase was added to each sensor, and the change in signal was recorded after 20 minutes of incubation. The coefficient of variation from all sensors was calculated to be 11%.

added. The peptide containing the substrate sequence was cleaved, releasing the MNPs into the solution in a time-dependent manner (Figure 4.5B). The signal from the scrambled peptide sequence remained unchanged in the assay. This confirmed that cleavage by HNE was specific for the RQPVnWG substrate and revealed that the enzyme does not cleave the streptavidin protein, which could non-specifically release the MNP due to the breakdown of the streptavidin-biotin interaction. Three independent assays were performed, and the coefficient of variation from all sensors after 20 min of incubation was calculated to be 11% (Figure 4.6).

Next, we evaluated the ability of the assay to distinguish between active and inhibited HNE. Sivelestat sodium is a clinically approved HNE inhibitor for treating acute lung injury or acute respiratory distress syndrome (Pu et al., 2017). HNE was added to RQPVnWG sensors that contained either 4 or 20 μg/mL of sivelestat sodium, and the reactions were monitored for 10 min. The change in magnetoresistance was compared to the HNE digestion assay without the inhibitor. In the absence of sivelestat sodium, the signal decreased by 28.4%, while in the presence of 4 μg/mL, the signal decreased by 16.2%. At 5× higher inhibitor concentration, the signal decreases by only 2.2%, revealing that the enzyme was mostly inactivated under these conditions (Figure 4.5C). These data showed that the release rate of MNPs correlates with the amount of active enzyme in the assay. We next performed a serial dilution of HNE from 125 nM to 4 nM and calculated the change in MR signal per second at each concentration. From these studies, a linear concentration curve was calculated with an R^2 value of 0.994 (Figure 4.5D), confirming that the change in MR signal directly correlates with enzyme concentration.

One of the most commonly used fluorogenic peptide substrates for monitoring HNE activity is Ala-Ala-Pro-Val-7-amino-4-methylcoumarin (AAPV-amc), where cleavage between V and amc results in an increase in fluorescence at 460 nm. To directly compare the peptide-MNP assay with a traditional fluorogenic peptide assay, the fluorogenic substrate was also assayed with 125 to 4 nM of HNE. The assay yielded an expected concentration-dependent increase in the reaction velocity. When comparing the velocities of both assays, a Pearson correlation coefficient of 0.974 was calculated, indicating a very strong positive correlation between the surface-based MNP release assay and the traditional solution-based fluorogenic assay (Figure 4.7A).

To evaluate the peptide-MNP assay using clinically relevant biofluids, we obtained sputum from 10 CF patients, diluted them 200-fold in assay buffer, and incubated it with both the peptide-MNP sensor and the fluorogenic substrate (Figure 4.7B). Each sputum sample contained sufficient HNE activity to release the MNPs, with the release rate ranging from 0.036 to 0.088 ppm/s. Compared with the fluorescent assay, the data was strongly correlative (Pearson correlation coefficient of 0.829). The velocity of MNP release by HNE in the sputum samples was then compared to the HNE concentration curve, and it was revealed that the amount of enzyme in each sample was between 8.8 and 24.6 μM (Table 4.1). This concentration of HNE in these sputum is comparable to previous studies on CF sputum that used a colorimetric substrate to quantify HNE in CF sputum at a range of 0.47–18.5 μM (Dittrich et al., 2018; Rees et al., 1997). This study shows that the peptide-MNP assay applies to quantifying HNE in patient sputum samples.

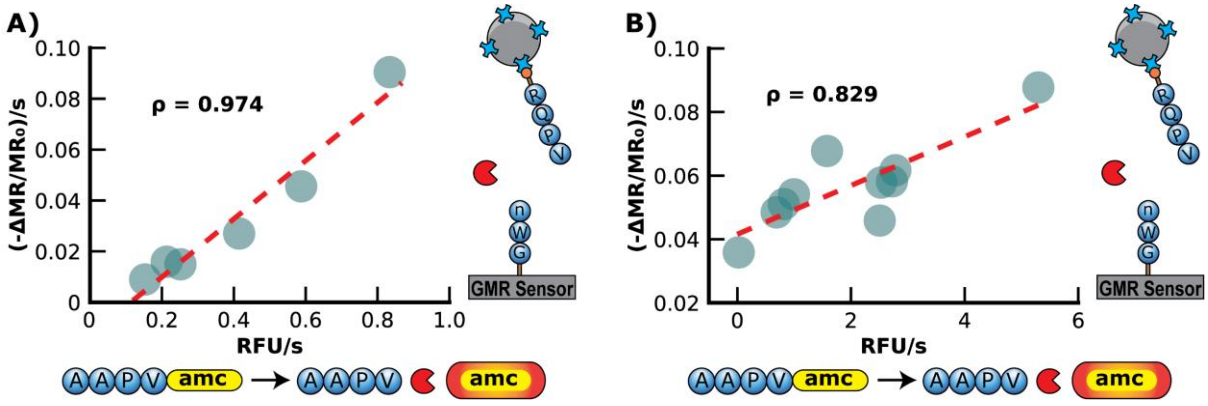

Figure 4.7: Validation of magnetic neutrophil elastase assay in buffer and sputum. (A) Validation of the magnetic human neutrophil elastase assay by comparison to a traditional AMC assay readout with a spectrometer. Each point represents a different concentration of human neutrophil elastase in buffer readout by the GMR readout station (shown in the y-axis) and the spectrometer (shown in the x-axis). The concentration ranges from 3.9 to 125 nM of human neutrophil elastase. (B) Validation of the magnetic human neutrophil elastase assay compared to a traditional amc assay readout with a spectrometer. Each point represents a different human sputum sample of patients with cystic fibrosis measured by the GMR station (y-axis) and the spectrometer (x-axis).

Table 4.1: CF sample concentrations calculated from HNE titration. The concentration both in the assay and in the sample (x200 to account for the dilution factor) for each CF sample.

CF Sample	$(-\Delta MR/MR_0)/s$	Assay HNE Concentration (nM)	Sample HNE Concentration (μM)
1	0.046	59.32	11.86
2	0.051	67.22	13.44
3	0.058	78.06	15.61
4	0.058	77.47	15.49
5	0.088	122.89	24.58
6	0.062	83.37	16.67
7	0.054	71.87	14.37
8	0.048	63.25	12.65
9	0.036	44.13	8.83
10	0.068	92.56	18.51

4.5 Nuclease activity assay

We evaluated the ability of hydrolytic enzymes to cleave a substrate sequence and, therefore, replaced the PEG_{11} linker from Chapter 2 with double-stranded DNA containing an amine group and biotin on each end (Figure 4.8A). We chose a sequence containing the restriction site for cleavage by Bcu I that corresponds to A*CTAGT, where * is the cleaved bond. This sequence is flanked by 4 bases on the 5′side and 20 bases on the 3′side and is coupled to the sensor surface as described for the PEG_{11} linker. Another DNA linker sequence was synthesized with a scrambled restriction site sequence, TACATG, which was expected to resist Bcu I cleavage. Upon cleavage of the DNA substrate, the bound MNPs are predicted to be released into solution, thereby reducing the magnetoresistance signal. We found that the DNA sequences could be coupled to the sensor surface using the same chemical protocol optimized using the PEG_{11} linker. Following the wash steps, the signal was evaluated for 5 min to ensure stability. To determine if the two DNA sequences are accessible for nuclease cleavage, we added DNase I, a broad-spectrum nuclease enzyme that nonspecifically cleaves the phosphodiester bonds in double-stranded DNA sequences.

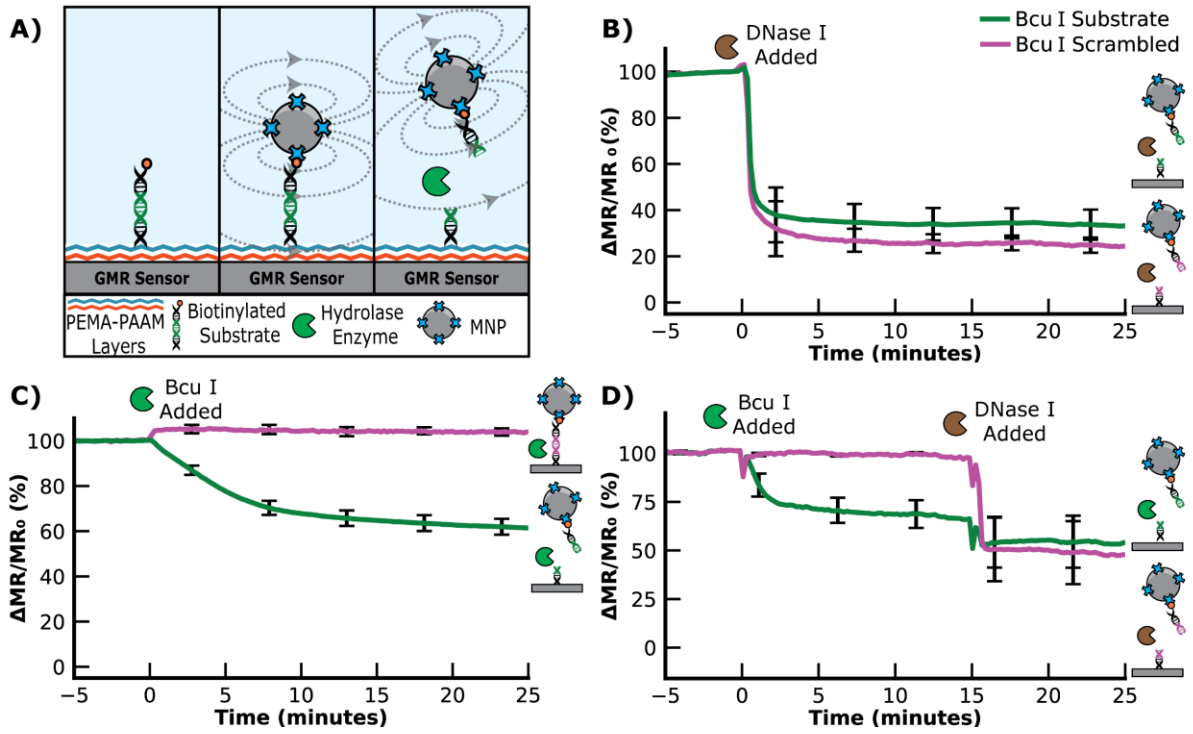

Figure 4.8: Nuclease assay. (A) Graphical illustration of the nuclease assay. The signal decreases when the nuclease cleaves the substrate. (B) Hydrolysis of the ACTAGT (Bcu I substrate) and TACATG (Bcu I scrambled) sequences by DNase I results in a time-dependent decrease in the MR signal. (C) Hydrolysis of ACTAGT and not TACATG by the restriction enzyme, Bcu I. (D) Sequential addition of Bcu I and DNase I shows that Bcu I specifically cleaves the ACTAGT substrate, while DNase I cleaves the TACATG sequence.

This enzyme rapidly cleaved both DNA sequences, decreasing the signal by 59.0% for the Bcu I substrate and 64.1% for the scrambled Bcu I substrate after only a 1-min incubation (Figure 4.8B). The signal stabilized, indicating that all available DNA linker sequences were hydrolyzed. These data confirm that the surface-tethered DNA sequence is accessible for cleavage by a nuclease. To assess the specificity of the Bcu I substrate over the scrambled sequence, we added Bcu I to a sensor containing both sequences. After incubation for 25 min with the scrambled substrate, no reduction in signal was detected, indicating that this DNA sequence was not cleaved. However, in the adjacent sensors containing the Bcu I substrate, a time-dependent change in signal was detectable, with 22.9% reduction in signal within 5 min and an additional 21.2% reduction over

the remaining 20 min (a total of 44.1% reduction in 25 min) (Figure 4.8C). We next set up an assay where Bcu I was incubated with the DNA sequences for 15 min, and then DNase I was added to the same sensor (Figure 4.8D). These studies showed that both DNA sequences are cleavable by DNase I, but only the ACTAGT sequence is a substrate for Bcu I. Knowing that the DNA sequences can be cleaved by nucleases, we evaluated their stability in saliva, a biofluid of interest for use in point-of-care applications. Saliva contains numerous hydrolytic enzymes such as salivary amylase, peptidases, lysozyme, and lipase (Chojnowska et al., 2018; des Gachons and Breslin, 2016; Feng et al., 2019; Mennella et al., 2014). When exposed to saliva, the Bcu I substrate and scrambled DNA sequence had only a 1.3% and 1.6% reduction in signal after 10 min of incubation, respectively (Figure 4.9). When compared to the reductions observed in the presence of Bcu I and DNase I, the signal change caused by saliva is statistically insignificant. These studies reveal that the DNA-MNP complex is stable in a complex biological sample containing numerous hydrolytic enzymes.

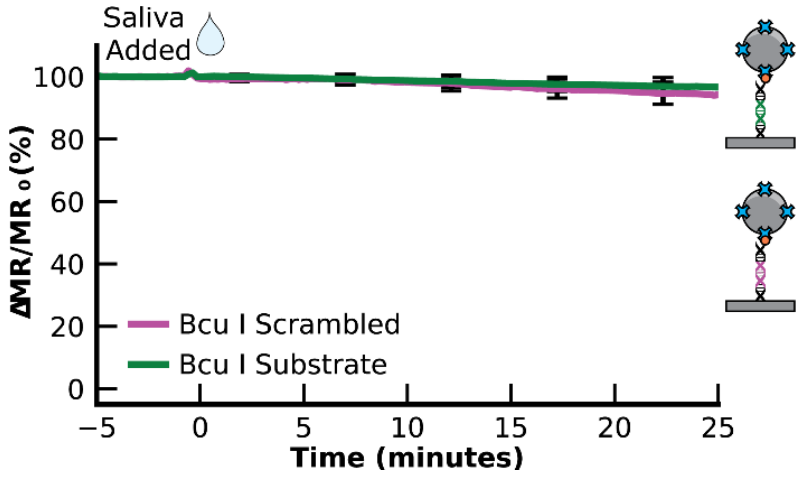

Figure 4.9: Assay stability in saliva. Assays showing the stability of the substrates in saliva over 25 minutes of incubation. The sensors show less than a 5% reduction in signal for either the Bcu I substrate sensors or the Bcu I scrambled substrate sensors.

Acknowledgements

Chapter 4, in part, is a reprint of the journal article “A GMR Enzymatic Assay for Quantifying Nuclease and Peptidase Activity” as it appears in *Frontiers in Bioengineering and Biotechnology* by Michael Sveiven, Ana Serrano, Joshua Rosenberg, Doug Conrad, Drew A. Hall, and Anthony J. O’Donoghue, Mar 2024. In addition, Chapter 4, in part, is a reprint of the journal article “Giant Magnetoresistive Biosensors for Real-Time Quantitative Detection of Protease Activity” as it appears in *Nature Scientific Reports* by Sandeep Adem, Sonal Jain, Michael Sveiven, Xiahan Zhou, Anthony J. O’Donoghue, and Drew A. Hall, May 2020. The dissertation author was the first author of the first paper and the third author of the second paper.

CHAPTER 5: DISCUSSION AND FUTURE DIRECTIONS

5.1 Point-of-care immunoassays

A magnetic immunoassay enables the possibility of POCT, greatly expanding accessibility and reducing the turnaround time. Since the sensor arrays have 80 sensors, there is room to add more biomarkers once identified. Microfluidics would allow for automation to reduce the expertise needed to run the assay and facilitate multiple sample dilutions to be run on the same chip. In addition, automated dilutions for logarithmic concentrations by microfluidics have been demonstrated and could be implemented for ease of use in a point-of-care setting and to allow a sample to be diluted 1:10 for IBP4 and 1:1000 for SHBG on a single sensor array (Kim et al., 2008). Paired with microfluidics, which can be developed in future work, these sensors could eventually lead to a comprehensive pregnancy panel, allowing ultra-personalized care.

Future work has various avenues for expediting the assay time. Promising strategies include active attraction of MNPs and wash-free assays (Choi et al., 2016; Su et al., 2019). While these approaches hold potential, it is worth highlighting that the present emphasis rests on establishing the fundamental viability of the assay concept. Should improving the assay's efficiency encounter challenges in significantly curtailing the assay time, one solution might involve incorporating a brief waiting period preceding an obstetrician appointment, which ensures that healthcare providers can access the assay results in tandem with the patient's visit.

Another significant advantage of the reported immunoassays is the low sample volume. All assays were run with less than 50 µL of sample, allowing them to be run from a single finger-puncture procedure (Serafin et al., 2020). This volume remains the same as more targets are added to the assay panel. The blood from a finger-puncture procedure could be diluted with microfluidics, and the assay steps automated. The clinical application of a resulting device will require full

analytical and clinical validation. Clinical validity must demonstrate discrimination and calibration for the association of the derived multi-analyte score with the risk of sPTB (Alba et al., 2017). The expansion of GMR sensor technology allows for personalized health monitoring of fetal development, and further automation will allow the test to be accessible to many pregnancies.

5.2 Potential use cases for the magnetic hydrolase activity assay

In the realm of hydrolase activity assays, the sputum samples used in this study were obtained from different patients; therefore, we could not perform a longitudinal study on how the HNE levels change when the patient is experiencing an exacerbation event. However, a potential application of this assay for patients with CF, COPD, or other lung diseases would be to monitor the HNE levels in sputum daily or weekly, thereby providing the healthcare team with data to monitor neutrophil levels in their lungs. The landscape of enzymes, their functions, and the impact of their dysfunction in disease states is vast. Table 5.1 lists a subset of these enzymes and the current methodologies used to measure their abundance. Nucleases and peptidases are activity-based markers for lung, inflammatory, and infectious diseases in addition to cancer. Many of these enzymes are currently assayed by ELISA, which cannot distinguish between active and inactive (inhibited enzymes or pro-enzymes). The standard fluorogenic methods for quantifying peptidase activity require a microplate reader and a trained technician. These methods can process many patient samples but are not amenable to point-of-care use. The magnetic enzymatic activity assay described here is designed for single-use in a point-of-care setting where the user (patient or healthcare provider) adds a biofluid sample to a preassembled substrate. The adaptability of the magnetic assay for other hydrolase substrates means that it can be readily modified to detect many different enzymes. The magnetic-based enzyme assay could greatly benefit the medical community as it seeks to diagnose patients and monitor their daily health.

Table 5.1: Potential applications of hydrolase activity assays.

Enzyme	Sample	Health Condition	Use	Current Assay Methods	References
Human Neutrophil Elastase	Sputum	COPD, Cystic fibrosis, antibody-deficiency Bronchiectasis	Exacerbation monitoring, Guide for antibiotic use	Activity-based immunoassay, Lateral flow device, Fluorogenic substrate-based kinetic assay, Mass spectrometry	(Chan et al., 2020; Oriano et al., 2019; Rofael et al., 2023; Thulborn et al., 2019; Voynow and Shinbashi, 2021)
Proteinase 3	Plasma, Sputum	α1-antitrypsin deficiency, Bronchiectasis	Exacerbation monitoring, Antitrypsin dosing guide	ELISA, Activity-based immunoassay	(Newby et al., 2019)
Wound Peptidases	Wound fluid	Chronic wounds	Early detection of non-healing wounds	Lateral flow device	(Serena et al., 2021)
Gingipain	Saliva	Gingivitis	Detection of *Porphyromonas gingivalis*	Immunoassay, FRET substrate, Photoacoustic	(Bikker et al., 2019; Hirai et al., 2020; Retout et al., 2023)
Human Nuclease	Tears	Dry eye disease	Disease monitoring	Gel Electrophoresis, FRET	(Sonawane et al., 2012)
Bacterial Nuclease	Urine	Urinary tract infection	Detection of urinary tract infections	FRET	(Flenker et al., 2017; Machado et al., 2019; Qing et al., 2019)
DNase I	Serum	Stomach, colon, pancreas, breast, and oral cancer	Diagnosis	SRED, Microchip electrophoresis, ELISA, Immunochemical	(Balian and Hernandez, 2021; Lauková et al., 2020)
Prostate-specific Antigen	Serum	Prostate cancer, prostatitis	Screening, Risk stratification, Post-treatment monitoring	Lateral flow	(Jung et al., 1999)
Trypsin	Blood	Acute pancreatitis, cystic fibrosis, and pancreatic cancer	Monitoring	ELISA, Colorimetry, Chemi-luminescence, Electrochemical, Photo-electrochemistry, and Fluorescence	(Bao et al., 2021; Ping et al., 2021)
Matrix Metallo-proteinase-8	Gingival crevicular fluid	Periodontitis	Diagnosis	ELISA, Immunofluorimetry	(Nazar Majeed et al., 2016)
Cathepsin S	Serum	Gastric cancer	Diagnosis and Prognosis	ELISA	(Liu et al., 2016)
RNase 5	Plasma	Pancreatic cancer	Patient stratification	ELISA	(Wang et al., 2018)
RNase A	Buffer	Many cancers	Diagnosis of malignant tumors and specific target for drug discovery	Electro-Chemiluminescence, Fluorescence, Chemiluminescence, Electrochemistry	(Ni et al., 2019)
Pepsin	Saliva, Sputum	GORD, laryngopharyn-geal reflux, VFL	Possible biomarker	ELISA, HPLC	(Stanforth et al., 2022)

5.3 Conclusions

To reiterate, the GMR SV sensors possess attributes that render them highly suitable for sensitive, multiplexed, matrix-agnostic, point-of-care assays. This study demonstrates their utility in immunoassays and hydrolase activity assays. The techniques and sensors described herein can be adapted for numerous biomarkers relevant to various disease states. However, applying GMR SV sensors in clinical settings will necessitate additional work, including the integration of microfluidics, scalability, and further clinical validation.

Microfluidics will be crucial for multiplexing specific assays. In immunoassays, the antibodies used may not be conducive to creating bioassays that perform effectively under the same dilution factor. The incorporation of microfluidics will enable multiple dilution factors to be tested on the same chip (Kim et al., 2008). Moreover, while Tween-20 and BSA in PBS solution serve as optimal buffers for immunoassays, the endonuclease assay yields optimal results in specific commercial buffers. The ability to employ multiple solutions on a microfluidics platform has already been demonstrated (Huang et al., 2021). Leveraging microfluidics to conduct bioassays in various buffers on the same chip can further enhance the performance of multiplexed assays.

As elucidated in chapter 2, the surface functionalization technique employed in magnetic bioassays is pivotal for achieving efficacy. Establishing covalent bonds between substrates and the sensor surface ensures robustness and stability. When adapting these sensors for future assays, researchers must prioritize a reliable and effective surface chemistry technique suitable for the substrates and affinity reagents employed. Furthermore, the choice of substrates is crucial. Chapter 3 demonstrates that while the IL-6 and IBP4 assays performed well with a traditional antibody-antigen sandwich assay, the SHBG assay necessitated a dual-binding assay for efficacy. This

underscores the critical role of reagents in assay performance. Future endeavors must assess the quality and consistency of affinity reagents utilized.

Hydrolase assays can benefit from lyophilized enzymes and pre-functionalized substrates on the sensor surface prior to sample addition. These enzymes can serve as controls for sample volume, viscosity, etc. For instance, when a smaller sputum sample is added to the sensor surface, the lyophilized control enzyme will cleave the control substrate at a rate proportional to the sample volume, as the concentration will be modulated by the sample volume.

5.4 Future directions

This work clearly demonstrates the utility of GMR assays for pregnancy monitoring. However, future research should expand the range of biomarkers measured by these assays. For instance, Placental Growth Factor and Pregnancy-associated Plasma Protein A have shown potential in predicting pre-eclampsia, a leading cause of fetal and maternal morbidity and mortality worldwide (Danielli et al., 2022). Incorporating a broader array of biomarkers into GMR sensor assays would significantly enhance the ability of obstetricians to provide comprehensive patient care. The development of such multiplexed assays will heavily rely on advancements in microfluidics.

Additionally, expanding the range of enzymes detectable by GMR sensors is critical. While an assay for Cas12a activity has been developed (Im et al., 2024), creating assays for other CRISPR-associated proteins, such as Cas9, would provide valuable tools for biomedical researchers developing genetic modification techniques. Furthermore, although this work has demonstrated assays for protease and nuclease activities, developing assays for lipase and carbohydrase activities would benefit both researchers and clinicians. Significant effort is required to create substrates for these enzymes, as they do not easily lend themselves to surface-based

assays like proteases and nucleases. For example, the hydrophobic nature of lipids necessitates the prevention of substrate crowding, and carbohydrates are challenging to conjugate to sensors and magnetic nanoparticles (MNPs). Overcoming these challenges to develop substrates for lipases and carbohydrases would enable the use of GMR sensors in multiplexed assays involving a wide array of enzymes relevant to both research and clinical applications.

In summary, the sensor platform presented in this study represents a step forward in magnetic bioassays. This platform offers an adaptable and point-of-care capable solution, addressing limitations inherent in traditional methods. With potential applications across diverse biomedical domains, this innovation lays the groundwork for precise enzymatic activity and antigen analysis, promising to empower researchers and clinicians in unraveling the complexities of multiple biomarkers and their implications in health and disease.

Acknowledgements

Chapter 5, in part, is a reprint of the journal article “A GMR Enzymatic Assay for Quantifying Nuclease and Peptidase Activity” as it appears in *Frontiers in Bioengineering and Biotechnology* by Michael Sveiven, Ana Serrano, Joshua Rosenberg, Doug Conrad, Drew A. Hall, and Anthony J. O’Donoghue, Mar 2024. In addition, Chapter 5, in part, is a reprint of the journal article “A Dual-Binding, Magnetic Immunoassay to Predict Spontaneous Preterm Birth” as it appears in *Frontiers in Bioengineering and Biotechnology* by Michael Sveiven, Andrew Gassman, Joshua Rosenberg, Jay Boniface, Matthew Chan, Anthony J. O’Donoghue, Louise Laurent, and Drew A. Hall, Sep 2023. The dissertation author was the first author of these papers.

APPENDICES

Diaza-Silane Surface Chemistry Protocol:

1. Wash with 600 µL each of Acetone, Methanol, and Isopropanol
2. 3 min in UV Ozone cleaner
3. Incubate sensors in 50 µL of 5 mg/mL succinic anhydride in dichloromethane and 50µL of 10% v/v diaza-silane (1x) in dichloromethane for 1 hr 30 min
4. Wash with 1 mL distilled water
5. 15 min of 100 µL of NHS-EDC 5% (1x)
6. Wash with 1 mL distilled water
7. Spot sensors with reagents
8. Incubate overnight at 4ºC in humidity chamber

Polyethylenimine Surface Chemistry Protocol:

1. Wash with 600 µL each of Acetone, Methanol, and Isopropanol
2. 10 minutes in UV Ozone Cleaner
3. Incubate 2% polyethylenimine in deionized water for 2 minutes
4. Wash with 1 mL of distilled water
5. Bake at 150ºC for 5 minutes to solidify adsorbed polyethylenimine
6. Spot with reagents
7. Incubate overnight at 4 degrees in humidity chamber

PEMA-PAAM Surface Chemistry Protocol:

1. Wash with 600 µL each of Acetone, Methanol, and Isopropanol
2. 10 min in UV Ozone cleaner
3. Boil 1.5% poly(ethylene-alt-maleic anhydride) 0.2 M MES buffer pH 6 until solution is clear
4. Add 100 µL of 1% polyallylamine in 0.2 M MES buffer pH 6 for 10 minutes
5. Wash with 600 µL of distilled water
6. Bake chip at 110ºC for 1 hr 30 min
7. Add 100 µL of 1.5% hydrolyzed poly(ethylene-alt-maleic anhydride) for 5 minutes
8. Wash with 1 mL of distilled water
9. Bake chip at 160ºC for 1 hr
10. Spot sensors with reagents
11. Incubate overnight at 4ºC in humidity chamber

NHS-EDC with PEMA-PAAM Surface Chemistry Protocol:

1. Wash with 600 µL each of Acetone, Methanol, and Isopropanol
2. 10 min in UV Ozone cleaner
3. Boil 1.5% poly(ethylene-alt-maleic anhydride) 0.2 M MES buffer pH 6 until solution is clear
4. Add 100 µL of 1% polyallylamine in 0.2 M MES buffer pH 6 for 10 minutes
5. Wash with 600 µL of distilled water
6. Bake chip at 110ºC for 1 hr 30 min
7. Add 100 µL of 1.5% hydrolyzed poly(ethylene-alt-maleic anhydride) for 5 minutes
8. Wash with 1 mL of distilled water
9. Bake chip at 160ºC for 1 hr
10. Add 10% NHS and 10% EDC in distilled water for 15 minutes
11. Wash with 1 mL of distilled water
12. Spot sensors with reagents
13. Incubate overnight at 4ºC in humidity chamber

APTES Surface Chemistry Protocol:

1. Wash with 600 µL each of Acetone, Methanol, and Isopropanol
2. 3 min in UV Ozone cleaner
3. 50 µL of 1% (50nM) KOH for 10 min at 37°C
4. Wash with 1 mL distilled water
5. Dry the surface
6. Add 100 µL of 0.25% APTES in PBS for 1 hr at 37°C
7. Use parafilm to seal the top of well
8. Wash with 1 mL 1X PBS (3 times)
9. Spot sensors with reagents
10. Incubate overnight at 4ºC in humidity chamber

REFERENCES

Adem, S., Jain, S., Sveiven, M., Zhou, X., O'Donoghue, A.J., Hall, D.A., 2020. Giant magnetoresistive biosensors for real-time quantitative detection of protease activity. Sci. Rep. 10, 7941. https://doi.org/10.1038/s41598-020-62910-2

Akinwunmi, B., Ming, W.-K., 2022. Evaluating Vaginal Progesterone in Preventing Recurrent Preterm Birth: A Call to Action. JAMA Netw. Open 5, e2242247. https://doi.org/10.1001/jamanetworkopen.2022.42247

Alba, A.C., Agoritsas, T., Walsh, M., Hanna, S., Iorio, A., Devereaux, P.J., McGinn, T., Guyatt, G., 2017. Discrimination and Calibration of Clinical Prediction Models: Users' Guides to the Medical Literature. JAMA 318, 1377–1384. https://doi.org/10.1001/jama.2017.12126

Anderson, D.C., 1974. Sex-Hormone-Binding Globulin. Clin. Endocrinol. (Oxf.) 3, 69–96. https://doi.org/10.1111/j.1365-2265.1974.tb03298.x

Antarnusa, G., Esmawan, A., Dwi Jayanti, P., Rizki Fitriani, S., Suherman, A., Kinarya Palupi, E., Umam, R., Ardimas, 2022. Synthesis of Fe3O4 at different reaction temperatures and investigation of its magnetic properties on giant magnetoresistance (GMR) sensors for bio-detection applications. J. Magn. Magn. Mater. 563, 169903. https://doi.org/10.1016/j.jmmm.2022.169903

Armbruster, D.A., Pry, T., 2008. Limit of Blank, Limit of Detection and Limit of Quantitation. Clin. Biochem. Rev. 29, S49–S52.

Armstrong, P.B., 2001. The contribution of proteinase inhibitors to immune defense. Trends Immunol. 22, 47–52. https://doi.org/10.1016/S1471-4906(00)01803-2

Arshavsky-Graham, S., Segal, E., 2022. Lab-on-a-Chip Devices for Point-of-Care Medical Diagnostics, in: Bahnemann, J., Grünberger, A. (Eds.), Microfluidics in Biotechnology, Advances in Biochemical Engineering/Biotechnology. Springer International Publishing, Cham, pp. 247–265. https://doi.org/10.1007/10_2020_127

Autran, C.A., Kellman, B.P., Kim, J.H., Asztalos, E., Blood, A.B., Spence, E.C.H., Patel, A.L., Hou, J., Lewis, N.E., Bode, L., 2018. Human milk oligosaccharide composition predicts risk of necrotising enterocolitis in preterm infants. Gut 67, 1064–1070. https://doi.org/10.1136/gutjnl-2016-312819

Balian, A., Hernandez, F.J., 2021. Nucleases as molecular targets for cancer diagnosis. Biomark. Res. 9, 86. https://doi.org/10.1186/s40364-021-00342-4

Bao, Q., Lin, D., Gao, Y., Wu, L., Fu, J., Galaa, K., Lin, X., Lin, L., 2021. Ultrasensitive off-on-off fluorescent nanosensor for protamine and trypsin detection based on inner-filter effect between N,S-CDs and gold nanoparticles. Microchem. J. 168, 106409. https://doi.org/10.1016/j.microc.2021.106409

Barnaś, J., Fuss, A., Camley, R.E., Grünberg, P., Zinn, W., 1990. Novel magnetoresistance effect in layered magnetic structures: Theory and experiment. Phys. Rev. B 42, 8110–8120. https://doi.org/10.1103/PhysRevB.42.8110

Baselt, D.R., Lee, G.U., Natesan, M., Metzger, S.W., Sheehan, P.E., Colton, R.J., 1998. A biosensor based on magnetoresistance technology1This paper was awarded the Biosensors & Bioelectronics Award for the most original contribution to the Congress.1. Biosens. Bioelectron. 13, 731–739. https://doi.org/10.1016/S0956-5663(98)00037-2

Betz, D., Fane, K., 2022. Human Chorionic Gonadotropin, in: StatPearls. StatPearls Publishing, Treasure Island (FL).

Biggio, J.R., Morris, T.C., Owen, J., Stringer, J.S.A., 2004. An outcomes analysis of five prenatal screening strategies for trisomy 21 in women younger than 35 years. Am. J. Obstet. Gynecol. 190, 721–729. https://doi.org/10.1016/j.ajog.2003.09.028

Bikker, F.J., Nascimento, G.G., Nazmi, K., Silbereisen, A., Belibasakis, G.N., Kaman, W.E., Lopez, R., Bostanci, N., 2019. Salivary Total Protease Activity Based on a Broad-Spectrum Fluorescence Resonance Energy Transfer Approach to Monitor Induction and Resolution of Gingival Inflammation. Mol. Diagn. Ther. 23, 667–676. https://doi.org/10.1007/s40291-019-00421-1

Boelig, R.C., Locci, M., Saccone, G., Gragnano, E., Berghella, V., 2022. Vaginal progesterone compared with intramuscular 17-alpha-hydroxyprogesterone caproate for prevention of recurrent preterm birth in singleton gestations: a systematic review and meta-analysis. Am. J. Obstet. Gynecol. MFM 4, 100658. https://doi.org/10.1016/j.ajogmf.2022.100658

Booker, W.A., Reed, E.G., Power, M.L., Schulkin, J., Gyamfi-Bannerman, C., Manuck, T., Berghella, V., Vink, J., 2021. OBGYN practice patterns regarding combination therapy for prevention of preterm birth: A national survey. Eur. J. Obstet. Gynecol. Reprod. Biol. 266, 23–30. https://doi.org/10.1016/j.ejogrb.2021.09.003

Boyle, A.K., Rinaldi, S.F., Norman, J.E., Stock, S.J., 2017. Preterm birth: Inflammation, fetal injury and treatment strategies. J. Reprod. Immunol. 119, 62–66. https://doi.org/10.1016/j.jri.2016.11.008

Bradford, C., Severinsen, R., Pugmire, T., Rasmussen, M., Stoddard, K., Uemura, Y., Wheelwright, S., Mentinova, M., Chelsky, D., Hunsucker, S.W., Kearney, P., Hickok, D., Fleischer, T.C., Ichetovkin, I., Boniface, J.J., Critchfield, G.C., Peltier, J.M., 2017. Analytical validation of protein biomarkers for risk of spontaneous preterm birth. Clin. Mass Spectrom. 3, 25–38. https://doi.org/10.1016/j.clinms.2017.06.002

Brock, D.J., Scrimgeour, J.B., Bolton, A.E., Wald, N., Peto, R., Barker, S., 1975. Effect of gestational age on screening for neural-tube defects by maternal plasma-A.F.P. measurement. Lancet Lond. Engl. 2, 195–196. https://doi.org/10.1016/s0140-6736(75)90669-8

Burchard, J., Polpitiya, A.D., Fox, A.C., Randolph, T.L., Fleischer, T.C., Dufford, M.T., Garite, T.J., Critchfield, G.C., Boniface, J.J., Saade, G.R., Kearney, P.E., 2021. Clinical Validation of a Proteomic Biomarker Threshold for Increased Risk of Spontaneous Preterm Birth and Associated Clinical Outcomes: A Replication Study. J. Clin. Med. 10, 5088. https://doi.org/10.3390/jcm10215088

Callen, J.L., Westbrook, J.I., Georgiou, A., Li, J., 2012. Failure to follow-up test results for ambulatory patients: a systematic review. J. Gen. Intern. Med. 27, 1334–1348. https://doi.org/10.1007/s11606-011-1949-5

Cannalire, G., Pilloni, S., Esposito, S., Biasucci, G., Franco, A.D., Street, M.E., 2023. Alkaline phosphatase in clinical practice in childhood: Focus on rickets. Front. Endocrinol. 14. https://doi.org/10.3389/fendo.2023.1111445

Cao, B., Wang, K., Xu, H., Qin, Q., Yang, J., Zheng, W., Jin, Q., Cui, D., 2020. Development of magnetic sensor technologies for point-of-care testing: Fundamentals, methodologies and applications. Sens. Actuators Phys. 312, 112130. https://doi.org/10.1016/j.sna.2020.112130

Casalino, L.P., Dunham, D., Chin, M.H., Bielang, R., Kistner, E.O., Karrison, T.G., Ong, M.K., Sarkar, U., McLaughlin, M.A., Meltzer, D.O., 2009. Frequency of failure to inform patients

of clinically significant outpatient test results. Arch. Intern. Med. 169, 1123–1129. https://doi.org/10.1001/archinternmed.2009.130

Chan, L.W., Anahtar, M.N., Ong, T.-H., Hern, K.E., Kunz, R.R., Bhatia, S.N., 2020. Engineering synthetic breath biomarkers for respiratory disease. Nat. Nanotechnol. 15, 792–800. https://doi.org/10.1038/s41565-020-0723-4

Chang, C.-C., 2021. Recent Advancements in Aptamer-Based Surface Plasmon Resonance Biosensing Strategies. Biosensors 11, 233. https://doi.org/10.3390/bios11070233

Chen, H., Zhang, J., Gao, Y., Liu, S., Koh, K., Zhu, X., Yin, Y., 2015. Sensitive cell apoptosis assay based on caspase-3 activity detection with graphene oxide-assisted electrochemical signal amplification. Biosens. Bioelectron. 68, 777–782. https://doi.org/10.1016/j.bios.2015.02.007

Chen, J.H.-K., Yip, C.C.-Y., Poon, R.W.-S., Chan, K.-H., Cheng, V.C.-C., Hung, I.F.-N., Chan, J.F.-W., Yuen, K.-Y., To, K.K.-W., 2020. Evaluating the use of posterior oropharyngeal saliva in a point-of-care assay for the detection of SARS-CoV-2. Emerg. Microbes Infect. 9, 1356–1359. https://doi.org/10.1080/22221751.2020.1775133

Chen, W., Jiang, X., Yang, Q., 2020. Glycoside hydrolase family 18 chitinases: The known and the unknown. Biotechnol. Adv. 43, 107553. https://doi.org/10.1016/j.biotechadv.2020.107553

Chen, Y.-T., Lee, Y.-C., Lai, Y.-H., Lim, J.-C., Huang, N.-T., Lin, C.-T., Huang, J.-J., 2020. Review of Integrated Optical Biosensors for Point-of-Care Applications. Biosensors 10, 209. https://doi.org/10.3390/bios10120209

Choi, J., Gani, A.W., Bechstein, D.J.B., Lee, J.-R., Utz, P.J., Wang, S.X., 2016. Portable, one-step, and rapid GMR biosensor platform with smartphone interface. Biosens. Bioelectron. 85, 1–7. https://doi.org/10.1016/j.bios.2016.04.046

Chojnowska, S., Baran, T., Wilińska, I., Sienicka, P., Cabaj-Wiater, I., Knaś, M., 2018. Human saliva as a diagnostic material. Adv. Med. Sci. 63, 185–191. https://doi.org/10.1016/j.advms.2017.11.002

Conde-Agudelo, A., Romero, R., 2022. Vaginal progesterone for the prevention of preterm birth: who can benefit and who cannot? Evidence-based recommendations for clinical use. J. Perinat. Med. https://doi.org/10.1515/jpm-2022-0462

Conde-Agudelo, A., Romero, R., Da Fonseca, E., O'Brien, J.M., Cetingoz, E., Creasy, G.W., Hassan, S.S., Erez, O., Pacora, P., Nicolaides, K.H., 2018. Vaginal progesterone is as effective as cervical cerclage to prevent preterm birth in women with a singleton gestation, previous spontaneous preterm birth, and a short cervix: updated indirect comparison meta-analysis. Am. J. Obstet. Gynecol. 219, 10–25. https://doi.org/10.1016/j.ajog.2018.03.028

Costantine, M.M., Weiner, S.J., 2009. Effects of Antenatal Exposure to Magnesium Sulfate on Neuroprotection and Mortality in Preterm Infants: A Meta-Analysis. Obstet. Gynecol. 114, 354–364. https://doi.org/10.1097/AOG.0b013e3181ae98c2

Crowther, J.R., 2008. ELISA: Theory and Practice. Springer Science & Business Media.

Danielli, M., Thomas, R.C., Gillies, C.L., Hu, J., Khunti, K., Tan, B.K., 2022. Blood biomarkers to predict the onset of pre-eclampsia: A systematic review and meta-analysis. Heliyon 8, e11226. https://doi.org/10.1016/j.heliyon.2022.e11226

de Freitas Nakata, K.C., da Silva Pereira, P.P., Salgado Riveros, B., 2021. Creatine kinase test diagnostic accuracy in neonatal screening for Duchenne Muscular Dystrophy: A systematic review. Clin. Biochem. 98, 1–9. https://doi.org/10.1016/j.clinbiochem.2021.09.010

des Gachons, C.P., Breslin, P.A.S., 2016. Salivary Amylase: Digestion and Metabolic Syndrome. Curr. Diab. Rep. 16, 102. https://doi.org/10.1007/s11892-016-0794-7

Ding, X., Yang, K.-L., 2014. Enzymatic Deposition of Silver Particles for Detecting Protease Activity. Part. Part. Syst. Charact. 31, 1300–1306. https://doi.org/10.1002/ppsc.201400107

Dittrich, A.S., Kühbandner, I., Gehrig, S., Rickert-Zacharias, V., Twigg, M., Wege, S., Taggart, C.C., Herth, F., Schultz, C., Mall, M.A., 2018. Elastase activity on sputum neutrophils correlates with severity of lung disease in cystic fibrosis. Eur. Respir. J. 51, 1701910. https://doi.org/10.1183/13993003.01910-2017

Doyle, L.W., Crowther, C.A., Middleton, P., Marret, S., Rouse, D., 2009. Magnesium sulphate for women at risk of preterm birth for neuroprotection of the fetus. Cochrane Database Syst. Rev. https://doi.org/10.1002/14651858.CD004661.pub3

Eatemadi, A., Aiyelabegan, H.T., Negahdari, B., Mazlomi, M.A., Daraee, H., Daraee, N., Eatemadi, R., Sadroddiny, E., 2017. Role of protease and protease inhibitors in cancer pathogenesis and treatment. Biomed. Pharmacother. 86, 221–231. https://doi.org/10.1016/j.biopha.2016.12.021

Ekelund, L., Laurell, C.-B., 1994. The pregnancy zone protein response during gestation: A metabolic challenge. Scand. J. Clin. Lab. Invest. 54, 623–629. https://doi.org/10.3109/00365519409087542

Feng, Y., Li, Q., Chen, J., Yi, P., Xu, X., Fan, Y., Cui, B., Yu, Y., Li, X., Du, Y., Chen, Q., Zhang, L., Jiang, J., Zhou, X., Zhang, P., 2019. Salivary protease spectrum biomarkers of oral cancer. Int. J. Oral Sci. 11, 1–11. https://doi.org/10.1038/s41368-018-0032-z

Flenady, V., Wojcieszek, A.M., Papatsonis, D.N., Stock, O.M., Murray, L., Jardine, L.A., Carbonne, B., 2014. Calcium channel blockers for inhibiting preterm labour and birth. Cochrane Database Syst. Rev. 2014, CD002255. https://doi.org/10.1002/14651858.CD002255.pub2

Flenker, K.S., Burghardt, E.L., Dutta, N., Burns, W.J., Grover, J.M., Kenkel, E.J., Weaver, T.M., Mills, J., Kim, H., Huang, L., Owczarzy, R., Musselman, C.A., Behlke, M.A., Ford, B., McNamara, J.O., 2017. Rapid Detection of Urinary Tract Infections via Bacterial Nuclease Activity. Mol. Ther. 25, 1353–1362. https://doi.org/10.1016/j.ymthe.2017.03.015

Fonseca, E.B., Celik, E., Parra, M., Singh, M., Nicolaides, K.H., Fetal Medicine Foundation Second Trimester Screening Group, 2007. Progesterone and the risk of preterm birth among women with a short cervix. N. Engl. J. Med. 357, 462–469. https://doi.org/10.1056/NEJMoa067815

Garcia Gonzalez, J., Hernandez, F.J., 2022. Nuclease activity: an exploitable biomarker in bacterial infections. Expert Rev. Mol. Diagn. 22, 265–294. https://doi.org/10.1080/14737159.2022.2049249

Garite, T.J., Manuck, T.A., 2022. Should case management be considered a component of obstetrical interventions for pregnancies at risk of preterm birth? Am. J. Obstet. Gynecol. https://doi.org/10.1016/j.ajog.2022.09.022

Gaster, R.S., Hall, D.A., Nielsen, C.H., Osterfeld, S.J., Yu, H., Mach, K.E., Wilson, R.J., Murmann, B., Liao, J.C., Gambhir, S.S., Wang, S.X., 2009. Matrix-insensitive protein assays push the limits of biosensors in medicine. Nat. Med. 15, 1327–1332. https://doi.org/10.1038/nm.2032

Gaster, R.S., Hall, D.A., Wang, S.X., 2013. Magneto-Nanosensor Diagnostic Chips, in: Issadore, D., Westervelt, R.M. (Eds.), Point-of-Care Diagnostics on a Chip, Biological and Medical

Physics, Biomedical Engineering. Springer, Berlin, Heidelberg, pp. 153–176. https://doi.org/10.1007/978-3-642-29268-2_7
Goldenberg, R.L., Culhane, J.F., Iams, J.D., Romero, R., 2008. Epidemiology and causes of preterm birth. The Lancet 371, 75–84. https://doi.org/10.1016/S0140-6736(08)60074-4
Gong, Y., Zheng, Y., Jin, B., You, M., Wang, J., Li, X., Lin, M., Xu, F., Li, F., 2019. A portable and universal upconversion nanoparticle-based lateral flow assay platform for point-of-care testing. Talanta 201, 126–133. https://doi.org/10.1016/j.talanta.2019.03.105
Grishkovskaya, I., Avvakumov, G.V., Sklenar, G., Dales, D., Hammond, G.L., Muller, Y.A., 2000. Crystal structure of human sex hormone-binding globulin: steroid transport by a laminin G-like domain. EMBO J. 19, 504–512. https://doi.org/10.1093/emboj/19.4.504
Haas, D.M., Caldwell, D.M., Kirkpatrick, P., McIntosh, J.J., Welton, N.J., 2012. Tocolytic therapy for preterm delivery: systematic review and network meta-analysis. BMJ 345, e6226. https://doi.org/10.1136/bmj.e6226
Haghighi, L., Rashidi, M., Najmi, Z., Homam, H., Hashemi, N., Mobasseri, A., Moradi, Y., 2017. Comparison of intramuscular progesterone with oral nifedipine for treating threatened preterm labor: A randomized controlled trial. Med. J. Islam. Repub. Iran 31, 56. https://doi.org/10.14196/mjiri.31.56
Hall, D.A., Gaster, R.S., Lin, T., Osterfeld, S.J., Han, S., Murmann, B., Wang, S.X., 2010a. GMR biosensor arrays: A system perspective. Biosens. Bioelectron. 25, 2051–2057. https://doi.org/10.1016/j.bios.2010.01.038
Hall, D.A., Gaster, R.S., Osterfeld, S.J., Murmann, B., Wang, S.X., 2010b. GMR biosensor arrays: Correction techniques for reproducibility and enhanced sensitivity. Biosens. Bioelectron. 25, 2177–2181. https://doi.org/10.1016/j.bios.2010.01.039
Hammond, E., Ferro, V., 2023. An Enzymatic Activity Assay for Heparanase That Is Useful for Evaluating Clinically Relevant Inhibitors and Studying Kinetics, in: Karamanos, N.K. (Ed.), Proteoglycans: Methods and Protocols, Methods in Molecular Biology. Springer US, New York, NY, pp. 227–238. https://doi.org/10.1007/978-1-0716-2946-8_16
Hao Ong, I.L., Yang, K.-L., 2017. Recent developments in protease activity assays and sensors. Analyst 142, 1867–1881. https://doi.org/10.1039/C6AN02647H
Hirai, K., Yamaguchi-Tomikawa, T., Eguchi, T., Maeda, H., Takashiba, S., 2020. Identification and Modification of Porphyromonas gingivalis Cysteine Protease, Gingipain, Ideal for Screening Periodontitis. Front. Immunol. 11.
Huang, E., Wang, Y., Yang, N., Shu, B., Zhang, G., Liu, D., 2021. A fully automated microfluidic PCR-array system for rapid detection of multiple respiratory tract infection pathogens. Anal. Bioanal. Chem. 413, 1787–1798. https://doi.org/10.1007/s00216-021-03171-4
Im, J., Kim, S., Park, S., Wang, S.X., Lee, J.-R., 2024. Evaluation of restriction and Cas endonuclease kinetics using matrix-insensitive magnetic biosensors. Biosens. Bioelectron. 249, 116017. https://doi.org/10.1016/j.bios.2024.116017
Jung, K., Zachow, J., Lein, M., Brux, B., Sinha, P., Lenk, S., Schnorr, D., Loening, S.A., 1999. Rapid detection of elevated prostate-specific antigen levels in blood: performance of various membrane strip tests compared11This study includes parts of the doctoral thesis of Jürgen Zachow. Urology 53, 155–160. https://doi.org/10.1016/S0090-4295(98)00419-1
Kafienah, W., Buttle, D.J., Burnett, D., Hollander, A.P., 1998. Cleavage of native type I collagen by human neutrophil elastase. Biochem. J. 330, 897–902.

Kårlund, A., Paukkonen, I., Gómez-Gallego, C., Kolehmainen, M., 2021. Intestinal Exposure to Food-Derived Protease Inhibitors: Digestion Physiology- and Gut Health-Related Effects. Healthcare 9, 1002. https://doi.org/10.3390/healthcare9081002

Kawabata, K., Hagio, T., Matsuoka, S., 2002. The role of neutrophil elastase in acute lung injury. Eur. J. Pharmacol. 451, 1–10. https://doi.org/10.1016/S0014-2999(02)02182-9

Kearney, P., Boniface, J.J., Price, N.D., Hood, L., 2018. The building blocks of successful translation of proteomics to the clinic. Curr. Opin. Biotechnol. 51, 123–129. https://doi.org/10.1016/j.copbio.2017.12.011

Kim, C., Lee, K., Hyun Kim, J., Sik Shin, K., Lee, K.-J., Song Kim, T., Yoon Kang, J., 2008. A serial dilution microfluidic device using a ladder network generating logarithmic or linear concentrations. Lab. Chip 8, 473–479. https://doi.org/10.1039/B714536E

Kim, D., Marchetti, F., Chen, Z., Zaric, S., Wilson, R.J., Hall, D.A., Gaster, R.S., Lee, J.-R., Wang, J., Osterfeld, S.J., Yu, H., White, R.M., Blakely, W.F., Peterson, L.E., Bhatnagar, S., Mannion, B., Tseng, S., Roth, K., Coleman, M., Snijders, A.M., Wyrobek, A.J., Wang, S.X., 2013. Nanosensor dosimetry of mouse blood proteins after exposure to ionizing radiation. Sci. Rep. 3, 2234. https://doi.org/10.1038/srep02234

Klein, T., Wang, W., Yu, L., Wu, K., Boylan, K.L.M., Vogel, R.I., Skubitz, A.P.N., Wang, J.-P., 2019. Development of a multiplexed giant magnetoresistive biosensor array prototype to quantify ovarian cancer biomarkers. Biosens. Bioelectron. 126, 301–307. https://doi.org/10.1016/j.bios.2018.10.046

Krishna, V.D., Wu, K., Perez, A.M., Wang, J.-P., 2016. Giant Magnetoresistance-based Biosensor for Detection of Influenza A Virus. Front. Microbiol. 7.

Kumar, S., Nodoushani, A., Khanam, F., DeCruz, A.T., Lambotte, P., Scott, R., Bogoch, I.I., Vaidya, K., Calderwood, S.B., Bhuiyan, T.R., Esfandiari, J., Ryan, E.T., Qadri, F., Andrews, J.R., Charles, R.C., 2020. Evaluation of a Rapid Point-of-Care Multiplex Immunochromatographic Assay for the Diagnosis of Enteric Fever. mSphere 5, e00253-20. https://doi.org/10.1128/mSphere.00253-20

Lauková, L., Konečná, B., Janovičová, Ľ., Vlková, B., Celec, P., 2020. Deoxyribonucleases and Their Applications in Biomedicine. Biomolecules 10, 1036. https://doi.org/10.3390/biom10071036

Li, S., Zhang, M., Tian, H., Liu, Z., Yin, X., Xi, B., 2014. Preterm birth and risk of type 1 and type 2 diabetes: systematic review and meta-analysis. Obes. Rev. 15, 804–811. https://doi.org/10.1111/obr.12214

Lichtenthaler, S.F., Tschirner, S.K., Steiner, H., 2022. Secretases in Alzheimer's disease: Novel insights into proteolysis of APP and TREM2. Curr. Opin. Neurobiol. 72, 101–110. https://doi.org/10.1016/j.conb.2021.09.003

Lin, C.-W., Chen, J.-M., Lin, Y.-J., Chao, L.-W., Wei, S.-Y., Wu, C.-H., Jeng, C.-C., Wang, L.-M., Chen, K.-L., 2019. Magneto-Optical Characteristics of Streptavidin-Coated Fe3O4@Au Core-Shell Nanoparticles for Potential Applications on Biomedical Assays. Sci. Rep. 9, 16466. https://doi.org/10.1038/s41598-019-52773-7

Lin, X., Nie, Y., 2022. Pregnant Populations which Benefit from Vaginal Progesterone for Preventing Preterm Birth at <34 Weeks and Neonatal Morbidities: A Systematic Review and Meta-analysis. Am. J. Perinatol. https://doi.org/10.1055/a-1877-5827

Liu, L., Johnson, H.L., Cousens, S., Perin, J., Scott, S., Lawn, J.E., Rudan, I., Campbell, H., Cibulskis, R., Li, M., Mathers, C., Black, R.E., 2012. Global, regional, and national causes

of child mortality: an updated systematic analysis for 2010 with time trends since 2000. The Lancet 379, 2151–2161. https://doi.org/10.1016/S0140-6736(12)60560-1

Liu, W.-L., Liu, D., Cheng, K., Liu, Y.-J., Xing, S., Chi, P.-D., Liu, X.-H., Xue, N., Lai, Y.-Z., Guo, L., Zhang, G., 2016. Evaluating the diagnostic and prognostic value of circulating cathepsin S in gastric cancer. Oncotarget 7, 28124–28138. https://doi.org/10.18632/oncotarget.8582

Lockwood, C.J., Senyei, A.E., Dische, M.R., Casal, D., Shah, K.D., Thung, S.N., Jones, L., Deligdisch, L., Garite, T.J., 1991. Fetal fibronectin in cervical and vaginal secretions as a predictor of preterm delivery. N. Engl. J. Med. 325, 669–674. https://doi.org/10.1056/NEJM199109053251001

Lucena, F., McDougall, J.J., 2021. Protease Activated Receptors and Arthritis. Int. J. Mol. Sci. 22, 9352. https://doi.org/10.3390/ijms22179352

Luu, T.M., Mian, M.O.R., Nuyt, A.M., 2017. Long-Term Impact of Preterm Birth: Neurodevelopmental and Physical Health Outcomes. Clin. Perinatol. 44, 305–314. https://doi.org/10.1016/j.clp.2017.01.003

Machado, I., Garrido, V., Hernandez, L.I., Botero, J., Bastida, N., San-Roman, B., Grilló, M.-J., Hernandez, F.J., 2019. Rapid and specific detection of Salmonella infections using chemically modified nucleic acid probes. Anal. Chim. Acta 1054, 157–166. https://doi.org/10.1016/j.aca.2018.12.027

Mahmoudi, T., de la Guardia, M., Baradaran, B., 2020. Lateral flow assays towards point-of-care cancer detection: A review of current progress and future trends. TrAC Trends Anal. Chem. 125, 115842. https://doi.org/10.1016/j.trac.2020.115842

Martha, J.W., Wibowo, A., Pranata, R., 2022. Prognostic value of elevated lactate dehydrogenase in patients with COVID-19: a systematic review and meta-analysis. Postgrad. Med. J. 98, 422–427. https://doi.org/10.1136/postgradmedj-2020-139542

Mecham, R.P., Broekelmann, T.J., Fliszar, C.J., Shapiro, S.D., Welgus, H.G., Senior, R.M., 1997. Elastin Degradation by Matrix Metalloproteinases: CLEAVAGE SITE SPECIFICITY AND MECHANISMS OF ELASTOLYSIS *. J. Biol. Chem. 272, 18071–18076. https://doi.org/10.1074/jbc.272.29.18071

Meis, P.J., Klebanoff, M., Thom, E., Dombrowski, M.P., Sibai, B., Moawad, A.H., Spong, C.Y., Hauth, J.C., Miodovnik, M., Varner, M.W., Leveno, K.J., Caritis, S.N., Iams, J.D., Wapner, R.J., Conway, D., O'Sullivan, M.J., Carpenter, M., Mercer, B., Ramin, S.M., Thorp, J.M., Peaceman, A.M., Gabbe, S., National Institute of Child Health and Human Development Maternal-Fetal Medicine Units Network, 2003. Prevention of recurrent preterm delivery by 17 alpha-hydroxyprogesterone caproate. N. Engl. J. Med. 348, 2379–2385. https://doi.org/10.1056/NEJMoa035140

Mennella, I., Fogliano, V., Vitaglione, P., 2014. Salivary lipase and α-amylase activities are higher in overweight than in normal weight subjects: Influences on dietary behavior. Food Res. Int. 66, 463–468. https://doi.org/10.1016/j.foodres.2014.10.008

Menon, S., Mathew, M.R., Sam, S., Keerthi, K., Kumar, K.G., 2020. Recent advances and challenges in electrochemical biosensors for emerging and re-emerging infectious diseases. J. Electroanal. Chem. Lausanne Switz. 878, 114596. https://doi.org/10.1016/j.jelechem.2020.114596

Moll, T., Shaw, P.J., Cooper-Knock, J., 2020. Disrupted glycosylation of lipids and proteins is a cause of neurodegeneration. Brain 143, 1332–1340. https://doi.org/10.1093/brain/awz358

Mondanelli, G., Iacono, A., Carvalho, A., Orabona, C., Volpi, C., Pallotta, M.T., Matino, D., Esposito, S., Grohmann, U., 2019. Amino acid metabolism as drug target in autoimmune diseases. Autoimmun. Rev. 18, 334–348. https://doi.org/10.1016/j.autrev.2019.02.004

Mostufa, S., Rezaei, B., Yari, P., Xu, K., Gómez-Pastora, J., Sun, J., Shi, Z., Wu, K., 2023. Giant Magnetoresistance Based Biosensors for Cancer Screening and Detection. ACS Appl. Bio Mater. 6, 4042–4059. https://doi.org/10.1021/acsabm.3c00592

Najeeb, S., Munir, T., Rehman, S., Hafiz, A., Gilani, M., Latif, M., 2015. Comparison of urine dipstick test with conventional urine culture in diagnosis of urinary tract infection. J. Coll. Physicians Surg.--Pak. JCPSP 25, 108–110.

Nazar Majeed, Z., Philip, K., Alabsi, A.M., Pushparajan, S., Swaminathan, D., 2016. Identification of Gingival Crevicular Fluid Sampling, Analytical Methods, and Oral Biomarkers for the Diagnosis and Monitoring of Periodontal Diseases: A Systematic Review. Dis. Markers 2016, 1804727. https://doi.org/10.1155/2016/1804727

Nelson, D.B., Lafferty, A., Venkatraman, C., McDonald, J.G., Eckert, K.M., McIntire, D.D., Spong, C.Y., 2022. Association of Vaginal Progesterone Treatment With Prevention of Recurrent Preterm Birth. JAMA Netw. Open 5, e2237600. https://doi.org/10.1001/jamanetworkopen.2022.37600

Newby, P.R., Crossley, D., Crisford, H., Stockley, J.A., Mumford, R.A., Carter, R.I., Bolton, C.E., Hopkinson, N.S., Mahadeva, R., Steiner, M.C., Wilkinson, T.M.A., Sapey, E., Stockley, R.A., 2019. A specific proteinase 3 activity footprint in α1-antitrypsin deficiency. ERJ Open Res. 5, 00095–02019. https://doi.org/10.1183/23120541.00095-2019

Ni, J., Lin, H., Yang, W., Liao, Y., Wang, Q., Luo, F., Guo, L., Qiu, B., Lin, Z., 2019. Homogeneous Electrochemiluminescence Biosensor for the Detection of RNase A Activity and Its Inhibitor. Anal. Chem. 91, 14751–14756. https://doi.org/10.1021/acs.analchem.9b04194

Norwitz, E.R., Caughey, A.B., 2011. Progesterone supplementation and the prevention of preterm birth. Rev. Obstet. Gynecol. 4, 60–72.

Nozeret, K., Boucharlat, A., Agou, F., Buddelmeijer, N., 2019. A sensitive fluorescence-based assay to monitor enzymatic activity of the essential integral membrane protein Apolipoprotein N-acyltransferase (Lnt). Sci. Rep. 9, 15978. https://doi.org/10.1038/s41598-019-52106-8

O'Donoghue, A.J., Jin, Y., Knudsen, G.M., Perera, N.C., Jenne, D.E., Murphy, J.E., Craik, C.S., Hermiston, T.W., 2013. Global Substrate Profiling of Proteases in Human Neutrophil Extracellular Traps Reveals Consensus Motif Predominantly Contributed by Elastase. PLoS ONE 8, e75141. https://doi.org/10.1371/journal.pone.0075141

Oishi, J., Asami, Y., Mori, T., Kang, J.-H., Niidome, T., Katayama, Y., 2008. Colorimetric Enzymatic Activity Assay Based on Noncrosslinking Aggregation of Gold Nanoparticles Induced by Adsorption of Substrate Peptides. Biomacromolecules 9, 2301–2308. https://doi.org/10.1021/bm800192d

Olazarra, A.S. de, Cortade, D.L., Wang, S.X., 2022. From saliva to SNP: non-invasive, point-of-care genotyping for precision medicine applications using recombinase polymerase amplification and giant magnetoresistive nanosensors. Lab. Chip 22, 2131–2144. https://doi.org/10.1039/D2LC00233G

O'Leary, P., Boyne, P., Flett, P., Beilby, J., James, I., 1991. Longitudinal assessment of changes in reproductive hormones during normal pregnancy. Clin. Chem. 37, 667–672. https://doi.org/10.1093/clinchem/37.5.667

Oriano, M., Terranova, L., Sotgiu, G., Saderi, L., Bellofiore, A., Retucci, M., Marotta, C., Gramegna, A., Miglietta, D., Carnini, C., Marchisio, P., Chalmers, J.D., Aliberti, S., Blasi, F., 2019. Evaluation of active neutrophil elastase in sputum of bronchiectasis and cystic fibrosis patients: A comparison among different techniques. Pulm. Pharmacol. Ther. 59, 101856. https://doi.org/10.1016/j.pupt.2019.101856

Orzechowski, K.M., Boelig, R.C., Berghella, V., 2016. Cervical Length Screening in Asymptomatic Women at High Risk and Low Risk for Spontaneous Preterm Birth. Clin. Obstet. Gynecol. 59, 241–251. https://doi.org/10.1097/GRF.0000000000000195

Osterfeld, S.J., Yu, H., Gaster, R.S., Caramuta, S., Xu, L., Han, S.-J., Hall, D.A., Wilson, R.J., Sun, S., White, R.L., Davis, R.W., Pourmand, N., Wang, S.X., 2008. Multiplex protein assays based on real-time magnetic nanotag sensing. Proc. Natl. Acad. Sci. 105, 20637–20640. https://doi.org/10.1073/pnas.0810822105

Parkinson, J.R.C., Hyde, M.J., Gale, C., Santhakumaran, S., Modi, N., 2013. Preterm Birth and the Metabolic Syndrome in Adult Life: A Systematic Review and Meta-analysis. Pediatrics 131, e1240–e1263. https://doi.org/10.1542/peds.2012-2177

Peaceman, A.M., Andrews, W.W., Thorp, J.M., Cliver, S.P., Lukes, A., Iams, J.D., Coultrip, L., Eriksen, N., Holbrook, R.H., Elliott, J., Ingardia, C., Pietrantoni, M., 1997. Fetal fibronectin as a predictor of preterm birth in patients with symptoms: a multicenter trial. Am. J. Obstet. Gynecol. 177, 13–18. https://doi.org/10.1016/s0002-9378(97)70431-9

Petrou, S., Yiu, H.H., Kwon, J., 2019. Economic consequences of preterm birth: a systematic review of the recent literature (2009–2017). Arch. Dis. Child. 104, 456–465. https://doi.org/10.1136/archdischild-2018-315778

Ping, J., Wu, W., Qi, L., Liu, Jie, Liu, Jinpeng, Zhao, B., Wang, Q., Yu, L., Lin, J.-M., Hu, Q., 2021. Hydrogel-assisted paper-based lateral flow sensor for the detection of trypsin in human serum. Biosens. Bioelectron. 192, 113548. https://doi.org/10.1016/j.bios.2021.113548

Prinz, G.A., 1998. Magnetoelectronics. Science 282, 1660–1663. https://doi.org/10.1126/science.282.5394.1660

Pu, S., Wang, D., Liu, D., Zhao, Y., Qi, D., He, J., Zhou, G., 2017. Effect of sivelestat sodium in patients with acute lung injury or acute respiratory distress syndrome: a meta-analysis of randomized controlled trials. BMC Pulm. Med. 17, 148. https://doi.org/10.1186/s12890-017-0498-z

Qing, T., Long, C., Wang, X., Zhang, K., Zhang, P., Feng, B., 2019. Detection of micrococcal nuclease for identifying Staphylococcus aureus based on DNA templated fluorescent copper nanoclusters. Mikrochim. Acta 186, 248. https://doi.org/10.1007/s00604-019-3363-3

Qiu, Q., Bell, M., Lu, X., Yan, X., Rodger, M., Walker, M., Wen, S.-W., Bainbridge, S., Wang, H., Gruslin, A., 2012. Significance of IGFBP-4 in the development of fetal growth restriction. J. Clin. Endocrinol. Metab. 97, E1429-1439. https://doi.org/10.1210/jc.2011-2511

Quinn, R.A., Adem, S., Mills, R.H., Comstock, W., DeRight Goldasich, L., Humphrey, G., Aksenov, A.A., Melnik, A.V., da Silva, R., Ackermann, G., Bandeira, N., Gonzalez, D.J., Conrad, D., O'Donoghue, A.J., Knight, R., Dorrestein, P.C., 2019. Neutrophilic proteolysis in the cystic fibrosis lung correlates with a pathogenic microbiome. Microbiome 7, 23. https://doi.org/10.1186/s40168-019-0636-3

Rack, J.G.M., Palazzo, L., Ahel, I., 2020. (ADP-ribosyl)hydrolases: structure, function, and biology. Genes Dev. 34, 263–284. https://doi.org/10.1101/gad.334631.119

Rees, D.D., Brain, J.D., Wohl, M.E., Humes, J.L., Mumford, R.A., 1997. Inhibition of neutrophil elastase in CF sputum by L-658,758. J. Pharmacol. Exp. Ther. 283, 1201–1206.

Retout, M., Amer, L., Yim, W., Creyer, M.N., Lam, B., Trujillo, D.F., Potempa, J., O'Donoghue, A.J., Chen, C., Jokerst, J.V., 2023. A Protease-Responsive Polymer/Peptide Conjugate and Reversible Assembly of Silver Clusters for the Detection of Porphyromonas gingivalis Enzymatic Activity. ACS Nano 17, 17308–17319. https://doi.org/10.1021/acsnano.3c05268

Richter, M.M., 2004. Electrochemiluminescence (ECL). Chem. Rev. 104, 3003–3036. https://doi.org/10.1021/cr020373d

Riise, R., Odqvist, L., Mattsson, J., Monkley, S., Abdillahi, S.M., Tyrchan, C., Muthas, D., Yrlid, L.F., 2019. Bleomycin hydrolase regulates the release of chemokines important for inflammation and wound healing by keratinocytes. Sci. Rep. 9, 20407. https://doi.org/10.1038/s41598-019-56667-6

Rofael, S., Leboreiro Babe, C., Davrandi, M., Kondratiuk, A.L., Cleaver, L., Ahmed, N., Atkinson, C., McHugh, T., Lowe, D.M., 2023. Antibiotic resistance, bacterial transmission and improved prediction of bacterial infection in patients with antibody deficiency. JAC-Antimicrob. Resist. 5, dlad135. https://doi.org/10.1093/jacamr/dlad135

Saade, G.R., Boggess, K.A., Sullivan, S.A., Markenson, G.R., Iams, J.D., Coonrod, D.V., Pereira, L.M., Esplin, M.S., Cousins, L.M., Lam, G.K., Hoffman, M.K., Severinsen, R.D., Pugmire, T., Flick, J.S., Fox, A.C., Lueth, A.J., Rust, S.R., Mazzola, E., Hsu, C., Dufford, M.T., Bradford, C.L., Ichetovkin, I.E., Fleischer, T.C., Polpitiya, A.D., Critchfield, G.C., Kearney, P.E., Boniface, J.J., Hickok, D.E., 2016. Development and validation of a spontaneous preterm delivery predictor in asymptomatic women. Am. J. Obstet. Gynecol. 214, 633.e1-633.e24. https://doi.org/10.1016/j.ajog.2016.02.001

Saetta, M., Turato, G., Maestrelli, P., Mapp, C.E., Fabbri, L.M., 2001. Cellular and Structural Bases of Chronic Obstructive Pulmonary Disease. Am. J. Respir. Crit. Care Med. 163, 1304–1309. https://doi.org/10.1164/ajrccm.163.6.2009116

Saigal, S., Doyle, L.W., 2008. An overview of mortality and sequelae of preterm birth from infancy to adulthood. The Lancet 371, 261–269. https://doi.org/10.1016/S0140-6736(08)60136-1

Salhi, A., Carriere, F., Grundy, M.M.-L., Aloulou, A., 2021. Enzymes Involved in Lipid Digestion, in: Grundy, M.M.-L., Wilde, P.J. (Eds.), Bioaccessibility and Digestibility of Lipids from Food. Springer International Publishing, Cham, pp. 3–28. https://doi.org/10.1007/978-3-030-56909-9_1

Sama, I.E., Ravera, A., Santema, B.T., van Goor, H., ter Maaten, J.M., Cleland, J.G.F., Rienstra, M., Friedrich, A.W., Samani, N.J., Ng, L.L., Dickstein, K., Lang, C.C., Filippatos, G., Anker, S.D., Ponikowski, P., Metra, M., van Veldhuisen, D.J., Voors, A.A., 2020. Circulating plasma concentrations of angiotensin-converting enzyme 2 in men and women with heart failure and effects of renin–angiotensin–aldosterone inhibitors. Eur. Heart J. 41, 1810–1817. https://doi.org/10.1093/eurheartj/ehaa373

Santa, P., Garreau, A., Serpas, L., Ferriere, A., Blanco, P., Soni, C., Sisirak, V., 2021. The Role of Nucleases and Nucleic Acid Editing Enzymes in the Regulation of Self-Nucleic Acid Sensing. Front. Immunol. 12, 629922. https://doi.org/10.3389/fimmu.2021.629922

Serafin, A., Malinowski, M., Prażmowska-Wilanowska, A., 2020. Blood volume and pain perception during finger prick capillary blood sampling: are all safety lancets equal? Postgrad. Med. 132, 288–295. https://doi.org/10.1080/00325481.2020.1717160

Serena, T.E., Bayliff, S.W., Brosnan, P.J., DiMarco, D.T., Doner, B.A., Guthrie, D.A., Patel, K.D., Sabo, M.J., Samies, J.H., Carter, M.J., 2021. Bacterial protease activity as a biomarker to assess the risk of non-healing in chronic wounds: Results from a multicentre randomised controlled clinical trial. Wound Repair Regen. Off. Publ. Wound Heal. Soc. Eur. Tissue Repair Soc. 29, 752–758. https://doi.org/10.1111/wrr.12941

S. Gaster, R., A. Hall, D., X. Wang, S., 2011. nanoLAB: An ultraportable, handheld diagnostic laboratory for global health. Lab. Chip 11, 950–956. https://doi.org/10.1039/C0LC00534G

Shpacovitch, V., Feld, M., Hollenberg, M.D., Luger, T.A., Steinhoff, M., 2008. Role of protease-activated receptors in inflammatory responses, innate and adaptive immunity. J. Leukoc. Biol. 83, 1309–1322. https://doi.org/10.1189/jlb.0108001

Singh, P., Yang, M., Dai, H., Yu, D., Huang, Q., Tan, W., Kernstine, K.H., Lin, D., Shen, B., 2008. Overexpression and Hypomethylation of Flap Endonuclease 1 Gene in Breast and Other Cancers. Mol. Cancer Res. 6, 1710–1717. https://doi.org/10.1158/1541-7786.MCR-08-0269

Son, M., Miller, E.S., 2017. Predicting preterm birth: Cervical length and fetal fibronectin. Semin. Perinatol. 41, 445–451. https://doi.org/10.1053/j.semperi.2017.08.002

Sonawane, S., Khanolkar, V., Namavari, A., Chaudhary, S., Gandhi, S., Tibrewal, S., Jassim, S.H., Shaheen, B., Hallak, J., Horner, J.H., Newcomb, M., Sarkar, J., Jain, S., 2012. Ocular Surface Extracellular DNA and Nuclease Activity Imbalance: A New Paradigm for Inflammation in Dry Eye Disease. Invest. Ophthalmol. Vis. Sci. 53, 8253–8263. https://doi.org/10.1167/iovs.12-10430

Stanforth, K.J., Wilcox, M.D., Chater, P.I., Brownlee, I.A., Zakhour, M.I., Banecki, K.M.R.M., Pearson, J.P., 2022. Pepsin properties, structure, and its accurate measurement: a narrative review. Ann. Esophagus 5, 31–31. https://doi.org/10.21037/aoe-20-95

Su, D., Wu, K., Krishna, V.D., Klein, T., Liu, J., Feng, Y., Perez, A.M., Cheeran, M.C.-J., Wang, J.-P., 2019. Detection of Influenza a Virus in Swine Nasal Swab Samples With a Wash-Free Magnetic Bioassay and a Handheld Giant Magnetoresistance Sensing System. Front. Microbiol. 10.

Sveiven, M., Gassman, A., Rosenberg, J., Chan, M., Boniface, J., O'Donoghue, A.J., Laurent, L.C., Hall, D.A., 2023. A dual-binding magnetic immunoassay to predict spontaneous preterm birth. Front. Bioeng. Biotechnol. 11, 1256267. https://doi.org/10.3389/fbioe.2023.1256267

Swamy, G.K., Simhan, H.N., Gammill, H.S., Heine, R.P., 2005. Clinical utility of fetal fibronectin for predicting preterm birth. J. Reprod. Med. 50, 851–856.

Tan, Y.H., Liu, M., Nolting, B., Go, J.G., Gervay-Hague, J., Liu, G., 2008. A Nanoengineering Approach for Investigation and Regulation of Protein Immobilization. ACS Nano 2, 2374–2384. https://doi.org/10.1021/nn800508f

Taylor, J.M., Yaneva, M., Velasco, K., Philip, J., Erdjument-Bromage, H., Ostrovnaya, I., Lilja, H.G., Bochner, B.H., Tempst, P., 2014. Aminopeptidase activities as prospective urinary biomarkers for bladder cancer. Proteomics Clin. Appl. 8, 317–326. https://doi.org/10.1002/prca.201300118

Thulborn, S.J., Mistry, V., Brightling, C.E., Moffitt, K.L., Ribeiro, D., Bafadhel, M., 2019. Neutrophil elastase as a biomarker for bacterial infection in COPD. Respir. Res. 20, 170. https://doi.org/10.1186/s12931-019-1145-4

Voynow, J.A., Shinbashi, M., 2021. Neutrophil Elastase and Chronic Lung Disease. Biomolecules 11, 1065. https://doi.org/10.3390/biom11081065

Waitzman, N.J., Jalali, A., Grosse, S.D., 2021. Preterm birth lifetime costs in the United States in 2016: An update. Semin. Perinatol., Economic Considerations in Neonatal Intensive Care 45, 151390. https://doi.org/10.1016/j.semperi.2021.151390

Walkowska, J., Zielinska, N., Tubbs, R.S., Podgórski, M., Dłubek-Ruxer, J., Olewnik, Ł., 2022. Diagnosis and Treatment of Acute Pancreatitis. Diagnostics 12, 1974. https://doi.org/10.3390/diagnostics12081974

Walsh, P.N., Ahmad, S.S., 2002. Proteases in blood clotting. Essays Biochem. Vol. 38.

Wang, D., Loo, J.F.C., Chen, J., Yam, Y., Chen, S.-C., He, H., Kong, S.K., Ho, H.P., 2019. Recent Advances in Surface Plasmon Resonance Imaging Sensors. Sensors 19, 1266. https://doi.org/10.3390/s19061266

Wang, K., Xie, C., Chen, D., 2014. Flap endonuclease 1 is a promising candidate biomarker in gastric cancer and is involved in cell proliferation and apoptosis. Int. J. Mol. Med. 33, 1268–1274. https://doi.org/10.3892/ijmm.2014.1682

Wang, Y.-N., Lee, H.-H., Chou, C.-K., Yang, W.-H., Wei, Y., Chen, C.-T., Yao, J., Hsu, J.L., Zhu, C., Ying, H., Ye, Y., Wang, W.-J., Lim, S.-O., Xia, W., Ko, H.-W., Liu, X., Liu, C.-G., Wu, X., Wang, H., Li, D., Prakash, L.R., Katz, M.H., Kang, Y., Kim, M., Fleming, J.B., Fogelman, D., Javle, M., Maitra, A., Hung, M.-C., 2018. Angiogenin/Ribonuclease 5 Is an EGFR Ligand and a Serum Biomarker for Erlotinib Sensitivity in Pancreatic Cancer. Cancer Cell 33, 752-769.e8. https://doi.org/10.1016/j.ccell.2018.02.012

Wei, T., Wang, F., Zhang, Z., Qiang, J., Lv, J., Chen, T., Li, J., Chen, X., 2019. Recent Progress in the Development of Fluorometric Chemosensors to Detect Enzymatic Activity. Curr. Med. Chem. 26, 3923–3957. https://doi.org/10.2174/0929867325666180214105552

Wilson, A., Hodgetts-Morton, V.A., Marson, E.J., Markland, A.D., Larkai, E., Papadopoulou, A., Coomarasamy, A., Tobias, A., Chou, D., Oladapo, O.T., Price, M.J., Morris, K., Gallos, I.D., 2022. Tocolytics for delaying preterm birth: a network meta-analysis (0924). Cochrane Database Syst. Rev. 8, CD014978. https://doi.org/10.1002/14651858.CD014978.pub2

Wolf, S.A., Awschalom, D.D., Buhrman, R.A., Daughton, J.M., Molnár, S. von, Roukes, M.L., Chtchelkanova, A.Y., Treger, D.M., 2001. Spintronics: A Spin-Based Electronics Vision for the Future. Science 294, 1488–1495. https://doi.org/10.1126/science.1065389

Wu, K., Tonini, D., Liang, S., Saha, R., Chugh, V.K., Wang, J.-P., 2022. Giant Magnetoresistance Biosensors in Biomedical Applications. ACS Appl. Mater. Interfaces 14, 9945–9969. https://doi.org/10.1021/acsami.1c20141

Xu, H., Feng, G., Wei, Y., Feng, Y., Yang, R., Wang, L., Zhang, H., Li, R., Qiao, J., 2020. Predicting Ectopic Pregnancy Using Human Chorionic Gonadotropin (hCG) Levels and Main Cause of Infertility in Women Undergoing Assisted Reproductive Treatment: Retrospective Observational Cohort Study. JMIR Med. Inform. 8, e17366. https://doi.org/10.2196/17366

Yao, C., Ng, E., Wang, S.X., 2022. An automated and mobile magnetoresistive biosensor system for early hepatocellular carcinoma diagnosis. Biosens. Bioelectron. 202, 113982. https://doi.org/10.1016/j.bios.2022.113982

Yohannes, G., Wiedmer, S.K., Elomaa, M., Jussila, M., Aseyev, V., Riekkola, M.-L., 2010. Thermal aggregation of bovine serum albumin studied by asymmetrical flow field-flow fractionation. Anal. Chim. Acta 675, 191–198. https://doi.org/10.1016/j.aca.2010.07.016

Yoo, E.-H., Lee, S.-Y., 2010. Glucose biosensors: an overview of use in clinical practice. Sensors 10, 4558–4576. https://doi.org/10.3390/s100504558

Zhang, G., 2004. Protease Assays, in: Markossian, S., Grossman, A., Brimacombe, K., Arkin, M., Auld, D., Austin, C., Baell, J., Chung, T.D.Y., Coussens, N.P., Dahlin, J.L., Devanarayan, V., Foley, T.L., Glicksman, M., Gorshkov, K., Haas, J.V., Hall, M.D., Hoare, S., Inglese, J., Iversen, P.W., Kales, S.C., Lal-Nag, M., Li, Z., McGee, J., McManus, O., Riss, T., Saradjian, P., Sittampalam, G.S., Tarselli, M., Trask, O.J., Wang, Y., Weidner, J.R., Wildey, M.J., Wilson, K., Xia, M., Xu, X. (Eds.), Assay Guidance Manual. Eli Lilly & Company and the National Center for Advancing Translational Sciences, Bethesda (MD).

Zhang, S., He, L., Dai, N., Guan, W., Shan, J., Yang, X., Zhong, Z., Qing, Y., Jin, F., Chen, C., Yang, Y., Wang, H., Baugh, L., Tell, G., Iii, D.M.W., Li, M., Wang, D., 2016. Serum APE1 as a predictive marker for platinum-based chemotherapy of non-small cell lung cancer patients. Oncotarget 7, 77482–77494. https://doi.org/10.18632/oncotarget.13030

Zhang, W., Wang, R., Luo, F., Wang, P., Lin, Z., 2020. Miniaturized electrochemical sensors and their point-of-care applications. Chin. Chem. Lett. 31, 589–600. https://doi.org/10.1016/j.cclet.2019.09.022

Zhou, X., Sveiven, M., Hall, D.A., 2019. A CMOS Magnetoresistive Sensor Front-End With Mismatch-Tolerance and Sub-ppm Sensitivity for Magnetic Immunoassays. IEEE Trans. Biomed. Circuits Syst. 13, 1254–1263. https://doi.org/10.1109/TBCAS.2019.2949725